LARGE FRAGMENT PRODUCTION CALCULATIONS IN RELATIVISTIC HEAVY-ION REACTIONS

by

Luiz Fernando Seixas de Oliveira

NOTICE

ABSTRACT

The abrasion-ablation model is briefly described and then used to calculate cross sections for production of large fragments resulting from target or projectile fragmentation in high-energy heavy-ion collisions.

The number of nucleons removed from the colliding nuclei in the abrasion stage and the excitation energy of the remaining fragments (primary products) are calculated with the geometrical picture of two different models: the fireball and the firestreak models. The charge-to-mass dispersion of the primary products is calculated using either a model which assumes no correlations between proton and neutron positions inside the nucleus (hypergeometric distribution) or a model based upon

the zero-point oscillations of the giant dipole resonance (NUC-GDR). Standard Weisskopf-Ewing statistical evaporation calculations are used to calculate final product distributions.

Results of the pure abrasion-ablation model are compared with a variety of experimental data. The comparisons show the insufficiency of the extra-surface energy term used in the abrasion calculations. A frictional spectator interaction (FSI) is introduced which increases the average excitation energy of the primary products, and improves the results considerably in most cases.

Agreements and discrepancies of the results calculated with the different theoretical assumptions and the experimental data are studied. Of particular relevance is the possibility of observing nuclear ground-state correlations. Results of the recently completed experiment on fragmentation of 213 MeV/A ^{40}Ar projectiles are studied and shown not to be capable of answering that question unambiguously. But predictions for the upcoming ^{48}Ca fragmentation experiment clearly show the possibility of observing correlation effects.

ACKNOWLEDGMENTS

I wish to express my sincere gratitude to Professor John O. Rasmussen, under whose supervision this work was performed. His friendly words of encouragement and support were essential to the completion of this thesis. I thank him for giving my not only an example of a great scientist but also of a great human being.

I deeply thank my friend Dr. Raul Donangelo. Without his brilliant ideas and continuous support it would have been extremely difficult for me to advance in this research. I also thank Dr. Dave Morrissey for his invaluable help in putting this thesis together and for the many discussions we have had on this subject.

Further, I extend my gratitude to Dr. Y. P. Viyogi, Dr. G. D. Westfall, Dr. D. K. Scott, Prof. J. Hüfner, and Prof. J. P. Bondorf for stimulating discussions. I am also grateful to Dr. M. Blann for making the ALICE code available and to Dr. W. Myers for generously giving and helping in the adaptation of key portions of his firestreak code.

Special thanks are due to Prof. S. G. Prussin for his invaluable help throughout my stay here in Berkeley. I am also indebted to Prof. S. N. Kaplan and Prof. L. Grossman. Their friendly advice and encouragment during those difficult first years were essential in making my transition from Rio de Janeiro to Berkeley a reasonably smooth one.

The excellent typing of the manuscript by Ms. Deberah Craig is deeply appreciated.

I wish to express my sincere appreciation to the many friends

of all languages, and in particular to Cesar and Ondina Leal, who made my stay in Berkeley a most pleasant one after all.

I express a sincere debt of gratitude to my parents for their enormous effort to give all their five children the best possible education. To my wife, Alix, and to my son, Renato, the least I can say is: I love you both. To them I dedicate this thesis.

I gratefully acknowledge financial support from Comissão Nacional de Energia Nuclear, Brazil. In particular, I would like to thank Prof. Bandeira de Mello and D. Nilza Eny de Almeida.

TABLE OF CONTENTS

Acknowledgments i

Table of Contents iii

I. INTRODUCTION 1
   1. Relativistic Heavy Ions 1
   2. Thesis Outline 5
   3. Survey of Relativistic Heavy-Ion Fragmentation Experiments 7

II. THE ABRASION-ABLATION MODEL 10
   1. Introduction 10
   2. Abrasion Models 11
   3. Charge Dispersion Relations 17
   4. The Ablation Stage 24

III. FIREBALL ABRASION 26
   1. Introduction 26
   2. Abrasion Cross Sections 26
   3. Primary Product Excitation 32
   4. Tabulation of Primary Product Cross Sections and Excitation Energies 35
   5. Discussion and Comparisons 58

IV. FINAL PRODUCT DISTRIBUTIONS 67
   1. Introduction 67
   2. Pure Abrasion-Ablation: Comparisons with Experimental Data 67
   3. Added Excitation Energy: Frictional Spectator Interaction . 77
   4. Abrasion-FSI-Ablation: New Comparisons 84
   5. Factorization of Fragmentation Cross Sections 97
   6. ^{40}Ar and ^{48}Ca Fragmentation Results 101

V. FIRESTREAK ABRASION
   1. Introduction 117
   2. Geometry and Kinematics 118
   3. Discussion 121

VI. CONCLUSIONS 128

APPENDICES 131

A. Derivation of Nuc-GDR Charge Dispersion 131

B. Table of ^{40}Ar and ^{48}Ca Fragmentation Cross Sections 136

REFERENCES 142

I. INTRODUCTION

I.1 Relativistic Heavy Ions

The first studies of high energy collisions between two nuclei date from the late 1940's, when $Z \geq 2$ components were discovered in the primary cosmic radiation.[1,2] However, the possibility of accelerating heavy ions to energies of hundreds to thousands of MeV per nucleon in the Berkeley Bevalac added a new dimension to research in this area, primarily because it allowed better control over the experimental conditions. Indeed, since 1971 when the first successful acceleration of relativistic heavy-ions was achieved in Berkeley,[3,4] a great wealth of new information has been gathered by the Bevalac experimentalists.[5] This very active research field has acquired an independent status and is known today as relativistic (or high energy) heavy-ion physics. The great interest in this new research area was prompted by suggestions that under the extreme conditions of a relativistic heavy-ion (RHI) collision many new exotic phenomena ("Lee-Wick abnormal nuclear matter",[6] "shock waves,"[7] "pion condensation"[8]) would be produced. Although experimental evidence of those processes has not been found yet, other interesting concepts, such as "factorization,"[9] "scaling,"[10] and "limiting fragmentation,"[11] have been experimentally verified.

The subdivision of high energy heavy-ion reactions into central and peripheral collisions is well established among nuclear physicists. These two qualitatively different types of collisions can be clearly differentiated in observations of streamer chamber[12] and nuclear emulsion[13] pictures.

In Fig. I.1 we show two clear examples of both types of collisions taken from Ref. 13. They result from the interaction of an ^{40}Ar projectile, E_{lab} = 1.8 GeV/nuc, with a Ag(Br) nucleus in Ilford G.5 emulsion. In both cases the beam enters the picture from the left. The central (impact parameter ≈ 0) collisions, which comprise about 10% of all cases,[14] are characterized by an almost complete destruction of both the projectile and target nuclei. A good example of this type of collision is shown in the lower part of Fig. I.1. A large number of high energy particles come out over a wide range of angles, i.e., these violent processes are high-multiplicity events. From the point of view of Swiatecki's participant-spectator model,[15] practically all nucleons in both colliding partners are participants in a central collision.

By contrast, in case of a peripheral event the momentum and energy transfers are relatively small. Only a few nucleons in the overlap zone effectively interact during the collision, i.e., the number of participant nucleons is much less than in a central collision. As a result, a few fragments are observed in the extreme forward cone of laboratory angles with velocities approximately equal to that of the projectile, as shown in the upper part of Fig. I.1. These particles originate from the fragmentation of the excited projectile. Simultaneously, other fragments are observed to have an almost isotropic distribution in the lab frame, and they are considered to be evaporation products from the excited target residue (target fragmentation).

Figure I.1. Ilford G.5 emulsion pictures resulting from the interaction of an ^{40}Ar projectile, E_{lab} = 1.8 GeV/nuc with a Ag(Br) nucleus. Part (a) is a clear example of a peripheral collision with characteristics of both projectile and target fragmentation. Part (b) is an example of a central collision. In both cases the beam enters the picture from the left.

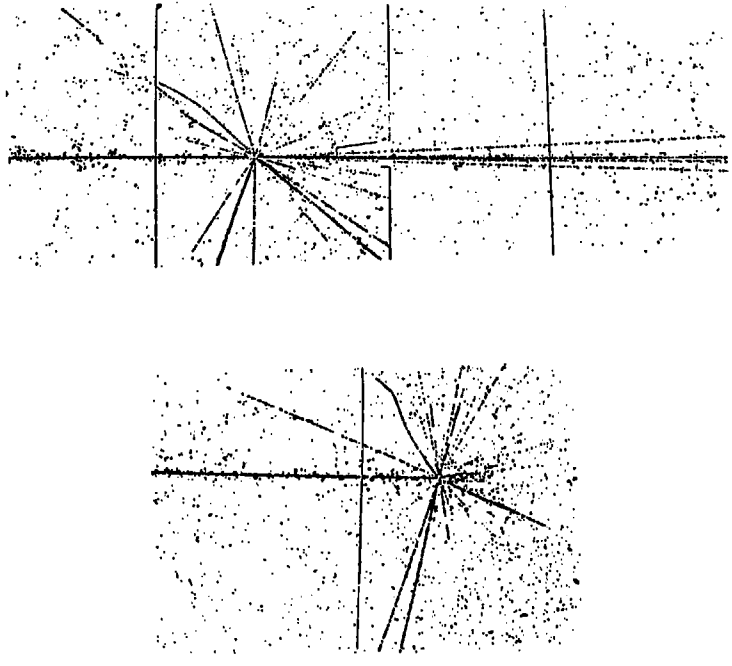

XBL 791-8104

Figure I.1

I.2 Thesis Outline

In this work we attempt to interpret results of target or projectile fragmentation experiments with high-energy heavy-ions. We calculate cross sections for production of heavy fragments considered to be produced in peripheral collisions.

An extensive survey of target and projectile fragmentation experiments is presented at the end of this introductory chapter. All experiments listed in Table I.1 have investigated the production of large fragments resulting from the collisions of two nuclei at high bombarding energies (from 0.2 to 2.1 GeV/nuc). The inclusion of such a table is meant to give an idea of the great variety of information gathered in the last five or six years in the area of peripheral RHI collisions. For a recent review of the general experimental situation, see Refs. 4 and 15.

All the calculations presented in this work are based on the abrasion-ablation model[16] which is presented in Chapter II. In section II.2 we give a brief description of the main theoretical assumptions behind the three abrasion pictures used here, namely, fireball,[16-19] firestreak,[19-21] and multiple scattering[22,23] abrasion. The fundamental question of ground state nucleon correlations[24-26] is investigated in section II.3, where we study several ways of specifying the neutron-proton composition (charge-to-mass dispersion) of the spectator nucleons. Chapter II ends with a description of the ablation (or evaporation) stage.

In Chapter III we give a detailed account of the fireball abrasion model. Cross section and excitation energy of the abrasion products

are calculated according to suggestions given by Swiatecki, and the results are compared to those of other models (multiple scattering abrasion[22,23] and Monte Carlo cascade.[28] Included in this chapter is an extensive tabulation of primary product distributions for the target-projectile systems studied in this work.

Chapter IV contains the final results (final product distribution) of our abrasion-ablation calculations, obtained with the fireball abrasion model. The computational procedure is explained, and the theoretical results are compared with a variety of experimental data. The possibility of observing ground state correlations is explored by comparing the theoretical results obtained with two different charge dispersion relations with experimental data. The target mass dependence of projectile fragmentation cross sections and the validity of the "factorization hypothesis" are discussed in section IV.5. This chapter ends with some predictions of new neutron-rich isotopes to be found in the fragmentation of a high-energy (~200 MeV/nuc) ^{48}Ca beam.

Chapter V discusses the application of the firestreak geometry and kinematics to the calculation of the abrasion stage. A description of the theoretical assumptions of the model is given in Section V.2. Results obtained with this approach are presented and a few modifications are suggested at the end of the chapter.

In Chapter VI we present our conclusions.

We remark that although we will be using the geometrical and kinematical assumptions of the fireball[14,17] and firestreak[20,21] models for the abrasion stage, we will not refer to the other hypotheses of those models, since here we do not deal with the fireball (or firestreak)

itself. Instead, we concentrate our attention on the fate of the spectator fragments.

I.3 Survey of Relativistic Heavy-Ion Fragmentation Experiments

In Table I.1 we have listed all the high-energy heavy-ion fragmentation experiments performed to date at the Bevalac. We included all those experiments which have the following characteristics:

1) Projectile lab energy is in the range 0.2 to 2.1 GeV/nuc.
2) Both colliding partners are heavy ions ($Z > 2$).
3) Heavy fragment production cross sections are the observed quantities, i.e., peripheral collisions are the dominant process;
4) Results are publicly available, either in a journal or as a laboratory report.

The first column gives the nuclei from which the fragments originated. They can be either projectile or target depending on whether it is a projectile or target fragmentation experiment (indicated in column 3).

TABLE I.1. Relativistic Heavy-ion fragmentation experiments.

Fragmented nucleus	Collision partner	Lab energy (GeV/nuc)	Type (projectile or target fragmentation)	Reference
^{12}C	Be C Al Cu Ag Pb	1.05 and 2.1	projectile	Lindstrom et al [29]
^{14}N	C	2.1	projectile	Heckman et al [29a]
^{16}O	Be C Al Cu Ag Pb	2.1	projectile	Lindstrom et al [29]
^{23}Na	^{12}C ^{4}He	0.25 and 0.40	target	Shibata et al [30]
^{32}S	^{12}C ^{4}He	0.25 and 0.40	target	Shibata et al [30]
^{40}Ca	^{12}C ^{4}He	0.25 and 0.40	target	Shibata et al [30]
^{40}Ar	^{12}C	0.21	projectile	Viyogi et al[31] Symons et al[32]
^{56}Fe	Li Be C S Cu Ag Ta Pb U	1.88	projectile	Westfall et al [33]
^{nat}Cu	^{14}N	0.28	target	Cumming et al[34]
^{nat}Cu	^{12}C	2.1	target	Cumming et al[35]
^{nat}Cu	^{40}Ar	2.0	target	Cumming et al[36]

TABLE I.1 (continued)

Fragmented nucleus	Collision partner	Lab energy (GeV/nuc)	Type (projectile or target fragmentation)	Reference
^{nat}Ag	^{12}C	2.1	target	Rudy and Porile [37]
^{197}Au	^{12}C	2.1	target	Loveland et al [38]
^{208}Pb	^{12}C	2.1	target	Loveland et al [38]
^{238}U	^{12}C	2.1	target	Loveland et al [39]
^{181}Ta	^{20}Ne	0.40	target	Morrissey et al [40]

II. THE ABRASION-ABLATION MODEL

II.1 Introduction

The abrasion-ablation model was introduced into the relativistic heavy-ion (RHI) field in 1973 by Bowman, Swiatecki and Tsang,[16] but its underlying assumptions were already formulated in 1954 by Y. Eisenberg.[41] In this chapter we describe the fundamental concepts of the model and discuss the different theoretical approaches which can be used in its application to the calculation of large fragment production cross sections in RHI reactions.

The basic idea behind the model, which is retained in all its variations, is the assumption that a RHI reaction occurs as a two-stage process. In the fast stage (abrasion) the nucleons within the overlap zone of the two collision partners interact with each other and are "kicked out" of their bound orbits, i.e., they are sheared away from either the projectile or the target. The projectile fragment follows its trajectory with essentially the same lab velocity as before, while the target fragment slowly recoils. Both fragments are excited as a result of the abrasion, and they later dissipate this excitation energy by undergoing particle evaporation (ablation stage). We should stress that the above description is meant to describe only those reactions which can be characterized as peripheral collisions, i.e., those which occur at large impact parameters, as described in Section I.1.

With present-day experimental techniques the only heavy fragments which can be observed in an RHI reaction are the final products of the ablation stage. Unfortunately the direct products of the abrasion, the so-called primary products (PP), or primary fragments, cannot be observed

due to their very fast decay. How does one calculate the cross sections for production (or yields) of the final products? First one must calculate the primary product distribution, i.e., the cross sections for removing one, two, three, ... nucleons, and the corresponding excitation energy of each primary product. These two results (cross section and excitation energy of each primary product) can then be fed into some kind of evaporation routine which will produce the final results. We will give more details of the computational procedure in Chapter IV.

There are at least three different ways of calculating the fast abrasion stage, and in the next section we will present a brief discussion of their differences and similarities.

Let us stress that by fast abrasion we mean that the abrasion process occurs in a time-interval which is shorter than the time it would take for the disturbance to spread appreciably toward the spectator pieces. Considering that the disturbance spreads with at least the Fermi velocity, this condition restricts one to projectile energies higher than approximately 50 MeV/A. All calculations described in this work have been applied to reactions in which the projectile energies are between 200 and 2000 MeV/A.

II.2 Abrasion Models

In the calculations we have done so far[18,19] we have used two distinct (though similar) geometrical pictures for the abrasion stage: the sharp surface (fireball) and the firestreak abrasion. A third way to calculate the fast stage has been proposed by Hüfner, Schäeffer and

Schürmann.[22] Since we intend to compare results calculated with different theoretical assumptions later in this work, let us first discuss each model separately.

Fireball abrasion

Two basic assumptions are included in the geometrical picture of the fireball model: both nuclei are assumed to have sharp spherical surfaces and to follow straight-line trajectories (at the energies we are considering, the orbit distortion caused by Coulomb repulsion can be neglected). Therefore, the separation between spectator and target nucleons is given by the intersection of the two nuclear surfaces. The two nuclei scrape each other, shearing away all nucleons located within their geometrical overlap zone (participant nucleons). A schematical view of this model is shown in Fig. II.1. The number of nucleons, a_T, removed from the target is therefore calculated from geometrical considerations alone, i.e., for a given system a_T depends only on the impact parameter b ($a_T = a_T(b)$). By calculating the product of the nuclear matter density times the overlap volume between a cylinder and a sphere, we can determine the impact parameters necessary for the removal of one, two, three, ... nucleons, and the corresponding cross sections.

In this model the excitation energy of the primary products is assumed (suggested by Swiatecki as a lower limit) to be proportional to the surface excess between the deformed abrasion product with a concave cylindrical surface and a spherical surface of equal volume. Further details will be given in Chapter III.

FIREBALL

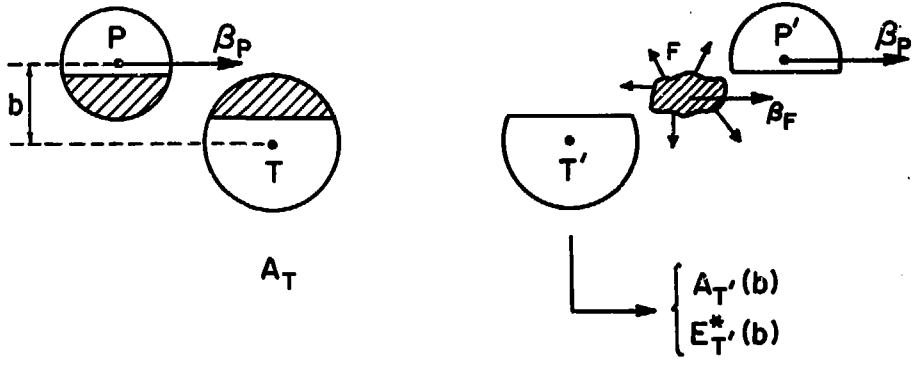

XBL784-4914

Fig. II.1. Abrasion stage with fireball geometry. Both nuclei are assumed to have sharp spherical surfaces and to follow straight line trajectories. The nucelons within the overlap zone are sheared away from both nuclei, which are excited in the process. The excitation energy is calculated from the excess surface of the distorted spectators.

Firestreak abrasion

In the firestreak model[20,21] the colliding nuclei are divided into a series of tubes (streaks) parallel to the direction of relative motion of the collision partners. Each projectile tube collides completely inelastically with the target tube directly in its path, again assuming straight-line trajectories (see Fig. II.2). By simple relativistic kinematics one can calculate the momentum and excitation energy of the compound tubes, which are completely characterized by the parameter

$$\eta = \frac{m_P}{m_P + m_T} \tag{1}$$

This parameter specifies the amount of material coming from the projectile which is present in the compound tube. One novelty of this approach is that a diffuse nuclear density distribution can be used instead of the uniform density used in the fireball abrasion description.

In order to calculate the cross section for removal of a_T nucleons from the target (or a_P nucleons from the projectile) we must first specify a criterion for deciding which tubes escape the target (or projectile) at a certain impact parameter b and which ones do not (escaping tube criterion). We have assumed that if the internal energy per particle of a tube is greater than a critical value ε_c the tube will escape, otherwise it will remain and deposit its energy in the spectator piece. With this criterion in mind we can calculate the cross sections and the excitation energy of the primary products. The possible values of ε_c and details of the actual calculation will be given in Chapter V.

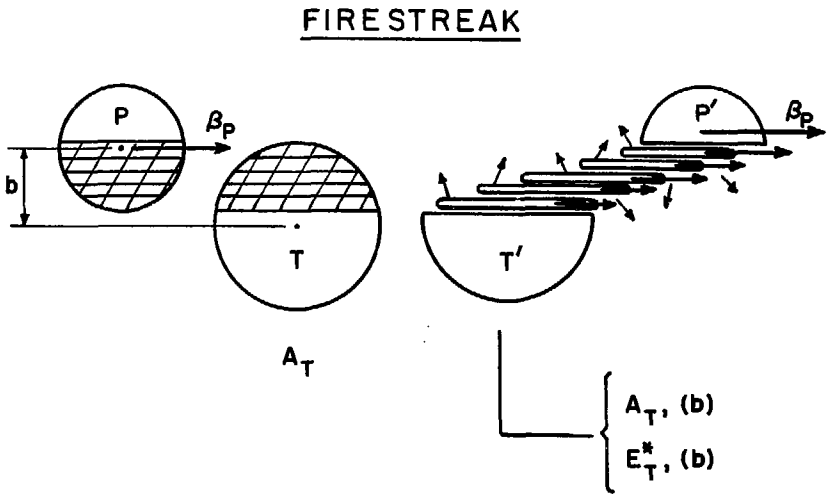

XBL 783-7702

Fig. II.2. Abrasion stage with firestreak geometry. Both nuclei are subdivided into tubes parallel to the direction of relative motion. Each projectile tube collides with a target tube directly in its path, and they form a composite tube (or streak). If the internal energy of a tube is greater than a critical value ε_c it leaves the spectators.

Abrasion calculation based on Glauber's multiple scattering theory

Hüfner and collaborators[22,23,42] have developed a picture of the abrasion stage based on the multiple scattering theory of Glauber.[43,44] This theory has been applied successfully to the description of the scattering of fast elementary particles by nuclei. It has also been used to calculate elastic and total cross sections between two heavy ions at high energies.[45-48] Hüfner et al. have extended Glauber's theory to the treatment of inelastic processes such as the removal of nucleons which occurs in the abrasion stage. We shall hereafter refer to Hüfner's formalism as multiple scattering abrasion (MSA).

In this section we give a brief overview of the MSA formalism. Abrasion cross sections obtained with this formalism will be compared to those predicted by the fireball abrasion model in Chapter III. For a detailed derivation of the following equations, see Ref. 2..

Starting from the inelastic scattering amplitude, as derived in Glauber theory, Hufner et al. showed that the cross section for abrasion of a_p nucleons from the projectile can be written as

$$\sigma(a_p) = \int d^2b \binom{A_p}{a_p} P(b)^{a_p} (1 - P(b))^{A_p - a_p} \tag{2}$$

where

$$P(b) = \int dz\, d^2s\, \rho_p(\vec{b} + \vec{s}, z) \left\{ 1 - \exp\left(-A_T\, \sigma_{NN}^{tot} \int_{-\infty}^{\infty} dz'\, \rho_T(\vec{s}, z') \right) \right\} \tag{3}$$

Here $\rho_p(\vec{x})$ and $\rho_T(\vec{x})$ are the single-particle densities of the projectile and target respectively, and the position vector $\vec{x}$ is decomposed into

a z-coordinate (beam direction) and a component $\vec{s}$ in the impact parameter ($\vec{b}$) plane.

The quantity P(b) can be readily interpreted as the probability of finding a target nucleon in the overlap zone at an impact parameter b, and the integrand of Eq. (2) is then the probability of finding a_p target nucleons in the direct path of the projectile and $(A_T - a_p)$ out of its way.

In the first paper on this subject,[22] Hüfner et al. used a generalized Thomas-Reich-Kuhn sum rule[49] to calculate the average excitation energy of the primary products. In a more recent work[42] they have proposed a semiclassical model of incoherent collisions. In this picture, the nucleons which are struck in the abrasion stage lose energy as they collide with other nucleons on their way out of the nucleus. Further details can be found in Ref. 23.

II.3 Charge Dispersion Relations[42a]

The abrasion stage, as described in the preceding section, only calculates the number of nucleons removed from the target, without specifying its proton-neutron ratio. Before proceeding with the evaporation stage we must specify that ratio, since that is what determines the isotopic composition of the primary products. The probability of a possible proton-neutron combination of the $a_T(b)$ abraded nucleons is determined by the nuclear charge-to-mass dispersion, or simply, charge dispersion.

The simplest limiting case for the calculation of the proton-neutron composition of the $a_T(b)$ abraded target nucleons is to assume no dispersion. This implies that for each impact parameter b, z(b) protons

and n(b) neutrons are ejected, which are determined by (in case of *target fragmentation*),

$$z(b) = \frac{Z_T}{A_T} a_T(b) \quad ,$$

$$n(b) = \frac{N_T}{A_T} a_T(b) \quad . \tag{4}$$

The opposite limit is to assume that each struck target nucleon has a Z_T/A_T probability of being a proton. Under this assumption, the fraction of the abrasion cross section of a_T nucleons which corresponds to the formation of a primary product $(Z_{T'}, A_{T'})$ is given by the hypergeometric distribution

$$P(Z_{T'}, A_{T'}) = \frac{\binom{Z_T}{z}\binom{N_T}{n}}{\binom{A_T}{a_T}} \quad , \tag{5}$$

where $z = Z_T - Z_{T'}$, $n = N_T - N_{T'}$, and $a_T = n + z$ are, respectively, the number of protons, neutrons, and nucleons removed from the target. Therefore, the cross section for formation of the primary product $(Z_{T'}, A_{T'})$ is given by

$$\sigma(Z_{T'}, A_{T'}) = P(Z_{T'}, A_{T'}) \times \sigma(A_{T'}) \tag{6}$$

where $\sigma(A_{T'})$ is the abrasion cross section for removal of $a_T = A_T - A_{T'}$ nucleons, and $P(Z_{T'}, A_{T'})$ is given in Eq. (5).

We understand that the above-mentioned charge dispersions (fixed composition and hypergeometric) correspond to limiting situations: the former corresponds to a situation of complete correlation among the nucleons, such as would be the case if nuclear matter were a two-component crystal. The latter, on the other hand, considers no correlation at all between the proton and neutron distributions, a situation analogous to that of two gases. The actual situation certainly lies between these two limiting cases.

A more sophisticated expression for the charge dispersion has been developed by Morrissey et al.,[24] which we shall refer to hereafter as Nuc-GDR (for nuclear giant dipole resonance). The basic assumption here is that fluctuations in the number of participant target protons are due to zero point vibrations of the giant dipole resonance of the target nucleus. In the Goldhaber-Teller picture, the giant dipole resonance is described as an out-of-phase vibration of the neutrons against the protons. The Nuc-GDR charge dispersion is then taken as having a Gaussian form:

$$\sigma(Z_{T'},A_{T'}) = \frac{1}{(2\pi\sigma_z^2)^{\frac{1}{2}}} \exp\left\{\frac{-[Z_{T'} - a_T(Z_T/A_T)]^2}{2\sigma_z^2}\right\} \sigma(A_{T'}) \qquad (7)$$

where all variables have the same meaning as in Eqs. (5) and (6) with the addition of σ_z which was not defined before. The width σ_z is given by

$$\sigma_z = \sigma_{disp}\left(\frac{da_T}{db}\right)\frac{Z_T}{A_T} \qquad (8)$$

where da_T/db is the derivative with respect to impact parameter of the

number of nucleons removed, and σ_{disp} is the width of the distribution in displacements of the neutrons relative to the protons (see derivation in Appendix A).

In Fig. II.3(a,b,c) we compare results of the primary product distribution obtained with the hypergeometric [Eq. (6)] and the Nuc-GDR [Eq. (7)] charge dispersions. (These results were calculated using the sharp-surface (fireball) abrasion model.) By examining those figures we see that while the widths of the two dispersions are not significantly different for the case of Mg fragmentation (a), they are very different for the Pb case (c). In fact, for the Fe case (b) they already show a significant distinction, the width of the hypergeometric being always broader than that of the Nuc-GDR. Whether or not this difference in width can survive the strong focusing effect of the subsequent evaporation stage toward the valley of stability is a point which will be discussed in Chapter IV, when we compare several theoretical results with experimental data.

An analysis with a similar orientation towards the proton-neutron distribution left in the spectator piece is that of Bondorf, Fai and Nielsen.[25,26] They investigate the influence of ground state correlations (such as isospin correlations) in the charge and mass distributions of the primary products by using a fluid-dynamic picture of the nucleus. We will not go into further detail of their work here, but we shall mention some of their interesting conclusions when we discuss the experimental results (Chapter IV).

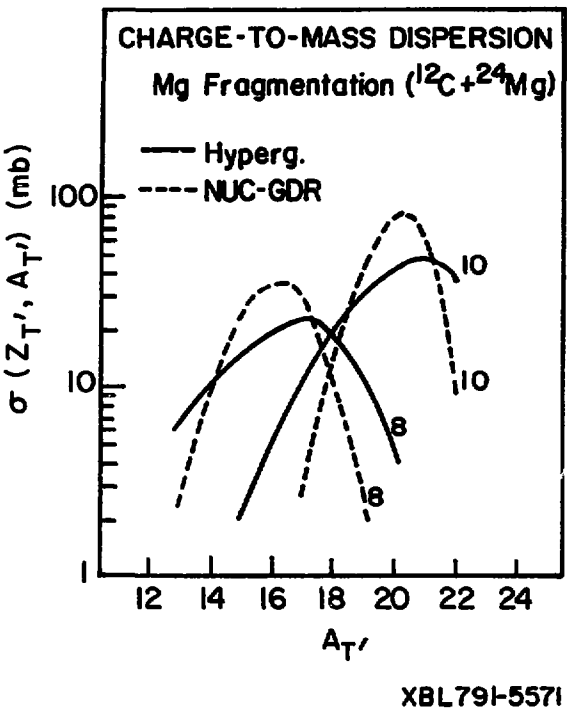

Fig. II.3(a). Charge-to-mass dispersion of primary products for $^{12}C + ^{24}Mg$. The numbers on the curves designate the charge ($Z_{T'}$) of the primary products.

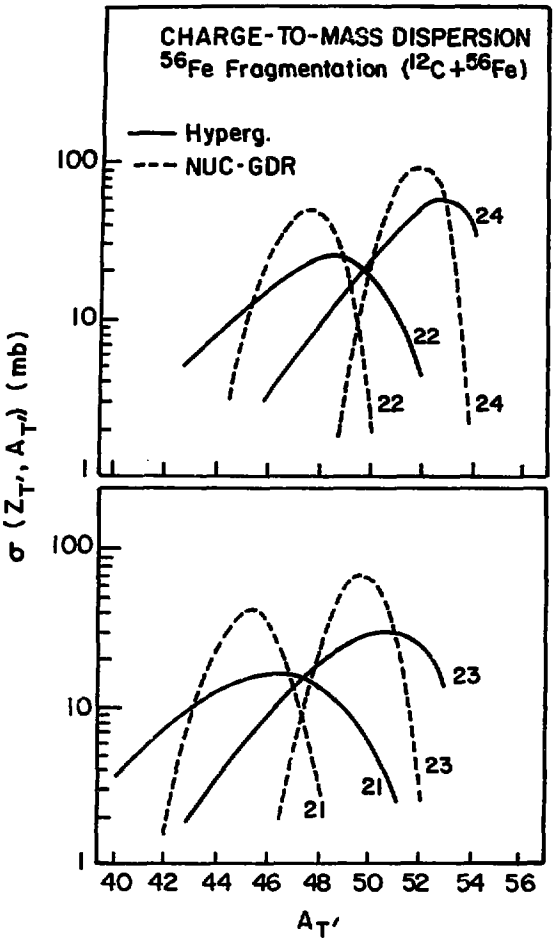

XBL 791-5570

Fig. II.3(b). Same as Fig. II.3(a) for $^{12}C + ^{56}Fe$.

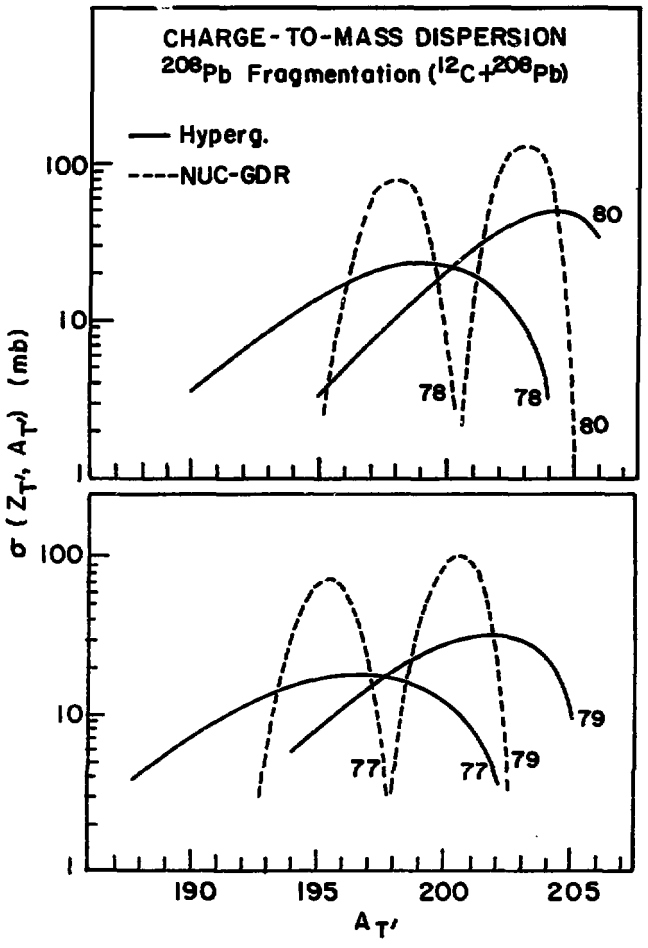

XBL791-5569

Fig. II.3(c). Same as Fig. II.3(a) for $^{12}C + ^{208}Pb$.

II.4 The Ablation Stage

After the fast stage of the collision the primary fragments are left with excitation energies which vary between 1 MeV and 80 MeV (for practically all cases reported in this work). How do these excited fragments decay? This is one question to which we do not have a definite answer yet. We assume that the excitation energy is thermalized before nucleon emission occurs. This thermalization hypothesis finds some support in the observed isotropy of black tracks in fragmentation reactions.[42] The excited nucleus can then be treated by standard statistical evaporation models.

To calculate the evaporation stage we use a subroutine which was adapted from the computer code OVERLAID ALICE.[50] This subroutine (which we called EVAPOR) performs standard Weisskopf-Ewing[51] (W-E) statistical evaporation of protons, neutrons, deuterons and alphas, from a given excited nucleus. In W-E theory the probability of emitting a particle ν with channel energy between ε and $\varepsilon + d\varepsilon$ from a nucleus at excitation energy E^* is given by

$$P_\nu(\varepsilon)d\varepsilon = \frac{(2s+1)_\nu\, \mu_\nu \varepsilon\, \sigma_\nu(\varepsilon)\, \rho(E_f)d\varepsilon}{\sum_{\nu=1}^{n} (2s+1)_\nu\, \mu_\nu \int_0^\infty \varepsilon\sigma_\nu(\varepsilon)\, \rho(E_f)d\varepsilon} \qquad (9)$$

where s is the particle spin, μ_ν the reduced mass, $\sigma_\nu(\varepsilon)$ the inverse reaction cross section, and $\rho(E_f)$ the residual nucleus level density at excitation energy $E_f = E^* - B_\nu - \varepsilon$ (B_ν = binding energy for particle ν). We used a Fermi gas level density

$$\rho(E) \propto E^{-2} \exp[2(aE)^{\frac{1}{2}}] \tag{10}$$

with level density parameter a = A/8. The inverse cross section $\sigma_\nu(\varepsilon)$ is related to the transmission coefficients $T_\ell^\nu(\varepsilon)$ for orbital angular momentum ℓ by

$$\sigma_\nu(\varepsilon) = \pi \lambda\!\!\!^{-}{}_\nu^2 \sum_{\ell=0}^{\infty} (2\ell+1)\ T_\ell^\nu(\varepsilon) \quad . \tag{11}$$

where $\lambda\!\!\!^{-}{}_\nu (= \sqrt{\hbar^2/2\mu_\nu\varepsilon}\ )$ is the reduced wave length. The transmission coefficients were calculated via the optical model[50] and the binding energies from the Myers-Swiatecki shell corrected mass formula.[52] The odd-even term was not included in the mass formula in order to compensate for the lacking of a pairing shift of the excitation energy in the level density formula [Eq. (10)]. The excited nucleus is allowed to evaporate neutrons, protons, deuterons, and alphas until the excitation energy of the residual nucleus falls below the binding energy of those particles.

III. FIREBALL ABRASION

III.1 Introduction

In this chapter we give a detailed description of our calculations of the primary products using the fireball abrasion picture introduced in Section II.2. The abrasion cross sections and excitation energies are discussed in Sections III.2 and III.3, respectively. In Section III.4 we present extensive tables of primary product distributions for some of the systems presented in Table I.1 using both the hypergeometric and the Nuc-GDR charge dispersions. In Section III.4 we compare the numerical results of the preceding section with those of the MSA (see Section II.2) for a few cases. A comparison with the Monte-Carlo cascade calculations of Fraenkel and Yariv[28] is also presented in this section.

III.2 Abrasion Cross Sections

Assuming the colliding nuclei to have sharp spherical surfaces and to follow straight line trajectories, the calculation of the number of participant nucleons for a given impact parameter becomes a purely geometrical problem. Let us calculate here the number of target participant nucleons. This can be done by numerically evaluating the intersection volume, V_T, between a sphere of radius R_T and a cylinder of radius R_P at impact parameter b, which can be written as

$$V_T(b) = 2\int d^2s \sqrt{R_T^2 - (\vec{s} - \vec{b})^2}\ \theta(R_T^2 - (\vec{s} - \vec{b})^2)\ \theta(R_P^2 - \vec{s}^2) \quad (1)$$

where $\vec{s}$ is in the plane perpendicular to the incident direction

(impact parameter plane). The step function $\theta(x)$ is chosen for positive arguments. The number of target participant nucleons is then simply

$$a_T(b) = \rho_{NM} V_T(b) \tag{2}$$

where ρ_{NM} is the normal nuclear matter density ($\rho_{NM} = 0.17\ fm^{-3}$). By interchanging the subindices T and P one obtains the projectile intersection volume.

Instead of performing the integration in Eq. (1), we use an analytical approximation derived by Swiatecki.[27] According to his formulation, the number of target participant nucleons at a given impact parameter b is given by

$$a_T(b) = A_T F(\nu,\beta) \tag{3}$$

where A_T is the target mass number and F is a function (given below) of the dimensionless parameters

$$\nu = \frac{R_T}{R_T + R_P} \tag{4}$$

and

$$\beta = \frac{b}{R_T + R_P} \tag{5}$$

The parameters ν and β (which specify the relative size of the collision partners and the impact parameter, respectively) range from 0 to 1. These limits define a square with unit side in the space of ν and β. Dividing this square as shown in Fig. III.1, the values of $F(\nu,\beta)$ in the four sectors are given by

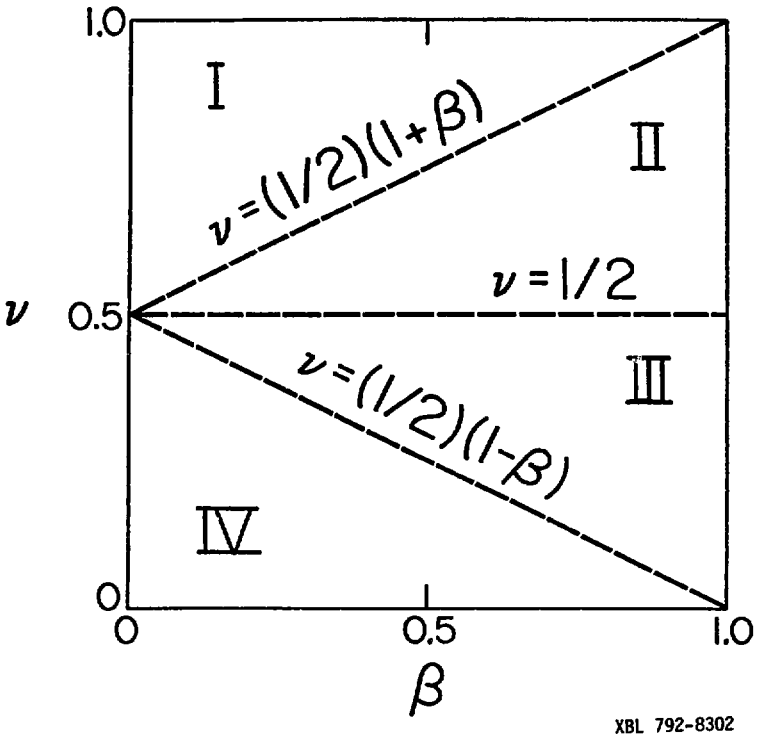

Fig. III.1. The four sectors of the ν,β space where the various values of $F(\nu,\beta)$ [Eq. (6)] apply.

$$F_I = [1-(1-\mu^2)^{3/2}]\,[1-(\beta/\nu)^2]^{1/2} \quad ,$$

$$F_{II} = \frac{3}{4}(1-\nu)^{1/2}\left(\frac{1-\beta}{\nu}\right)^2 - \frac{1}{8}\left\{\frac{3(1-\nu)^{1/2}}{\mu} - \frac{[1-(1-\mu^2)^{3/2}][1-(1-\mu)^2]^{1/2}}{\mu^3}\right\}\left(\frac{1-\beta}{\nu}\right)^3 \quad ,$$

$$F_{III} = \frac{3}{4}(1-\nu)^{1/2}\left(\frac{1-\beta}{\nu}\right)^2 - \frac{1}{8}[3(1-\nu)^{1/2}-1]\left(\frac{1-\beta}{\nu}\right)^3 \quad , \tag{6}$$

$$F_{IV} = 1 \quad .$$

where $\mu = \frac{1}{\nu} - 1 = \frac{R_p}{R_T}$.

The four sectors of Fig. III.1 correspond to the following physical situations:

i) A cylindrical hole is gouged in the target nucleus ($A_T > A_p$).

ii) A cylindrical channel is gouged in the target A_T, with a radius smaller than that of A_T ($A_T > A_p$).

iii) A cylindrical channel is gouged in the target A_T, with a radius larger than that of A_T ($A_T < A_p$).

iv) The target nucleus is completely obliterated by the projectile ($A_T < A_p$).

In this work we restrict ourselves to cases (ii) and (iii) because we are dealing with peripheral collisions only.

In Fig. III.2 we compare the results of Eqs. (2) and (3) for the $^{12}C + {}^{40}Ca$ and $^{12}C + {}^{56}Fe$ reactions. We see that the analytical

Fig. III.2. Number of target participant nucleons as a function of impact parameter. This figure shows that the results obtained with the approximate analytical formulation [Eq. (3)] agree very well with those calculated by the numerical integration of Eq. (2), particularly for large impact parameter values.

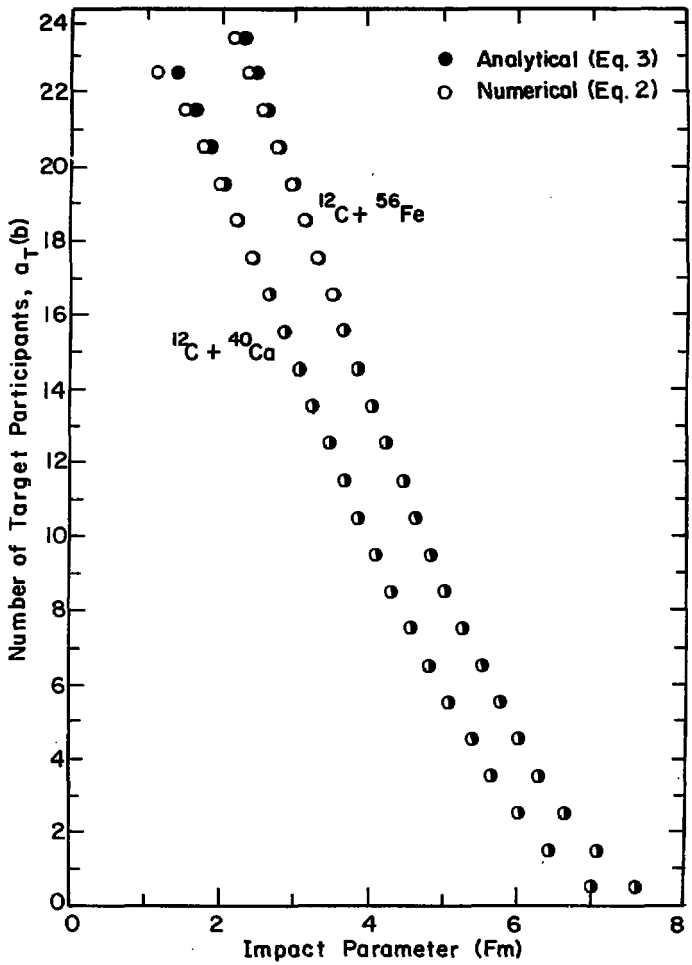

XBL791-5562

Fig. III.2

formulation [Eq. (3)] is an excellent approximation to the exact numerical integration, especially for large impact parameters (which is exactly the region that we are interested in). The rationale for using the approximate formulation lies in the amount of computation time that is saved by the analytical approximation.

With $a_T(b)$ calculated from Eq. (3), the mass number for the primary residue produced at impact parameter b is simply given by

$$A_{T'}(b) = A_T - a_T(b) \quad . \tag{7}$$

From the inverse function $b(A_{T'})$, the cross section for a primary product of mass $A_{T'}$ is determined by

$$\sigma(A_{T'}) = \pi[b(A_T + 0.5)^2 - b(A_{T'} - 0.5)^2] \tag{8}$$

In the upper part of Fig. III.3 we show the abrasion cross sections obtained with the above equations for the cases of $^{12}C + {}^{40}Ca$ and $^{12}C + {}^{56}Fe$.

III.3 Excitation Energy

As a result of the sharp cut suffered in the abrasion stage, a primary product is left with a concave cylindrical channel as part of its surface. Assuming its ground state configuration to be spherical, we have calculated (as suggested in Ref. 27) its excitation energy by multiplying the nuclear surface-energy coefficient (taken as 0.95 MeV/fm^2) by the calculated value of the fragment excess surface. This excess is given by the difference between the area of the deformed abrasion product (with a concave cylindrical surface gouged in it) and the area

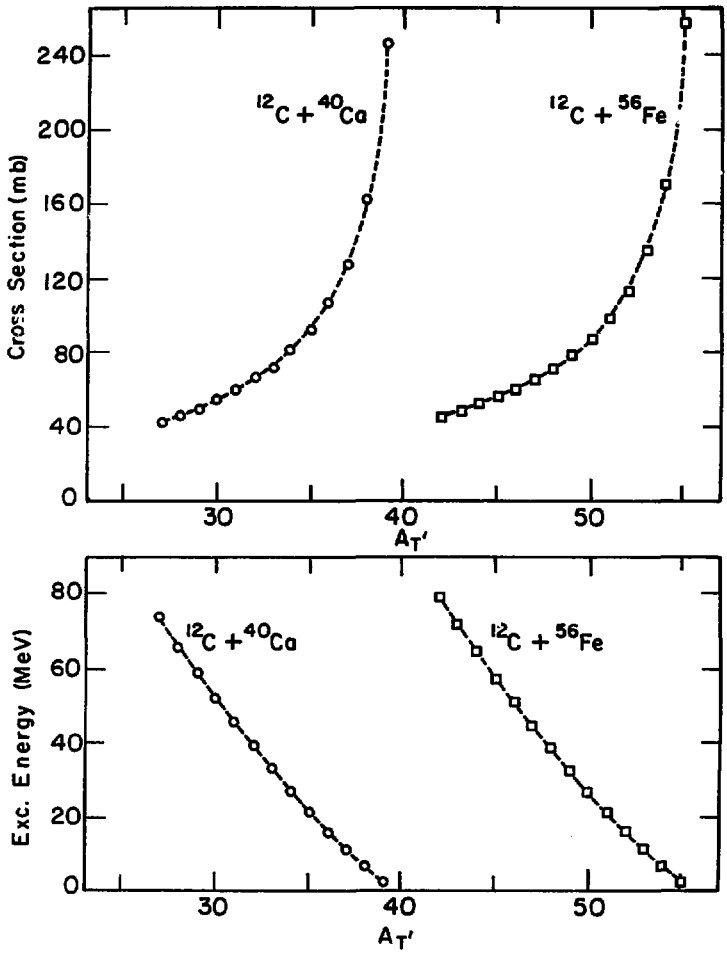

XBL 784-4921

Fig. III.3. Cross section and excitation energy as a function of the primary product mass number ($A_{T'}$). The cross sections were obtained from Eq. (7) and the excitation energies from the surface excess of the deformed abrasion products, Eq. (8).

of a sphere of equal volume. To calculate this excess surface area we have used the approximate analytical expressions given by Swiatecki:[27]

$$\Delta(\text{area}) = 4\pi R_T^2 \left[1 + S(\nu,\beta) - 1 - F(\nu,\beta)^{2/3}\right] , \qquad (9)$$

where

$$S_I = \left[\frac{1}{\nu}(1-\mu^2)^{1/2} - 1\right]\left[1 - (\beta/\nu)^2\right]^{1/2}$$

$$S_{II} = \frac{1}{8}(\mu\nu)^{1/2}\left(\frac{1}{\mu} - 2\right)\left(\frac{1-\beta}{\nu}\right)^2 - \frac{1}{8}\left[\frac{1}{2}\left(\frac{\nu}{\mu}\right)^{1/2}\left(\frac{1}{\mu} - 2\right) - \frac{\left[\frac{1}{\nu}(1-\mu^2)^{1/2} - 1\right]\left[(2-\mu)\mu\right]^{1/2}}{\mu^3}\right]\left(\frac{1-\beta}{\nu}\right)^3 , \qquad (10)$$

$$S_{III} = \frac{1}{8}(\mu\nu)^{1/2}\left(\frac{1}{\mu} - 2\right)\left(\frac{1-\beta}{\nu}\right)^2 - \frac{1}{8}\left[\frac{1}{2}(\mu\nu)^{1/2}\left(\frac{1}{\mu} - 2\right) + 1\right]\left(\frac{1-\beta}{\nu}\right)^3 ,$$

$$S_{IV} = -1 .$$

All variables have the same meaning as in Eq. (6), which also determines the corresponding values of $F(\nu,\beta)$ used in Eq. (9).

In the lower part of Fig. III.3 we have plotted the excitation energy [Eq. (9)] as a function of the mass number of the primary product for the cases of $^{12}C + {}^{40}Ca$ and $^{56}Fe + {}^{12}C$.

Let us stress that although all equations in Sections III.2 and III.3 are written for the target spectrators, they can be equally applied to the projectile spectators by simply exchanging the subindices P and T.

III.4 Tabulation of Primary Product Cross Sections and Excitation Energies Calculated with the Fireball Abrasion Model

In Table III.1 we present the results of the fireball abrasion calculations for the primary products (before evaporation); column 1 gives the mass number of the primary product, and columns 2 and 3 the abrasion cross section (in mb) and excitation energy (in MeV) for the corresponding number of nucleons removed from the target, respectively. In columns 4 to 13 (4 to 8 for ^{16}O fragmentation) we list the results for the abrasion cross section of those isotopes which are obtained with the mass number of column 1, calculated with the charge dispersion expression indicated on top of each section of the table. For each collision system, we present first the results of the hypergeometric charge dispersion, and in the following section those of the Nuc-GDR charge dispersion. The systems included in Table III.1 are (see Table I.1 for experimental references):

$^{16}O + {}^{9}Be$	for	^{16}O fragmentation
$^{40}Ar + {}^{12}C$	for	^{40}Ar fragmentation
$^{12}C + {}^{40}Ca$	for	^{40}Ca fragmentation
$^{48}Ca + {}^{12}C$	for	^{48}Ca fragmentation
$^{56}Fe + {}^{12}C$ $^{56}Fe + {}^{64}Cu$ $^{56}Fe + {}^{108}Ag$ $^{56}Fe + {}^{181}Ta$ $^{56}Fe + {}^{208}Pb$	}	^{56}Fe fragmentation

$$\left.\begin{array}{l} {}^{40}Ar + {}^{63}Cu \\ {}^{40}Ar + {}^{65}Cu \end{array}\right\} \quad {}^{nat}Cu \text{ fragmentation}$$

Let us mention here that in examples where the fragments of a target with natural isotopic abundance are observed, such as is the case for Cu, one must calculate the results of the fragmentation of all significant isotopes separately and sum the results weighted by the corresponding isotopic abundance in order to obtain cross sections which can be compared to the experimental data. On the other hand, if one is using a natural abundance target but is looking at the fragments of the projectile, then it suffices to use an average target mass number in the calculations (^{64}Cu, ^{108}Ag, etc.). This is because, in the latter case, the results of projectile fragmentation are merely dependent on the radius of curvature of the target nucleus.

TABLE III.1 Fireball abrasion.

$^{16}O + {}^{9}Be$ (^{16}O fragmentation)

Primary product distribution — Hyper-geom charge dispersion

A	sigma	Exc.en	Z=	4	5	6	7	8
15	217.40	1.99	--				108.698	108.698
14	139.33	7.07	--			32.510	74.309	32.510
13	106.08	12.49	--		10.608	42.432	42.432	10.608
12	86.09	18.22	--	3.311	21.191	37.083	21.191	3.311
11	71.72	24.30	--	9.195	25.747	25.747	9.195	0.920
10	61.03	30.74	--	14.938	23.900	14.938	3.414	0.213

$^{16}O + {}^{9}Be$ (^{16}O fragmentation)

Primary product distribution — NuclearGDR charge dispersion

15	217.40	1.99	--				106.738	110.656
14	139.33	7.07	--			11.284	115.168	11.874
13	106.08	12.49	--		1.263	51.301	52.176	1.339
12	86.09	18.22	--	0.121	13.486	58.455	13.895	0.129
11	71.72	24.30	--	2.377	33.215	33.638	2.475	
10	61.03	30.74	--	11.438	37.283	11.713	0.305	

TABLE III.1 (CONT.) AR-40 + C-12 (AR-40 FRAGMENTATION)

PRIMARY PRODUCT DISTRIBUTION ..... HYPER-GEOM CHARGE DISPERSION

A	SIGMA	EXC.EN.	Z=	9	10	11	12	13	14	15	16	17	18
39	247.50	1.94	..									111.373	136.122
38	162.73	6.37	..								31.920	82.617	48.193
37	127.46	11.12	..							10.527	43.424	53.641	19.867
36	106.13	16.15	..						3.553	20.847	41.042	32.190	8.495
35	91.94	21.44	..					1.197	9.406	26.338	32.923	18.398	3.680
34	80.94	27.01	..				.391	3.975	14.906	26.500	23.601	9.996	1.573
33	72.36	32.83	..			.124	1.585	7.682	18.290	23.167	15.638	5.213	.662
32	65.83	38.90	..		.037	.599	3.671	11.294	19.159	18.393	9.771	2.628	.274
31	59.48	45.28	..	.011	.209	1.599	6.219	13.634	17.530	13.245	5.676	1.252	.108
30	54.82	51.88	..	.069	.654	3.170	8.783	14.592	14.766	9.000	3.164	.579	.042
29	50.18	58.80	..	.244	1.463	5.053	10.611	13.876	11.328	5.664	1.652	.253	.015
28	46.25	65.99	..	.620	2.650	6.938	11.467	12.097	8.101	3.360	.819	.105	.005
27	42.72	73.48	..	1.263	4.091	8.430	11.240	9.727	5.404	1.873	.383	.041	
26	39.35	81.28	..	2.171	5.535	9.202	10.064	7.226	3.355	.976	.168	.015	
25	36.30	89.39	..	3.274	6.734	9.183	8.333	5.000	1.948	.476	.069	.005	
24	33.53	97.83	..	4.423	7.464	8.444	6.404	3.224	1.056	.217	.026		
23	30.83	106.62	..	5.402	7.563	7.151	4.550	1.925	.529	.091	.009		
22	28.35	115.79	.	6.047	7.075	5.613	3.002	1.066	.245	.035	.003		
21	25.77	125.34	..	6.172	6.060	4.040	1.813	.538	.102	.012			
20	23.51	135.27	..	5.849	4.825	2.699	1.012	.249	.039	.004			
19	21.24	145.65	..	5.086	3.521	1.646	.512	.103	.013				
18	27.16	157.86	..	5.794	3.352	1.300	.332	.054	.005				
17	56.09	165.74	..	9.828	4.717	1.501	.309	.040	.003				
16	5.84	172.44	..	.770	.303	.078	.013						

TABLE III.1 (CONT.) AR-40 + C-12 (AR-40 FRAGMENTATION)

PRIMARY PRODUCT DISTRIBUTION ..... NUCLEARGDR CHARGE DISPERSION

A	SIGMA	EXC.EN.	Z=	9	10	11	12	13	14	15	16	17	18
39	247.50	1.94	..									87.524	159.971
38	162.73	6.37	..								1.091	152.981	8.659
37	127.46	11.12	..							.011	39.121	87.946	.381
36	106.13	16.15	..							2.501	82.073	21.539	.014
35	91.94	21.44	..						.066	23.720	65.462	2.693	
34	80.94	27.01	..						2.393	52.340	26.003	.206	
33	72.36	32.83	..					.104	15.627	50.987	5.630	.011	
32	65.83	38.90	..				.002	1.931	36.157	27.006	.730		
31	59.48	45.28	..				.108	10.686	40.488	8.143	.060		
30	54.82	51.88	..			.003	1.440	25.757	26.113	1.506	.003		
29	50.18	58.80	..			.092	7.425	32.488	10.002	.173			
28	46.25	65.99	..		.003	1.021	18.596	24.243	2.375	.013			
27	42.72	73.48	..		.069	5.137	25.999	11.161	.355				
26	39.35	81.28	..	.002	.693	13.476	21.927	3.213	.034				
25	36.30	89.39	..	.046	3.483	20.541	11.640	.586	.002				
24	33.53	97.83	..	.449	9.692	19.386	3.932	.068					
23	30.83	106.62	..	2.307	16.043	11.609	.839	.005					
22	28.35	115.79	..	6.820	16.685	4.456	.113						
21	25.77	125.34	..	12.176	11.039	1.075	.009						
20	23.51	135.27	..	13.855	4.717	.163							
19	21.24	145.65	..	10.102	1.267	.015							
18	27.16	157.86	..	6.718	.297								
17	56.09	165.74	..										
16	5.84	172.44	..										

TABLE III.1 (CONT.) C-12 + CA-40 (CA-40 FRAGMENTATION)

PRIMARY PRODUCT DISTRIBUTION ..... HYPER-GEOM CHARGE DISPERSION

A	SIGMA	EXC.EN.	Z= 11	12	13	14	15	16	17	18	19	20
39	247.50	1.94	..								123.748	123.748
38	162.73	6.37	..							39.639	83.451	39.639
37	127.46	11.12	..						14.707	49.022	49.022	14.707
36	106.13	16.15	..					5.626	26.477	41.921	26.477	5.626
35	91.94	21.44	..				2.166	13.540	30.265	30.265	13.540	2.166
34	80.94	27.01	..			.817	6.539	19.412	27.406	19.412	6.539	.817
33	72.36	32.83	..		.201	3.009	11.433	21.437	21.437	11.433	3.009	.301
32	65.83	38.90	..	.108	1.327	6.304	15.128	20.093	15.128	6.304	1.327	.108
31	59.48	45.28	.. .037	.548	3.204	9.612	16.341	16.341	9.612	3.204	.548	.037
30	54.82	51.88	.. .217	1.548	5.715	12.145	15.546	12.145	5.715	1.548	.217	.012
29	50.18	58.80	.. .693	3.117	8.152	13.044	13.044	8.152	3.117	.693	.080	.004
28	46.25	65.99	.. 1.585	5.053	9.950	12.437	9.950	5.053	1.585	.291	.028	
27	42.72	73.48	.. 2.889	6.934	10.667	10.667	6.934	2.889	.748	.113	.009	
26	39.35	81.28	.. 4.415	8.278	10.188	8.278	4.415	1.518	.325	.041	.003	
25	36.30	89.39	.. 5.875	8.812	8.812	5.875	2.585	.734	.130	.013		
24	33.53	97.83	.. 6.946	8.465	6.946	3.820	1.389	.326	.047	.004		
23	30.83	106.62	.. 7.352	7.352	4.977	2.262	.679	.131	.015			
22	28.35	115.79	.. 7.054	5.819	3.256	1.221	.301	.047	.004			
21	25.77	125.34	.. 6.092	4.154	1.917	.590	.118	.015				
20	23.51	135.27	.. 4.811	2.706	1.025	.256	.041	.004				
19	21.24	145.65	.. 3.423	1.580	.486	.097	.012					
18	27.16	157.86	.. 3.119	1.170	.288	.045	.004					
17	56.09	165.74	.. 4.115	1.235	.237	.028						
16	5.84	172.44	.. .242	.057	.008							

TABLE III.1 (CONT.) C-12 + CA-40 (CA-40 FRAGMENTATION)

PRIMARY PRODUCT DISTRIBUTION ..... NUCLEARGDR CHARGE DISPERSION

A	SIGMA	EXC.EN.	Z=	11	12	13	14	15	16	17	18	19	20
39	247.50	1.94	..									120.715	126.781
38	162.73	6.37	..								5.143	152.003	5.583
37	127.46	11.12	..							.207	62.777	64.246	.228
36	106.13	16.15	..						.007	10.639	84.353	11.119	.008
35	91.94	21.44	..						.996	44.556	45.332	1.057	
34	80.94	27.01	..					.061	11.543	57.346	11.929	.065	
33	72.36	32.83	..				.003	1.684	34.208	34.699	1.764	.003	
32	65.83	38.90	..				.154	11.118	42.965	11.426	.163		
31	59.48	45.28	..			.009	2.088	27.432	27.774	2.172	.010		
30	54.82	51.88	..			.247	10.192	33.683	10.440	.259			
29	50.18	58.80	..		.019	2.263	22.641	22.895	2.343	.020			
28	46.25	65.99	..		.315	9.120	27.163	9.321	.330				
27	42.72	73.48	..	.028	2.266	18.930	19.127	2.340	.030				
26	39.35	81.28	..	.353	8.054	22.348	8.219	.368					
25	36.30	89.39	..	2.145	15.857	16.013	2.211	.037					
24	33.53	97.83	..	7.028	18.594	7.166	.375	.002					
23	30.83	106.62	..	13.331	13.458	2.011	.040						
22	28.35	115.79	..	15.474	6.144	.355	.003						
21	25.77	125.34	..	11.174	1.751	.039							
20	23.51	135.27	..	5.132	.317	.003							
19	21.24	145.65	..	1.467	.034								
18	27.16	157.86	..	.366	.003								
17	56.09	165.74	..										
16	5.84	172.44	..										

TABLE III.1 (CONT.) CA-48 + C-12 (CA-48 FRAGMENTATION)

PRIMARY PRODUCT DISTRIBUTION ..... HYPER-GEOM CHARGE DISPERSION

A	SIGMA	EXC.EN.	Z=	11	12	13	14	15	16	17	18	19	20
47	253.00	1.96	..									105.416	147.583
46	166.85	6.33	..								28.104	82.832	55.912
45	130.65	11.01	..							8.611	40.186	57.107	24.746
44	109.59	15.97	..						2.729	17.978	40.451	36.902	11.532
43	94.82	21.21	..					.859	7.512	23.862	34.467	22.676	5.442
42	84.34	26.70	..				.266	2.984	12.588	25.669	26.739	13.510	2.589
41	75.35	32.48	..			.079	1.111	5.998	16.244	23.888	19.110	7.711	1.212
40	68.55	38.48	..		.023	.394	2.662	9.227	18.022	20.355	13.004	4.302	.565
39	62.79	44.75	..	.006	.132	1.097	4.754	11.885	17.827	16.079	8.422	2.327	.259
38	57.93	51.29	..	.042	.422	2.249	7.029	13.495	16.166	11.955	5.230	1.223	.116
37	53.09	58.11	..	.149	.970	3.730	8.951	13.725	13.479	8.326	3.084	.617	.050
36	49.53	65.17	..	.391	1.834	5.417	10.382	13.052	10.706	5.598	1.773	.305	.022
35	45.89	72.54	..	.818	2.945	6.947	10.917	11.463	7.960	3.559	.971	.145	.009
34	42.65	80.18	..	1.460	4.197	8.117	10.654	9.470	5.623	2.165	.511	.066	.004
33	39.56	88.10	..	2.290	5.397	8.718	9.687	7.362	3.765	1.255	.257	.029	
32	37.19	96.32	..	3.280	6.458	8.831	8.390	5.491	2.431	.704	.126	.012	
31	34.31	104.89	..	4.219	7.032	8.222	6.727	3.812	1.466	.370	.057	.005	
30	32.07	113.74	..	5.090	7.254	7.304	5.174	2.547	.853	.187	.025		
29	29.72	122.95	..	5.675	6.965	6.072	3.736	1.601	.467	.089	.011		
28	27.58	132.50	..	5.943	6.314	4.782	2.562	.956	.243	.040	.004		
27	25.47	142.43	..	5.832	5.383	3.549	1.656	.538	.119	.017			
26	23.52	152.75	..	5.401	4.340	2.493	1.013	.286	.055	.007			
25	21.46	163.49	..	4.670	3.269	1.635	.577	.141	.023	.002			
24	49.33	180.46	..	9.619	5.862	2.546	.778	.164	.023	.002			
23	58.88	182.12	..	9.718	5.145	1.935	.509	.092	.011				

TABLE III.1 (CONT.) CA-48 + C-12 (CA-48 FRAGMENTATION)

PRIMARY PRODUCT DISTRIBUTION ..... NUCLEARGDR CHARGE DISPERSION

A	SIGMA	EXC.EN.	Z=	11	12	13	14	15	16	17	18	19	20
47	253.00	1.96	..									61.403	191.597
46	166.85	6.33	..								.129	156.563	10.156
45	130.65	11.01	..								22.193	108.113	.345
44	109.59	15.97	..							.366	76.295	32.921	.009
43	94.82	21.21	..							10.412	80.028	4.375	
42	84.34	26.70	..						.295	41.426	42.304	.320	
41	75.35	32.48	..					.002	5.243	58.773	11.320	.015	
40	68.55	38.48	..					.180	23.219	43.492	1.662		
39	62.79	44.75	..				.002	2.688	41.982	17.972	.144		
38	57.93	51.29	..				.098	13.189	40.375	4.259	.008		
37	53.09	58.11	..				1.349	28.694	22.434	.593			
36	49.53	65.17	..			.048	7.344	34.510	7.580	.052			
35	45.89	72.54	..			.661	19.054	24.637	1.537	.003			
34	42.65	80.18	..		.022	3.962	27.609	10.870	.192				
33	39.56	88.10	..		.306	12.012	24.263	2.964	.015				
32	37.19	96.32	..	.009	2.063	21.007	13.602	.509					
31	34.31	104.89	..	.133	7.238	22.152	4.729	.053					
30	32.07	113.74	..	1.004	14.911	15.105	1.047	.004					
29	29.72	122.95	..	4.119	18.851	6.549	.143						
28	27.58	132.50	..	9.952	15.349	1.806	.012						
27	25.47	142.43	..	14.898	8.066	.310							
26	23.52	152.75	..	14.393	2.715	.033							
25	21.46	163.49	..	8.961	.566	.002							
24	49.33	180.46	..	9.064	.181								
23	58.88	182.12	..										

TABLE III.1 (CONT.) FE-56 + C-12 (FE-56 FRAGMENTATION)

PRIMARY PRODUCT DISTRIBUTION ..... HYPER-GEOM CHARGE DISPERSION

A	SIGMA	EXC.EN.	Z=	17	18	19	20	21	22	23	24	25	26
55	257.60	1.98	..									119.599	137.998
54	170.01	6.28	..								35.878	86.108	48.022
53	134.17	10.89	..							12.585	47.193	54.744	19.652
52	112.27	15.80	..						4.570	23.843	43.216	32.268	8.377
51	97.97	20.96	..					1.687	11.503	29.009	33.843	18.275	3.655
50	86.65	26.41	..				.614	5.266	17.355	28.171	23.769	9.888	1.585
49	78.23	32.09	..			.222	2.330	9.653	20.475	24.036	15.624	5.208	.687
48	71.38	38.04	..		.079	.992	5.033	13.420	20.588	18.618	9.697	2.660	.294
47	65.29	44.25	..	.027	.404	2.466	8.055	15.535	18.359	13.304	5.702	1.311	.123
46	60.17	50.70	..	.158	1.148	4.513	10.662	15.841	15.001	8.945	3.214	.629	.051
45	55.92	57.39	..	.510	2.382	6.770	12.321	14.668	11.429	5.715	1.746	.293	.021
44	51.89	64.35	..	1.179	3.978	8.710	12.703	12.444	8.131	3.457	.907	.132	.008
43	48.58	71.57	..	2.201	5.723	10.040	12.048	9.896	5.498	2.008	.456	.058	.003
42	45.41	79.08	..	3.483	7.257	10.477	10.542	7.363	3.514	1.111	.220	.024	
41	42.38	86.85	..	4.838	8.294	10.040	8.590	5.154	2.130	.586	.101	.010	
40	39.93	94.91	..	6.099	8.767	9.023	6.632	3.445	1.240	.299	.045	.004	
39	37.13	103.26	..	6.928	8.468	7.487	4.765	2.155	.678	.143	.019		
38	35.05	111.88	..	7.379	7.748	5.931	3.287	1.300	.359	.067	.008		
37	32.91	120.85	..	7.254	6.594	4.396	2.131	.739	.179	.029	.003		
36	30.64	130.13	..	6.658	5.271	3.073	1.306	.398	.085	.012			
35	28.70	139.73	..	5.760	3.988	2.039	.761	.204	.038	.005			
34	26.79	149.58	..	4.680	2.841	1.276	.419	.099	.016				
33	24.92	159.99	..	3.575	1.907	.753	.217	.045	.006				
32	23.21	170.67	..	2.583	1.211	.420	.106	.019	.002				
31	43.11	185.55	..	3.514	1.447	.440	.097	.015					

TABLE III.1 (CONT.) FE-56 + C-12 (FE-56 FRAGMENTATION)

PRIMARY PRODUCT DISTRIBUTION ..... NUCLEARGDR CHARGE DISPERSION

A	SIGMA	EXC.EN.	Z= 17	18	19	20	21	22	23	24	25	26
55	257.60	1.98	..								97.861	159.736
54	170.01	6.28	..							.840	164.239	4.929
53	134.17	10.89	..						.005	46.310	87.751	.108
52	112.27	15.80	..						2.646	93.875	15.750	
51	97.97	20.96	..					.055	29.982	66.734	1.202	
50	86.65	26.41	..					2.956	63.039	20.603	.051	
49	78.23	32.09	..				.114	21.217	53.882	3.020		
48	71.38	38.04	..			.002	2.709	45.878	22.554	.237		
47	65.29	44.25	..			.147	15.668	44.603	4.857	.011		
46	60.17	50.70	..		.004	2.283	34.518	22.788	.577			
45	55.92	57.39	..		.152	11.840	37.460	6.425	.040			
44	51.89	64.35	..	.005	1.855	26.729	22.269	1.027				
43	48.58	71.57	..	.140	9.037	31.663	7.641	.098				
42	45.41	79.08	.. .005	1.470	21.065	21.336	1.531	.006				
41	42.38	86.85	.. .118	6.888	26.720	6.475	.183					
40	39.93	94.91	.. 1.135	16.680	20.063	2.034	.013					
39	37.13	103.26	.. 5.230	22.527	8.984	.291						
38	35.05	111.88	.. 13.158	18.521	2.488	.026						
37	32.81	120.85	.. 19.074	9.283	.417							
36	30.64	130.13	.. 16.818	2.864	.043							
35	28.70	139.73	.. 9.258	.544	.003							
34	26.79	149.68	.. 3.162	.063								
33	24.92	159.99	.. .662	.004								
32	23.21	170.67	.. .084									
31	43.11	185.55	.. .013									

TABLE III.1 (CONT.) FE-56 + CU-64 (FE-56 FRAGMENTATION)

PRIMARY PRODUCT DISTRIBUTION ..... HYPER-GEOM CHARGE DISPERSION

A	SIGMA	EXC.EN.		Z= 17	18	19	20	21	22	23	24	25	26
55	315.11	.76	..									146.302	168.810
54	212.35	3.10	..								44.815	107.556	59.983
53	169.92	5.35	..							15.938	59.768	69.330	24.888
52	144.42	7.50	..						5.878	30.670	55.589	41.506	10.776
51	127.53	9.56	..					2.196	14.973	37.759	44.052	23.788	4.758
50	114.76	11.54	..				.814	6.975	22.986	37.311	31.481	13.096	2.099
49	104.73	13.43	..			.297	3.119	12.921	27.409	32.175	20.914	6.971	.919
48	97.16	15.24	..		.107	1.350	6.850	18.268	28.024	25.344	13.200	3.621	.400
47	90.44	16.99	..	.037	.560	3.416	11.159	21.521	25.434	18.431	7.899	1.817	.171
46	84.51	18.66	..	.222	1.613	6.338	14.974	22.247	21.068	12.562	4.514	.883	.071
45	79.73	20.25	..	.728	3.396	9.653	17.569	20.915	16.297	8.149	2.490	.418	.029
44	75.60	21.77	..	1.717	5.796	12.691	18.507	18.130	11.846	5.036	1.322	.192	.012
43	71.62	23.22	..	3.245	8.437	14.801	17.762	14.590	8.106	2.960	.673	.085	.005
42	68.21	24.59	..	5.233	10.991	15.737	15.835	11.060	5.278	1.669	.330	.037	
41	65.34	25.88	..	7.458	12.785	15.476	13.241	7.945	3.283	.904	.156	.015	
40	62.55	27.11	..	9.553	13.732	14.133	10.388	5.396	1.942	.468	.071	.006	
39	59.85	28.27	..	11.168	13.650	12.070	7.681	3.475	1.093	.231	.031	.002	
38	57.23	29.35	..	12.050	12.653	9.686	5.368	2.123	.586	.109	.013		
37	55.44	30.33	..	12.255	11.141	7.427	3.599	1.249	.303	.049	.005		
36	52.96	31.27	..	11.505	9.109	5.310	2.257	.688	.147	.021			
35	51.25	32.10	..	10.285	7.120	3.640	1.359	.364	.068	.009			
34	49.58	32.85	..	8.658	5.257	2.361	.775	.182	.030	.003			
33	47.60	33.54	..	6.828	3.642	1.438	.414	.086	.012				
32	45.99	34.13	..	5.119	2.399	.832	.210	.038	.005				
31	44.42	34.64	..	3.620	1.491	.453	.100	.016					

TABLE III.1 (CONT.) FE-56 + CU-64 (FE-56 FRAGMENTATION)

PRIMARY PRODUCT DISTRIBUTION ..... NUCLEARGDR CHARGE DISPERSION

A	SIGMA	EXC.EN.	Z=	17	18	19	20	21	22	23	24	25	26
55	315.11	.76	..									122.588	192.523
54	212.35	3.10	..								1.883	201.824	8.647
53	169.92	5.35	..							.025	60.730	108.842	.327
52	144.42	7.50	..							5.020	116.012	23.376	.011
51	127.53	9.56	..						.188	40.917	83.856	2.566	
50	114.76	11.54	..					.004	5.556	79.533	29.490	.179	
49	104.73	13.43	..					.359	30.154	68.535	5.670	.009	
48	97.16	15.24	..				.013	5.216	59.373	31.887	.674		
47	90.44	16.99	..				.460	23.376	57.933	8.623	.054		
46	84.51	18.66	..			.023	4.594	46.175	32.254	1.457	.003		
45	79.73	20.25	..			.490	18.495	49.547	11.037	.164			
44	75.60	21.77	.		.030	3.961	37.272	31.894	2.426	.013			
43	71.62	23.22	..		.476	14.895	42.948	12.943	.355				
42	68.21	24.59	..	.034	3.341	30.509	30.840	3.455	.036				
41	65.34	25.88	..	.437	12.157	37.676	14.436	.625	.003				
40	62.55	27.11	..	2.799	25.449	29.682	4.504	.078					
39	59.85	28.27	..	9.933	33.088	15.478	.957	.007					
38	57.23	29.35	..	21.205	28.096	5.462	.141						
37	55.44	30.33	..	29.311	16.272	1.342	.015						
36	52.96	31.27	..	26.601	6.370	.226							
35	51 25	32.10	..	16.694	1.750	.027							
34	49.58	32.85	..	7.245	.335	.002							
33	47.60	33.54	..	2.175	.045								
32	45.99	34.13	..	.459	.004								
	44.42	34.64	..	.068									

TABLE III.1 (CONT.) FE-56 + AG-108 (FE-56 FRAGMENTATION)

PRIMARY PRODUCT DISTRIBUTION ..... HYPER-GEOM CHARGE DISPERSION

A	SIGMA	EXC.EN.	Z=	17	18	19	20	21	22	23	24	25	26
55	342.62	.65	..									159.076	183.549
54	232.20	2.87	..								49.004	117.609	65.590
53	186.53	5.02	..							17.495	65.607	76.104	27.320
52	159.34	7.09	..						6.486	33.839	61.333	45.795	11.889
51	141.57	9.07	..					2.438	16.622	41.917	48.903	26.408	5.282
50	127.70	10.98	..				.905	7.761	25.577	41.516	35.029	14.572	2.335
49	117.37	12.82	..			.333	3.496	14.482	30.719	36.061	23.440	7.813	1.030
48	108.66	14.59	..		.120	1.509	7.661	20.428	31.339	28.341	14.761	4.049	.448
47	101.42	16.29	..	.042	.627	3.930	12.513	24.132	28.520	20.666	8.857	2.037	.192
46	96.07	17.91	..	.253	1.834	7.206	17.023	25.292	23.950	14.281	5.132	1.004	.081
45	90.41	19.49	..	.825	3.851	10.946	19.922	23.716	18.480	9.240	2.823	.474	.033
44	85.99	20.98	..	1.954	6.594	14.437	21.053	20.624	13.476	5.729	1.504	.219	.013
43	82.23	22.41	..	3.726	9.687	16.994	20.393	16.751	9.306	3.399	.772	.098	.005
42	78.10	23.80	..	5.991	12.481	18.018	18.131	12.663	6.044	1.911	.378	.042	
41	75.55	25.08	..	8.624	14.783	17.896	15.311	9.186	3.796	1.045	.181	.018	
40	72.13	26.33	..	11.016	15.835	16.298	11.979	6.223	2.239	.539	.082	.007	
39	69.73	27.49	..	13.012	15.904	14.062	8.949	4.048	1.274	.269	.036	.003	
38	66.94	28.60	..	14.094	14.799	11.329	6.278	2.484	.685	.127	.015		
37	65.11	29.62	..	14.394	13.086	8.724	4.228	1.467	.356	.058	.006		
36	62.88	30.59	..	13.662	10.816	6.306	2.680	.817	.174	.025	.002		
35	60.71	31.48	..	12.183	8.434	4.312	1.610	.431	.081	.010			
34	58.59	32.31	..	10.233	6.213	2.790	.916	.215	.035	.004			
33	57.32	33.03	..	8.224	4.386	1.731	.499	.103	.015				
32	55.67	33.69	..	6.195	2.904	1.007	.255	.046	.006				
31	53.65	34.29	..	4.373	1.801	.548	.121	.019	.002				

TABLE III.1 (CONT.) FE-56 + AG-108 (FE-56 FRAGMENTATION)

PRIMARY PRODUCT DISTRIBUTION ..... NUCLEARGOR CHARGE DISPERSION

A	SIGMA	EXC.EN.	Z=	17	18	19	20	21	22	23	24	25	26
55	342.62	.65	..									134.029	208.596
54	232.20	2.87	..								2.328	219.715	10.160
53	186.53	5.02	..							.036	67.136	118.928	.427
52	159.34	7.09	..							5.961	126.862	26.503	.016
51	141.57	9.07	..						.248	45.807	92.400	3.113	
50	127.70	10.98	..					.006	6.571	87.625	33.258	.236	
49	117.37	12.82	..					.463	34.124	76.049	6.724	.013	
48	108.66	14.59	..				.019	6.170	65.760	35.858	.848		
47	101.42	16.29	..				.584	26.500	64.215	10.044	.073		
46	96.07	17.91	..			.032	5.504	52.050	36.675	1.804	.005		
45	90.41	19.49	..			.624	21.233	55.494	12.846	.216			
44	85.99	20.98	..		.042	4.744	42.090	36.155	2.945	.018			
43	82.23	22.41	..		.609	17.339	48.700	15.121	.458				
42	78.10	23.80	..	.046	4.025	34.728	35.095	4.159	.049				
41	75.55	25.08	..	.560	14.273	43.039	16.877	.792	.004				
40	72.13	26.33	..	3.395	29.222	33.960	5.397	.104					
39	69.73	27.49	..	11.767	38.112	18.143	1.201	.010					
38	66.94	28.60	..	24.738	32.571	6.578	.185						
37	65.11	29.62	..	34.065	19.159	1.674	.020						
36	62.88	30.59	..	31.292	7.732	.297							
35	60.71	31.48	..	19.769	2.177	.037							
34	58.59	32.31	..	8.702	.430	.003							
33	57.32	33.03	..	2.723	.061								
32	55.67	33.69	..	.595	.006								
31	53.65	34.29	..	.090									

TABLE III.1 (CONT.) FE-56 + TA-181 (FE-56 FRAGMENTATION)

PRIMARY PRODUCT DISTRIBUTION ..... HYPER-GEOM CHARGE DISPERSION

A	SIGMA	EXC.EN.		Z= 17	18	19	20	21	22	23	24	25	26
55	375.14	.55	..									174.172	200.967
54	255.76	2.68	..								53.975	129.540	72.244
53	206.26	4.74	..							19.346	72.547	84.154	30.209
52	177.10	6.74	..						7.209	37.610	68.169	50.899	13.214
51	157.64	8.65	..					2.715	18.509	46.676	54.455	29.406	5.881
50	143.11	10.51	..				1.015	8.698	28.665	46.529	39.259	16.332	2.617
49	131.20	12.31	..			.372	3.907	16.188	34.338	40.310	26.202	8.734	1.152
48	122.34	14.03	..		.135	1.700	8.625	23.001	35.285	31.910	16.620	4.559	.504
47	115.07	15.69	..	.047	.712	4.346	14.198	27.381	32.359	23.449	10.050	2.311	.217
46	108.08	17.30	..	.285	2.063	8.107	19.152	28.454	26.945	16.067	5.774	1.129	.091
45	103.14	18.83	..	.941	4.394	12.487	22.726	27.055	21.082	10.541	3.221	.541	.038
44	98.37	20.32	..	2.235	7.542	16.513	24.082	23.591	15.414	6.553	1.720	.250	.015
43	93.75	21.75	..	4.247	11.043	19.374	23.249	19.098	10.610	3.875	.881	.112	.006
42	89.84	23.12	..	6.892	14.358	20.727	20.856	14.566	6.952	2.198	.435	.048	.002
41	86.61	24.42	..	9.887	16.949	20.517	17.553	10.532	4.352	1.198	.207	.020	
40	84.02	25.65	..	12.831	18.445	18.985	13.954	7.249	2.608	.628	.095	.008	
39	80.41	26.86	..	15.005	18.339	16.216	10.319	4.668	1.469	.310	.041	.003	
38	78.48	27.96	..	16.524	17.350	13.283	7.361	2.912	.804	.149	.017		
37	75.56	29.04	..	16.704	15.185	10.123	4.906	1.702	.413	.067	.007		
36	73.73	30.02	..	16.019	12.682	7.393	3.142	.958	.204	.029	.003		
35	71.93	30.95	..	14.434	9.993	5.109	1.907	.511	.096	.012			
34	69.66	31.82	..	12.167	7.387	3.318	1.089	.256	.042	.005			
33	67.93	32.61	..	9.746	5.198	2.052	.591	.122	.018				
32	66.23	33.34	..	7.371	3.455	1.198	.303	.055	.007				
31	64.55	33.99	..	5.262	2.167	.659	.146	.023	.002				

TABLE III.1 (CONT.) FE-56 + TA-181 (FE-56 FRAGMENTATION)

PRIMARY PRODUCT DISTRIBUTION ..... NUCLEARGDR CHARGE DISPERSION

A	SIGMA	EXC.EN.	Z=	17	18	19	20	21	22	23	24	25	26
55	375.14	.55	..									147.420	227.719
54	255.76	2.68	..								2.844	241.025	11.889
53	206.26	4.74	..							.049	74.692	130.968	.547
52	177.10	6.74	..							7.063	139.845	30.168	.023
51	157.64	8.65	..						.322	51.388	102.180	3.752	
50	143.11	10.51	..					.009	7.773	97.310	37.715	.307	
49	131.20	12.31	..					.588	38.472	84.218	7.907	.018	
48	122.34	14.03	..				.026	7.299	73.389	40.564	1.060		
47	115.07	15.69	..				.741	30.357	72.084	11.790	.098		
46	108.08	17.30	..			.044	6.497	58.082	41.259	2.194	.907		
45	103.14	18.83	..			.788	24.486	62.588	14.996	.281			
44	98.37	20.32	..		.057	5.686	47.811	41.213	3.574	.025			
43	93.75	21.75	..	.003	.766	20.013	54.871	17.512	.580				
42	89.84	23.12	..	.063	4.849	39.724	40.134	5.006	.066				
41	86.61	24.42	..	.705	16.592	48.777	19.541	.989	.006				
40	84.02	25.65	..	4.142	33.898	39.262	6.511	.138					
39	80.41	26.86	..	13.780	43.465	21.037	1.485	.014					
38	78.48	27.96	..	28.927	37.860	7.923	.243						
37	75.56	29.04	..	39.127	22.278	2.057	.028						
36	73.73	30.02	..	36.355	9.253	.382	.002						
35	71.93	30.95	..	23.409	2.701	.050							
34	69.66	31.82	..	10.505	.554	.005							
33	67.93	32.61	..	3.351	.081								
32	66.23	33.34	..	.756	.008								
31	64.55	33.99	..	.120									

TABLE III.1 (CONT.) FE-56 + PB-208 (FE-56 FRAGMENTATION)

PRIMARY PRODUCT DISTRIBUTION ..... HYPER-GEOM CHARGE DISPERSION

A	SIGMA	EXC.EN.	Z=	17	18	19	20	21	22	23	24	25	26
55	385.13	.52	..									178.811	206.321
54	263.20	2.63	..								55.546	133.311	74.346
53	211.62	4.69	..							19.849	74.434	86.343	30.995
52	182.42	6.65	..						7.425	38.740	70.216	52.428	12.611
51	162.45	8.56	..					2.798	19.074	48.100	56.116	30.303	6.061
50	147.55	10.40	..				1.046	8.968	29.554	47.971	40.476	16.838	2.698
49	135.34	12.18	..			.384	4.031	16.698	35.420	41.580	27.027	9.009	1.188
48	126.91	13.88	..		.140	1.763	8.948	23.860	36.604	33.103	17.241	4.729	.523
47	118.17	15.55	..	.049	.731	4.463	14.580	28.119	33.232	24.081	10.320	2.374	.223
46	112.30	17.14	..	.296	2.143	8.423	19.899	29.564	27.996	16.693	5.999	1.173	.095
45	106.62	18.68	..	.973	4.542	12.908	23.493	27.968	21.793	10.896	3.329	.559	.039
44	101.75	20.16	..	2.312	7.801	17.081	24.910	24.401	15.944	6.778	1.779	.259	.016
43	97.62	21.58	..	4.423	11.500	20.176	24.211	19.888	11.049	4.035	.917	.116	.006
42	93.63	22.95	..	7.182	14.962	21.599	21.734	15.180	7.245	2.291	.453	.050	.002
41	89.75	24.26	..	10.244	17.562	21.259	18.188	10.913	4.509	1.242	.215	.021	
40	87.12	25.50	..	13.306	19.127	19.686	14.469	7.516	2.705	.651	.099	.008	
39	83.99	26.69	..	15.674	19.157	16.939	10.779	4.876	1.535	.324	.043	.003	
38	81.50	27.82	..	17.158	18.016	13.792	7.643	3.024	.834	.155	.018		
37	79.06	28.88	..	17.477	15.888	10.592	5.133	1.781	.432	.070	.007		
36	77.20	29.88	..	16.774	13.279	7.742	3.290	1.003	.214	.031	.003		
35	74.86	30.83	..	15.021	10.399	5.317	1.985	.532	.100	.012			
34	72.56	31.71	..	12.673	7.694	3.456	1.134	.267	.044	.005			
33	71.33	32.50	..	10.233	5.458	2.154	.621	.128	.018				
32	69.11	33.26	..	7.691	3.605	1.250	.316	.057	.007				
31	67.91	33.91	..	5.535	2.279	.693	.153	.024	.003				

TABLE III.1 (CONT.) FE-56 + PB-208 (FE-56 FRAGMENTATION)

PRIMARY PRODUCT DISTRIBUTION ..... NUCLEARGDR CHARGE DISPERSION

A	SIGMA	EXC.EN.	Z= 17	18	19	20	21	22	23	24	25	26
55	385.13	.52	..								151.524	233.608
54	263.20	2.63	..							3.008	247.763	12.432
53	211.62	4.69	..						.054	76.765	134.218	.585
52	182.42	6.65	..						7.394	143.737	31.262	.025
51	162.45	8.56	..					.345	53.054	105.107	3.944	
50	147.55	10.40	..				.010	8.124	100.088	39.000	.329	
49	135.34	12.18	..				.626	39.767	86.663	8.259	.020	
48	126.91	13.88	..			.029	7.666	75.958	42.129	1.128		
47	118.17	15.55	..			.783	31.253	73.815	12.216	.105		
46	112.30	17.14	..		.048	6.828	60.225	42.865	2.323	.007		
45	106.62	18.68	..		.837	25.381	64.506	15.595	.300			
44	101.75	20.16	..	.062	5.950	49.365	42.590	3.751	.028			
43	97.62	21.58	..	.003	.817	20.904	56.972	18.306	.620			
42	93.63	22.95	..	.068	5.113	41.335	41.760	5.277	.072			
41	89.75	24.26	..	.749	17.253	50.386	20.299	1.048	.006			
40	87.12	25.50	..	4.346	35.111	40.632	6.813	.148				
39	83.99	26.69	..	14.450	45.274	22.004	1.579	.015				
38	81.50	27.82	..	30.016	39.224	8.284	.260					
37	79.06	28.88	..	40.830	23.321	2.184	.030					
36	77.20	29.88	..	37.975	9.741	.410	.003					
35	74.86	30.83	..	24.358	2.846	.054						
34	72.56	31.71	..	10.986	589	.005						
33	71.33	32.50	..	3.554	.088							
32	69.11	33.26	..	.803	.009							
31	67.91	33.91	..	.130								

TABLE III.1 (CONT.) AR-40 + CU-63 (CU-63 FRAGMENTATION)

PRIMARY PRODUCT DISTRIBUTION ..... HYPER-GEOM CHARGE DISPERSION

A	SIGMA	EXC.EN.	Z=	20	21	22	23	24	25	26	27	28	29
62	296.17	1.12	..									136.334	159.840
61	198.98	4.01	..								41.366	100.460	57.158
60	157.80	6.97	..							14.520	54.851	64.646	23.778
59	133.71	9.96	..						5.332	27.888	51.128	38.955	10.410
58	117.76	12.98	..					1.990	13.529	34.343	40.702	22.532	4.662
57	105.70	16.04	..				.739	6.281	20.729	34.016	29.292	12.554	2.092
56	96.23	19.14	..			.271	2.809	11.587	24.719	29.473	19.649	6.783	.936
55	88.63	22.28	..		.098	1.214	6.099	16.263	25.207	23.268	12.496	3.570	.416
54	81.88	25.45	..	.035	.505	3.029	9.833	19.052	22.863	17.001	7.556	1.821	.181
53	76.74	28.65	..	.204	1.446	5.608	13.227	19.840	19.179	11.802	4.426	.913	.079
52	72.24	31.88	..	.659	3.013	8.492	15.507	18.737	14.990	7.783	2.498	.446	.034
51	67.95	35.17	..	1.526	5.069	11.059	16.267	16.267	10.981	4.880	1.356	.211	.014
50	64.23	38.48	..	2.850	7.328	12.879	15.679	13.229	7.644	2.940	.713	.098	.006
49	61.05	41.83	..	4.550	9.425	13.710	14.082	10.170	5.085	1.707	.364	.044	.002
48	57.98	45.22	..	6.394	10.962	13.453	11.828	7.393	3.226	.951	.179	.019	
47	55.39	48.65	..	8.145	11.782	12.377	9.417	5.137	1.969	.513	.085	.008	
46	52.89	52.12	..	9.494	11.755	10.686	7.096	3.400	1.151	.266	.039	.003	
45	50.81	55.64	..	10.311	11.048	8.765	5.113	2.163	.649	.133	.018		
44	48.13	59.21	..	10.309	9.639	6.718	3.460	1.298	.346	.063	.007		
43	46.52	62.78	..	9.882	8.117	4.995	2.280	.760	.181	.029	.003		
42	44.62	66.43	..	8.873	6.435	3.510	1.424	.423	.090	.013			
41	42.78	70.13	..	7.541	4.848	2.350	.849	.225	.042	.006			
40	40.99	73.86	..	6.080	3.474	1.500	.483	.114	.019	.002			
39	39.83	77.63	..	4.726	2.405	.926	.266	.056	.008				
38	37.83	81.49	..	3.416	1.550	.532	.136	.026	.003				

TABLE III.1 (CONT.) AR-40 + CU-63 (CU-63 FRAGMENTATION)

PRIMARY PRODUCT DISTRIBUTION ..... NUCLEARGOR CHARGE DISPERSION

A	SIGMA	EXC.EN.	Z=	20	21	22	23	24	25	26	27	28	29
62	296.17	1.12	..									109.562	186.611
61	198.98	4.01	..								1.003	191.290	6.690
60	157.80	6.97	..							.007	52.578	105.025	.185
59	133.71	9.96	..							3.182	109.433	21.093	.004
58	117.76	12.98	..						.077	34.476	81.241	1.963	
57	105.70	16.04	..						3.633	74.098	27.860	.110	
56	96.23	19.14	..					.165	24.796	66.372	4.890	.004	
55	88.63	22.28	..				.004	3.407	54.083	30.635	.502		
54	81.88	25.45	..				.220	18.579	55.203	7.841	.033		
53	76.74	28.65	..			.008	2.975	41.228	31.309	1.215			
52	72.24	31.88	..			.241	14.428	46.978	10.474	.121			
51	67.95	35.17	..		.011	2.520	32.370	30.872	2.167	.008			
50	64.23	38.48	..		.236	11.279	39.923	12.500	.293				
49	61.05	41.83	..	.013	2.093	25.893	29.774	3.246	.027				
48	57.98	45.22	..	.216	8.930	34.229	14.048	.556					
47	55.39	48.65	..	1.715	20.957	28.284	4.358	.065					
46	52.89	52.12	..	7.122	29.503	15.164	.906	.005					
45	50.81	55.64	..	17.150	26.670	5.456	.130						
44	48.13	59.21	..	25.248	15.748	1.317	.013						
43	46.52	62.78	..	24.749	6.433	.224							
42	44.62	66.43	..	16.218	1.796	.027							
41	42.78	70.13	..	7.297	.349	.002							
40	40.99	73.86	..	2.283	.048								
39	39.83	77.63	..	.508	.005								
38	37.83	81.49	..	.078									

TABLE III.1 (CONT.) AR-40 + CU-65 (CU-65 FRAGMENTATION)

PRIMARY PRODUCT DISTRIBUTION ..... HYPER-GEOM CHARGE DISPERSION

A	SIGMA	EXC.EN.		Z= 20	21	22	23	24	25	26	27	28	29
64	296.97	1.13	..									132.494	164.475
63	198.77	4.02	..								38.798	99.767	60.204
62	158.49	6.97	..							13.258	53.032	66.290	25.907
61	134.29	9.96	..						4.711	26.091	50.733	41.070	11.684
60	117.78	13.00	..					1.693	12.192	32.824	41.334	24.358	5.376
59	106.18	16.06	..				.611	5.496	19.235	33.537	30.742	14.054	2.504
58	96.21	19.18	..			.216	2.363	10.339	23.435	29.744	21.151	7.806	1.154
57	89.06	22.32	..		.076	.991	5.281	14.962	24.687	24.307	13.954	4.272	.534
56	82.29	25.52	..	.026	.398	2.531	8.730	18.007	23.048	18.321	8.724	2.259	.242
55	77.14	28.73	..	.155	1.165	4.802	12.057	19.291	19.934	13.143	5.294	1.176	.110
54	72.22	32.00	..	.509	2.473	7.419	14.450	18.665	15.998	8.922	3.084	.595	.048
53	68.35	35.29	..	1.213	4.290	9.984	15.700	16.821	12.195	5.837	1.751	.296	.021
52	64.62	38.64	..	2.322	6.368	11.964	15.605	14.142	8.800	3.655	.960	.143	.009
51	61.06	42.02	..	3.780	8.369	13.043	14.389	11.192	6.044	2.198	.509	.067	.004
50	58.39	45.42	..	5.492	10.088	13.297	12.591	8.499	4.018	1.288	.264	.031	
49	55.80	48.89	..	7.199	11.184	12.652	10.397	6.144	2.560	.727	.133	.014	
48	52.95	52.40	..	8.590	11.454	11.246	8.090	4.213	1.556	.393	.064	.006	
47	50.90	55.93	..	9.634	11.148	9.582	6.075	2.804	.921	.208	.030	.003	
46	48.90	59.52	..	10.103	10.234	7.753	4.356	1.789	.525	.106	.014		
45	46.63	63.17	..	9.900	8.840	5.934	2.967	1.088	.286	.052	.006		
44	44.76	66.85	..	9.239	7.310	4.367	1.949	.640	.151	.024	.003		
43	43.25	70.56	..	8.241	5.802	3.095	1.236	.364	.077	.011			
42	41.47	74.35	..	6.943	4.364	2 083	.746	.197	.037	.005			
41	39.73	78.18	..	5.575	3.136	1.342	.431	.102	.017	.002			
40	38.62	82.04	..	4.337	2.187	.839	.242	.051	.008				

TABLE III.1 (CONT.) AR-40 + CU-65 (CU-65 FRAGMENTATION)

PRIMARY PRODUCT DISTRIBUTION ..... NUCLEARGDR CHARGE DISPERSION

A	SIGMA	EXC.EN.	Z=	20	21	22	23	24	25	26	27	28	29
64	296.97	1.13	..									96.253	200.716
63	198.77	4.02	..								.488	190.793	7.489
62	158.49	6.97	..								43.273	115.012	.200
61	134.29	9.96	..							1.677	106.812	25.795	.005
60	117.78	13.00	..						.023	26.193	89.010	2.551	
59	106.18	16.06	..						1.834	69.262	34.934	.148	
58	96.21	19.18	..					.049	17.460	71.878	6.815	.006	
57	89.06	22.32	..					1.606	48.019	38.674	.763		
56	82.29	25.52	..				.063	12.174	58.637	11.359	.054		
55	77.14	28.73	..				1.296	34.552	39.303	1.982	.003		
54	72.22	32.00	..			.064	8.682	47.934	15.326	.217			
53	68.35	35.29	..			1.005	25.476	38.159	3.688	.016			
52	64.62	38.64	..		.057	6.281	39.268	18.451	.567				
51	61.06	42.02	..		.756	18.917	35.693	5.631	.058				
50	58.39	45.42	..	.047	4.556	32.042	20.601	1.134	.004				
49	55.80	48.89	..	.563	14.319	33.054	7.709	.154					
48	52.95	52.40	..	3.291	25.935	21.765	1.905	.014					
47	50.90	55.93	..	10.759	29.781	9.621	.324						
46	48.90	59.52	..	21.147	22.418	2.873	.038						
45	46.63	63.17	..	26.397	11.288	.585	.003						
44	44.76	66.85	..	22.117	3.921	.084							
43	43.25	70.56	..	12.749	.951	.008							
42	41.47	74.35	..	5.056	.161								
41	39.73	78.18	..	1.402	.019								
40	38.62	82.04	..	.278									

III.5 Discussion and Comparisons

The abrasion cross sections calculated here are based on geometrical considerations alone, and therefore, assumed to be completely independent of the projectile bombarding energy. This may not constitute a major problem because it is well known that many aspects of high energy physics are indeed energy-independent over a very wide range of energies. One such example was presented by Cleghorn, Freier and Waddington.[53] In their studies of the mean-free path data for heavy cosmic-ray nuclei in emulsion, they concluded that the reaction cross sections of nuclei are essentially independent of energy from 0.1 to 30 GeV. They also concluded that the average number of i-type nuclei produced in the fragmentation of a j-type projectile is consistent with energy independence over the same energy range.

Since the introduction of high-energy heavy-ion accelerators, experiments have been performed[4,15] which have proven to be consistent with the hypothesis of "limiting fragmentation" for heavy ions from 0.8 to 2.1 GeV/A. According to this hypothesis, first formulated in the study of high energy particle processes,[54,55] a distribution of products with finite energies in the rest frame of projectile or target approaches a limiting form as the bombardment energy increases. Of particular significance to our work is the fragmentation experiment of Lindstrom et al.[29] In this study cross sections for production of several isotopes in the fragmentation of ^{12}C at 1.05 GeV/A and at 2.1 GeV/A incident on several different targets were measured. Their results showed that for all fragments $\sigma^F(2.1)/\sigma^F(1.05) = 1.01 \pm 0.01$, which indicates that the element and isotope production cross sections

studied in this work, can be treated as essentially independent of bombarding energies, at least within the 1.0 to 2.1 GeV/A range (limiting fragmentation). Whether or not the energy independence of the isotope production cross sections can be extended down to projectile energies of the order of 0.2 GeV/A is a point which remains to be established experimentally. In particular, we should mention the in-beam γ-ray experiment of Shibata et al.[30] They have studied the fragmentation of a ^{40}Ca target bombarded with 0.25 and 0.40 GeV/A ^{12}C beams from the Berkeley Bevalac. Their data, which motivated our original calculations,[19] are different for the two beam energies, and the results of our calculations fit the 0.40 GeV/A data better than the data at the lower energy. On the other hand, these calculations fit the more recent ^{40}Ar fragmentation cross sections of Viyogi et al[31] at 0.213 GeV/A very well (see Section IV.6). Unfortunately, because there are no systematic experimental studies of isotope production cross sections which span the entire 0.2 to 2.0 GeV/A range, the dependence on beam energy over this range remains to be settled. The fact that the simple fireball abrasion model is capable of reproducing many experimental results over this range would indicate that isotope production is fairly independent of bombarding energy from 0.2 to 2.0 GeV/A.

Let us now compare the fireball abrasion cross sections with those predicted by the multiple scattering abrasion (MSA) of Hüfner et al.[22] As introduced in Section II.2 (see derivation in Appendix A), the MSA cross section for the abrasion of a_P nucleons from a projectile (Z_P,A_P) which collides with a target (Z_T,A_T) is given by

$$\sigma_{a_p} = \int_0^\infty 2\pi b \, db \binom{A_p}{a_p} P(b)^{A_p} \, (1 - P(b))^{A_p - a_p} \tag{11}$$

where

$$P(b) = \int d^2s \, dz \, \rho_p(\vec{b} + \vec{s}, z) \left\{ 1 - \exp\left(-A_T \, \sigma_{NN}^{tot} \int_{-\infty}^{\infty} dz' \rho_T(\vec{s}, z') \right) \right\} \tag{12}$$

See the text following Eq. (II-3) for the definitions of the variables and the geometrical coordinates in Eq. (12).

In the derivation of Eq. (12), all nucleon-nucleon correlations were neglected, then the MSA cross section for removal of z protons and n neutrons ($n+z = a_p$) is obtained by multiplying Eq. (11) by the hypergeometric charge dispersion (see Section II.3), i.e.,

$$\sigma_{nz} = \binom{N_p}{n} \binom{Z_p}{z} \int_0^\infty 2\pi b \, db \, P(b)^{n+z} \, (1 - P(b))^{A_p - n - z} \tag{13}$$

In Ref. 22 the densities σ_p and σ_T in Eq. (12) were built from harmonic oscillator wave functions with the oscillator constants chosen in such a way as to reproduce the experimental rms radii for projectile and target. For the case of $^{16}O + {}^{9}Be$ (only case calculated in Ref. 22), the integration of Eq. (9) can be quite easily performed because the wave functions are composed of two orbitals (s and p) only. However, because we would like to present a more general comparison, we have also calculated the MSA cross sections for two heavier systems ($^{40}Ca + {}^{12}C$ and $^{56}Fe + {}^{64}Cu$).

For ^{9}Be, ^{12}C and ^{16}O the density distributions are assumed to be Gaussian

$$\rho(r) = \frac{1}{(a\sqrt{\pi})^3} e^{-(r/a)^2} \tag{14}$$

where

$$a = R_{rms} (1.5)^{-\frac{1}{2}} \tag{15}$$

and R_{rms} is the experimental rms radius.[48]

For the heavier nuclei (^{40}Ca, ^{56}Fe and ^{64}Cu) we assumed the density distributions to have the usual Fermi distribution form[48]

$$\rho(r) = \frac{\rho_0}{1 + e^{(r-c)4.4/t}} \tag{16}$$

where c is the half-central-density radius, usually taken as $1.07 \times A^{1/3}$, t is the 90%-10% surface skin thickness parameter,[56] and ρ_0 is a normalization constant. Both density distributions used in Eq. (12) are normalized to unity

$$4\pi \int_0^\infty \rho(r)\, r^2 dr = 1 \tag{17}$$

A comparison between the fireball abrasion cross sections and those predicted by the multiple scattering abrasion (MSA) is presented in Table III-2, together with the parameters actually used in the calculations. We see that the results are indeed very close, with the exception of those for the removal of one nucleon, for which the MSA results are larger. This is obviously due to the extended picture (diffuse density distribution) used by the MSA, in contrast to the sharp density of the fireball abrasion model. However, as soon as the

TABLE III.2 Comparison between fireball abrasion and MSA cross sections. The hypergeometric charge dispersion is used in both models.

(A) $^{16}O + ^{9}Be$ (^{16}O fragmentation)

$R_{rms}(^{16}O) = 2.65$ fm

$R_{rms}(^{9}Be) = 2.35$ fm

A_Z	Fireball abrasion [a] (mb)	MSA [b] (mb)
^{15}O	109	145 (131)
^{14}O	33	35 (33)
^{13}O	11	10 (10)
^{12}O	3	3 (3)
^{15}N	109	145 (131)
^{14}N	74	80 (75)
^{13}N	42	41 (40)
^{12}N	21	19 (19)
^{11}N	9	8 (8)
^{14}C	33	35 (33)
^{13}C	42	41 (40)
^{12}C	37	34 (33)
^{11}C	26	23 (21)

(B) $^{40}Ca + ^{12}C$ (^{40}Ca fragmentation)

$R_{rms}(^{12}C) = 2.37$ fm

$^{40}Ca \rightarrow c = 3.659$ fm, $t = 2.2$ fm

A_Z	Fireball abrasion (mb)	MSA (mb)
^{39}Ca	124	170
^{38}Ca	40	44
^{37}Ca	15	15
^{39}K	124	170
^{38}K	84	93
^{37}K	49	49
^{36}K	26	25
^{35}K	14	12
^{38}Ar	40	44
^{37}Ar	49	49
^{36}Ar	42	39
^{35}Ar	30	27
^{34}Ar	19	17

(C) $^{56}Fe + ^{64}Cu$ (^{56}Fe fragmentation)

$^{56}Fe \rightarrow c = 4.34$ fm, $t = 2.15$ fm

$^{64}Cu \rightarrow c = 4.34$ fm, $t = 2.15$ fm

A_Z	Fireball abrasion (mb)	MSA (mb)
^{55}Fe	169	219
^{54}Fe	60	70
^{53}Fe	25	27
^{55}Mn	147	190
^{54}Mn	108	126
^{53}Mn	69	75
^{52}Mn	42	42
^{51}Mn	24	23
^{54}Cr	45	52
^{53}Cr	60	64
^{52}Cr	56	56
^{51}Cr	44	43
^{50}Cr	31	29

(continued . . .)

TABLE III.2 (continued)

(A) $^{16}O + {}^{9}Be$ (^{16}O fragmentation)

$R_{rms}(^{16}O) = 2.65$ fm
$R_{rms}(^{9}Be) = 2.35$ fm

A_Z	Fireball abrasion[a] (mb)	MSA[b] (mb)
^{13}B	11	10 (10)
^{12}B	21	19 (19)
^{11}B	26	23 (21)

(B) $^{40}Ca + {}^{12}C$ (^{40}Ca fragmentation)

$R_{rms}(^{12}C) = 2.37$ fm
^{40}Ca c = 3.659 fm, t = 2.2 fm

A_Z	Fireball abrasion (mb)	MSA (mb)
^{37}Cl	15	15
^{36}Cl	26	25
^{35}Cl	30	27
^{34}Cl	27	24
^{33}Cl	31	19
^{34}S	19	17
^{33}S	21	19
^{32}S	20	17
^{31}S	16	14
^{30}S	12	10

(C) $^{56}Fe + {}^{64}Cu$ (^{56}Fe fragmentation)

^{56}Fe c = 4.34 fm, t = 2.15 fm
^{64}Cu c = 4.34 fm, t = 2.15 fm

A_Z	Fireball abrasion (mb)	MSA (mb)
^{53}V	16	17
^{52}V	31	31
^{51}V	38	37
^{50}V	37	35
^{49}V	32	29
^{48}V	25	23
^{52}Ti	6	5
^{51}Ti	15	15
^{50}Ti	23	22
^{49}Ti	27	25
^{48}Ti	28	25
^{47}Ti	25	22
^{46}Ti	21	18

[a]In all fireball abrasion calculations: $R_P = r_0 A_P^{1/3}$ and $R_T = r_0 A_T^{1/3}$, where $r_0 = 1.36$ fm.

[b]The numbers in parentheses (shown for comparison) are those of Ref. 22, with density distributions built from harmonic oscillator wave functions.

collision becomes a little less peripheral, the results of the two models become practically identical. Therefore, the derivation of the abrasion cross sections based on Glauber's multiple-scattering theory has been viewed as a formal derivation of the fireball abrasion model.[22]

Let us now turn our attention to the second aspect of the fireball abrasion process, that of the excitation energy of the primary products. In particular, let us concentrate on the excitation energy of those fragments formed by the removal of one or two nucleons. Looking at Table III.1 we see that for the same projectile (target), e.g., ^{56}Fe, the larger the mass of the collision partner, the smaller is the excitation energy left. This is because the larger the radius of the partner, the larger the radius of curvature of the "cutting" surface will be, and consequently the surface excess of the abraded nucleus will be smaller. But the important point is the fact that even for the smallest partner (^{12}C), the excitation energy left after the removal of one or two nucleons is of the order of 6 MeV. Such a low excitation is, in general, less than a nucleon binding energy, and therefore cannot induce particle evaporation. As a result, after the evaporation process these nuclei will retain their full abrasion cross sections. The effects of this fact on the final results of our calculations (abrasion-ablation) will be analyzed in Chapter IV, when we compare our results with the experimental data.

In Fig. III.4 we show the excitation energy distributions of target residues left after the fast cascade process, calculated with the computer code ISABEL of Yariv and Fraenkel[28] for the case of $^{12}C + {}^{40}Ca$ at 400 MeV/A incident energy. This code is an extensive development of

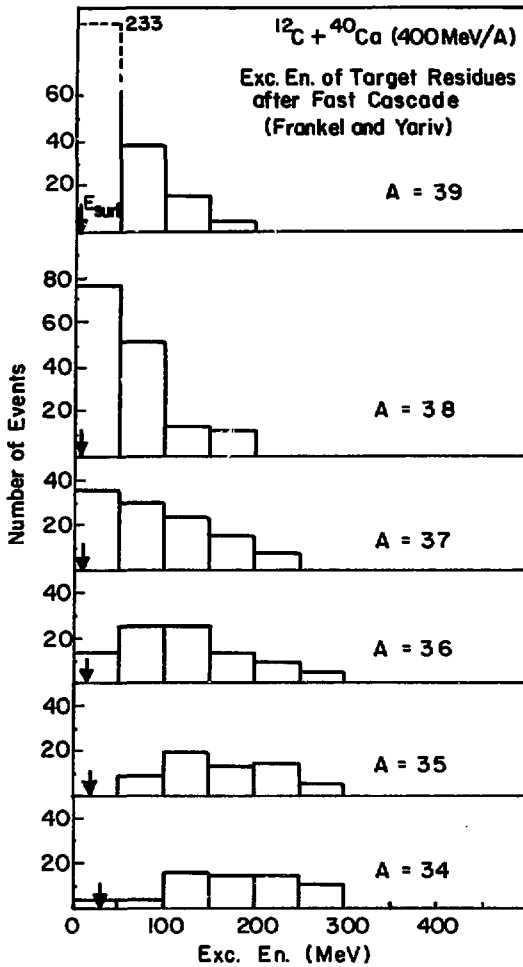

Fig. III.4. Excitation energy of target residues after fast cascade process calculated with Monte Carlo cascade code ISABEL of Yariv and Fraenkel.[28] The excitation energies have been sorted into 50 MeV wide bins to emphasize the high excitation energies obtained in this model.

the earlier Monte Carlo cascade code VEGAS[51] which was used for proton-nucleus reactions only. In ISABEL, a nucleus-nucleus collision is treated by allowing each nucleon within the projectile to interact with the target nucleons individually, without including any kind of collective interaction. The histograms shown in Fig. III.4 were calculated for 1000 ^{12}C ions at 400 MeV/A incident on a ^{40}Ca target at random impact parameter. From the figure we see that this treatment allows for some events of very high excitation energy (although with low probability). Also indicated in that figure are the results of the surface energy excitation (double arrow) predicted by the fireball abrasion model, and we see that these results are too low compared to those of the Monte Carlo cascade calculations. Indeed, as a preview of the next chapter, we would like to mention that the surface energy excitation cannot account for all the energy needed to reproduce the experimental observations. We will propose another physical process which will supplement the pure abrasion-ablation model by increasing the average excitation energy of the primary residues.

IV. FINAL PRODUCT DISTRIBUTIONS

IV.1 Introduction

This chapter contains the final results of our calculations with the fireball abrasion followed by evaporation, and comparisons with data from various experiments. In section IV.2 we discuss the results of the pure abrasion-ablation model. In section IV.3 we introduce a new process, frictional spectator interaction (FSI), which increases the average excitation energy of the primary products over that predicted by the excess surface energy. The final yields of the abrasion-FSI-ablation model are then compared with the experimental data, and the implications of this three-stage model are discussed in section IV.4. The dependence of projectile (target) fragmentation cross sections on target (projectile) mass number is investigated in section IV.5, and its consistency with the idea of "factorization" of high-energy fragmentation cross sections is studied. An interesting aspect of high-energy HI reactions is the possibility of producing isotopes far away from the β-stability line. In section IV.6 we discuss the results of our calculations in connection with the recently completed experiment on fragmentation of an ^{40}Ar beam[31,32] and the planned experiment with a ^{48}Ca beam[58] at the Bevalac. The possibility of observing nuclear ground state correlations is also discussed in this section.

IV.2 Pure Abrasion-Ablation: Comparisons with Experimental Data

Computational Procedure

Before proceeding with the theory-experiment comparisons let us give a comprehensive review of the computational procedure used in the

calculations, which is illustrated in Fig. IV.1. Let us suppose we would like to obtain the results of a projectile fragmentation process.

The input to our code consists simply of the charge and mass number of the projectile-target system to be studied.

The first step is to calculate the abrasion cross sections, that is, the cross sections for removal of one, two, three, ..., n nucleons from the projectile. Simultaneously to the abrasion cross sections we obtain the corresponding excitation energy of the primary residues resulting from the excess surface energy. Secondly, we must calculate the primary product charge distribution. By applying a charge dispersion (hypergeometric or Nuc-GDR) the cross section for producing a given (Z_p', A_p') primary residue is obtained.

The cross sections and excitation energies obtained for each primary residue are then used as input for the evaporation subroutine (EVAPOR), which was described in section II.4. This comprises the so-called "ablation stage," from which we obtain a series of partial yields of the final (observed) fragments. Finally, we sum the partial yields of each final fragment over all primary residues, and obtain the final yields (cross sections), which are to be compared with the experimental values.

Comparison with Experimental Data

Following the scheme outlined above we have calculated the elemental cross sections (summed over A for the same Z) resulting from the fragmentation of an ^{56}Fe beam. Westfall et al[33] have studied the fragmentation of ^{56}Fe at 1.8 GeV/A by several targets at the Bevalac. In Fig. IV.2(a,b,c) the calculated results are compared with the data for the cases of ^{12}C,

COMPUTATIONAL PROCEDURE

(Pure Abrasion–Ablation Calculation)

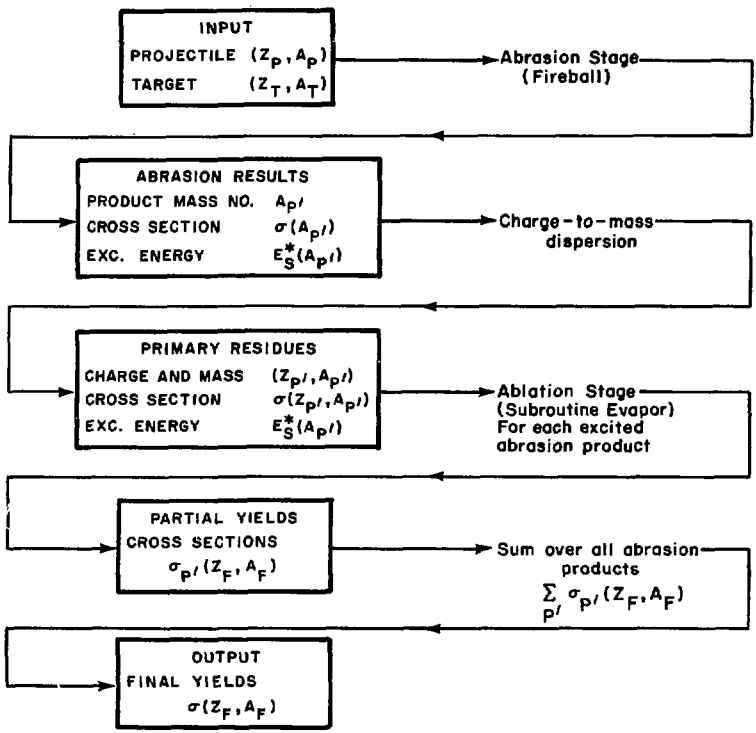

XBL 792-8240

Fig. IV.1

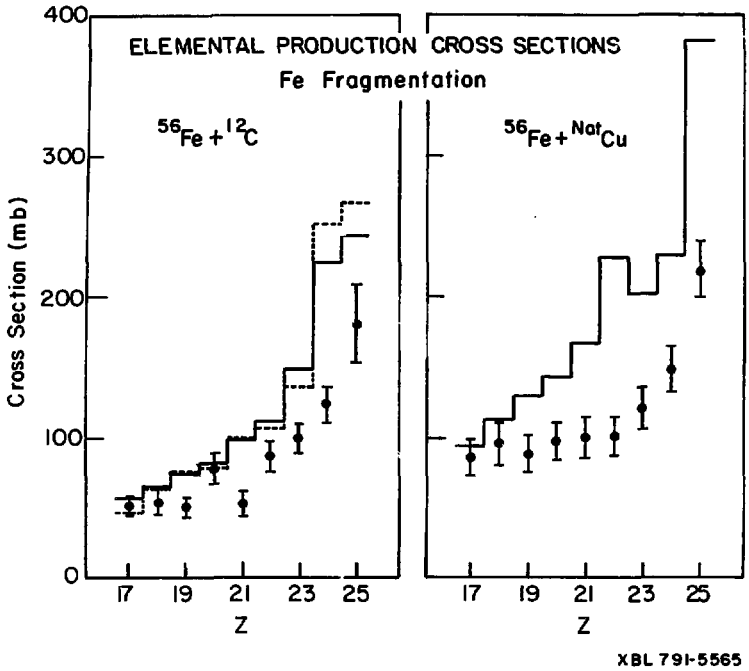

Fig. IV.2(a). Comparison between the abrasion-ablation results and the ^{56}Fe (1.88 GeV/nuc) fragmentation data of Westfall et al.[33] The solid lines were calculated with the hypergeometric charge dispersion and the traced lines (in the ^{12}C target case) with the Nuc-GDR charge dispersion.

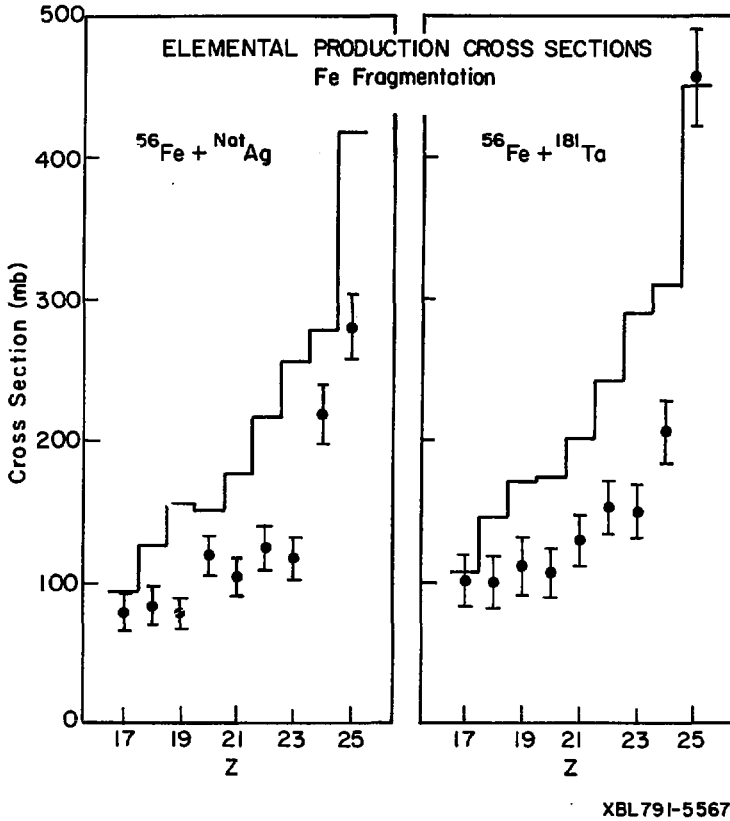

Fig. IV.2(b). Same as Fig. IV.2(a) for ^{nat}Ag and ^{181}Ta targets.

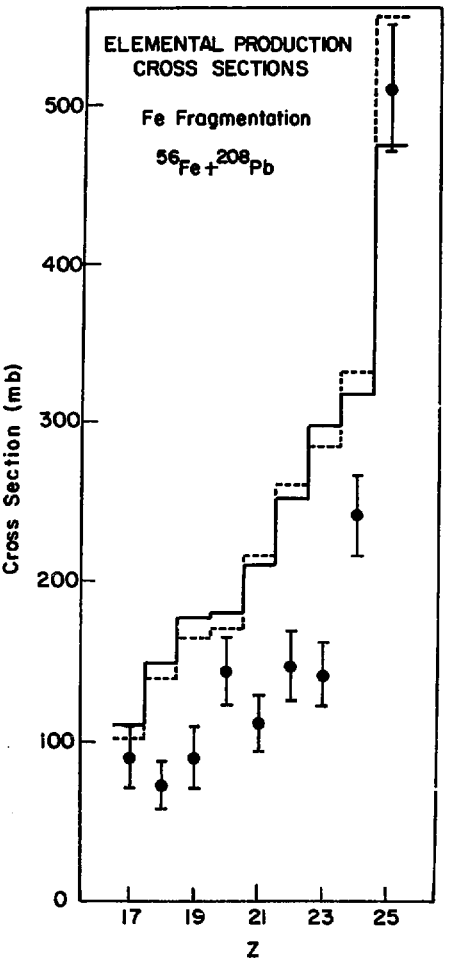

XBL 791-5563

Fig. IV.2(c). Same as Fig. IV.2(b) for ^{208}Pb target.

^{nat}Cu, ^{nat}Ag, ^{181}Ta, and ^{208}Pb targets. The dotted lines in the ^{12}C and ^{208}Pb figures were obtained with the Nuc-GDR charge dispersion and the solid lines in all figures were calculated with the hypergeometric charge dispersion. The corresponding primary product distributions are listed in Table III.1. From the figures we see that both charge dispersions predict very similar results for the elemental cross sections, although they predict somewhat different isotope production cross sections as can be seen from Fig. IV.3. This means that element production cross sections are not sensitive to details of ground state correlations, but that isotope production cross sections should be an interesting probe of those correlations. Unfortunately the latter were not resolved in the experiment of Ref. 33. This point will come up again in section IV.6 in connection with the discussion of the ^{40}Ar fragmentation experiment of Viyogi et al.[31]

Let us concentrate our attention on the first three cases (^{12}C, ^{nat}Cu, and ^{nat}Ag targets). The experimental results for the other two targets present a particularity at $Z = 25$ which will be discussed in section IV.4. An interesting feature of the first three cases is that the theoretical results are higher than the data, especially for the near projectile fragments. Furthermore, one can see from Fig. IV.2 that the discrepancy is not just a normalization problem, as the data are much flatter than the theoretical results. The same applies for the other two target results, except at $Z = 25$. This has an important bearing on the discussion of the excitation energy of the primary products. It definitely tells us that the excitation energy calculated with the surface term is far less than what is needed to reproduce the data.

Fig. IV.3(a). Comparison between theoretical isotope production cross sections obtained with the hypergeometric (solid line) and the Nuc-GDR charge dispersions. The corresponding values of the elemental production cross sections (σ_Z = 21) are also indicated in the figure.

Fig. IV.3(b). Same as Fig. IV.3(a) for the $_{20}$Ca isotopes.

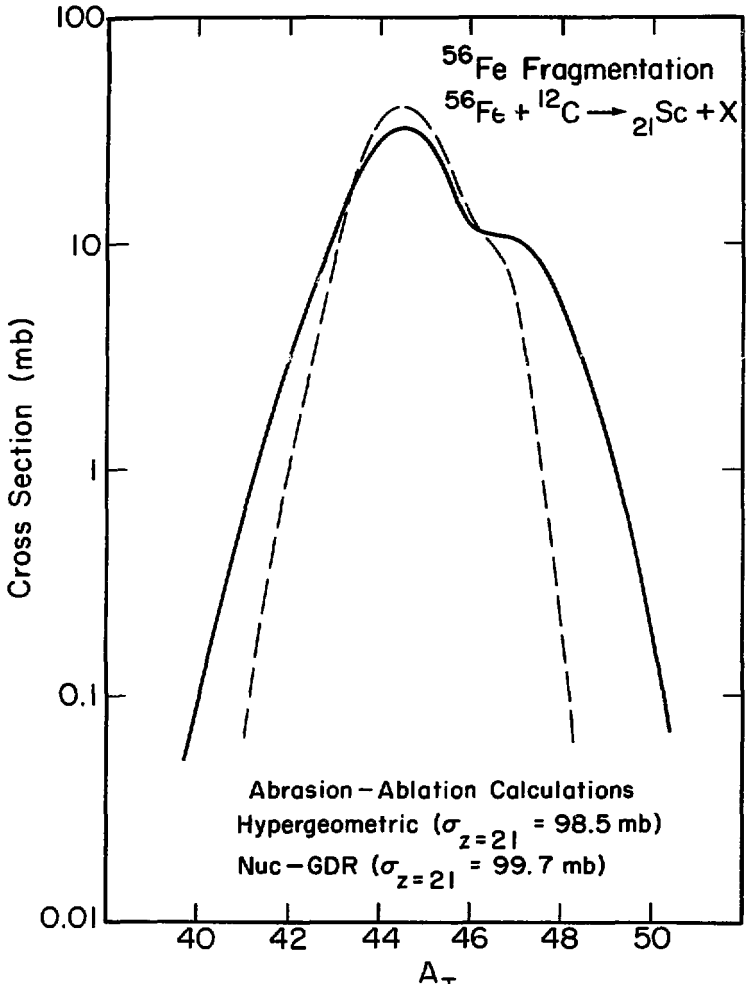

XBL 792-8243

Fig. IV.3(a)

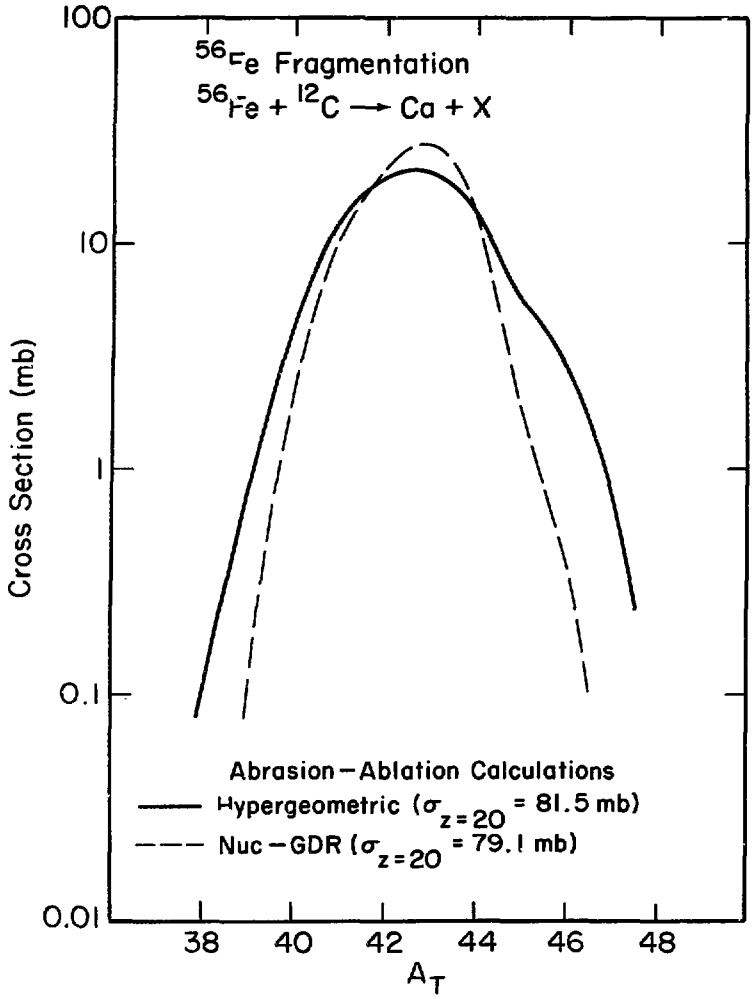
^{56}Fe Fragmentation
^{56}Fe + ^{12}C → Ca + X
Cross Section (mb)
100
10
1
0.1
0.01
38
40
42
44
46
48
A_T
Abrasion–Ablation Calculations
Hypergeometric ($\sigma_{z=20}$ = 81.5 mb)
Nuc–GDR ($\sigma_{z=20}$ = 79.1 mb)
XBL 792-8242

Fig. IV.3(b)

As we had anticipated in section III.4, a look at Table III.1 or Fig. III.3 shows that the abrasion cross sections for the elements one or two nucleons removed from the target are quite high, whereas the corresponding surface energy excitations are not enough to induce appreciable particle evaporation from those nuclei. An examination of Fig. IV.7 (which will be explained in section IV.4) also corroborates the need of higher excitation energies than those calculated with the extra-surface energy equation alone. Following an idea of Hüfner, Schäfer and Schürmann,[22] we introduced a mechanism which increases the average excitation energy of the primary fragments. The physics of this process (which was called "final state interaction" in Ref. 22) is described in the next section. We prefer to call it "frictional spectator interaction," retaining the same initials (FSI), but avoiding confusion with other uses of the expression "final state interaction."[59,60]

IV.3 Added Excitation Energy: Frictional Spectator Interaction

Since the nucleon-nucleon elastic scattering cross section at high energies is largely forward-peaked, it is a good approximation to assume (at such energies) that the incident projectile nucleon follows a straight-line trajectory, while a struck target nucleon moves in the plane perpendicular to the projectile direction (impact parameter plane). This means that the momentum transfer is approximately perpendicular to the incident momentum, as is shown in Fig. IV.4. This picture is obviously the same in the projectile frame of reference, with the projectile and target roles reversed. Therefore, a struck nucleon is either immediately kicked out of the nucleus (without FSI) or it has to

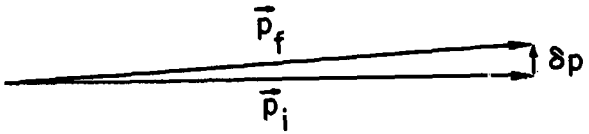

XBL 791-8105

Fig. IV.4. Small angle scattering momentum conservation. Because of the smallness of the scattering angle at high energies, the momentum transfer, δp, is, to a very good accuracy, perpendicular to the incident momentum.

go through the spectator piece, depositing energy in further nucleon-nucleon collisions. This latter possibility is what has been called the frictional spectator interaction (FSI) mechanism. Based on geometrical arguments, we assume that a struck nucleon has a 50% chance of undergoing FSI.

We must then calculate the average energy deposited by a struck nucleon which undergoes FSI. Let us view the collision in the target (lab) reference frame.

In Ref. 61, the differential elastic scattering nucleon-nucleon cross section is presented as a function of t — the square of the four-momentum transfer to the target nucleon, for bombarding energy from 0.5 to 2.0 GeV. From this angular distribution we evaluated the average four-momentum transfer $\langle t \rangle$ by

$$\langle t \rangle = \frac{\int_0^\infty t \frac{d\sigma}{dt} dt}{\int_0^\infty \frac{d\sigma}{dt} dt} \quad . \tag{1}$$

Let us consider an individual nucleon-nucleon collison. Assuming the target nucleon to be at rest before collision, its four-momentum is $P = (0, m_N)$, where m_N is the nucleon mass. After the collision its four-momentum becomes $P_f = (p_f, E_f)$. The square of the four-momentum transfer t is defined as[62]

$$t = (P_f - P)^2 \quad . \tag{2}$$

Substituting the four-momentum coordinates, Eq. (2) becomes

$$t = (p_f, E_f - m_N)^2 = E_f^2 - 2m_N E_f + m_n^2 - p_f^2 \quad . \tag{3}$$

Using the relativistic expression for p_f ,

$$p_f^2 = E_f^2 - m_N^2 \quad , \tag{4}$$

in Eq. (3) we obtain

$$t = -2m_N(E_f - m_N) \quad . \tag{5}$$

Since

$$E_f - m_N = E_{recoil} \quad , \tag{6}$$

where E_{recoil} is the kinetic energy of the recoiling target nucleon, we finally obtain a relation between t and E_{recoil},

$$t = -2m_N E_{recoil} \quad . \tag{7}$$

Therefore, disregarding a negative sign, we can write

$$\langle t \rangle = 2m_N \langle E_{recoil} \rangle \quad . \tag{8}$$

From the energy dependence of $d\sigma/dt$ and Eqs. (1) and (8) we obtained the average recoil energy $\langle E_{recoil} \rangle$ as a function of the lab energy/nucleon of the projectile.

The real physical situation between colliding heavy-ions is more complicated than this simple picture of individual nucleon-nucleon collisions. Therefore, we believe that the calculations presented above give only an upper limit to the energy imparted to a target nucleon during the collision and are valid for the most grazing collisions, where the situation is closer to that of an individual N-N collision.

As the recoiling nucleon advances through the spectator piece it loses energy in further N-N collisions. We calculate the deposited energy by assuming the recoiling nucleon energy to be given by[10]

$$\frac{dE}{dx} = -\frac{\alpha}{\lambda} E \tag{9}$$

subject to the condition

$$E(x=0) = \langle E_{recoil} \rangle \quad . \tag{10}$$

In Eq. (9), λ is the nucleon mean free path, and α is the fraction of energy lost in each collision. In the calculations presented here we take $\alpha = 0.25$ (see Ref. 63), and

$$\lambda = \frac{1}{\rho\sigma_{NN}} \tag{11}$$

where $\rho = 0.17\ Fm^{-3}$ is the nuclear matter density and σ_{NN} is the N-N cross section, assumed to be $\approx 300/E\ Fm^2$ (a fair approximation for $50 < E < 150$ MeV).

Finally, the average deposited energy $\langle E_{FSI} \rangle$ is calculated by averaging over all orientations of the nucleon trajectory through the spectator piece:

$$\langle E_{FSI} \rangle = \frac{1}{\pi} \int_0^{\pi} E_{dep}(\theta)\, d\theta \tag{12}$$

where θ is the scattering angle in the plane perpendicular to the incident direction.

Table IV.1 presents the values we obtained for the three cases studied in the next section.

TABLE IV.1. Average energy deposited by a nucleon undergoing FSI.

Spectator	Lab energy (MeV/N)	$\langle E_{FSI} \rangle$ (MeV)
^{40}Ca	400	35.3
^{56}Fe	1800	38.8
Cu	2000	41.5

As stated before, we assume that each struck nucleon has a 50% chance of passing through the spectator, depositing $\langle E_{FSI} \rangle$ of excitation on the average. Therefore, each primary residue with mass number $A_{T'} = A_T - a_T$ may have from zero to a_T final state interactions according to a binomial distribution given by:

$$\text{Prob}\,(m_{FSI}) = \frac{\binom{a_T}{m_{FSI}}}{2^{a_T}} \quad . \tag{13}$$

The total excitation energy of a primary fragment ($A_{T'}$), which has undergone m_{FSI} final state interactions is given by

$$E^* = E_{surf}(a_T) + m_{FSI} \cdot \langle E_{FSI} \rangle \tag{14}$$

where $E_{surf}(a_T)$ is the extra surface energy term, which is a function only of the number of nucleons removed.

The new computational procedure (with FSI) is shown in Fig. IV.5.

Before closing this section, let us mention a limitation of the FSI scheme proposed above. Because of the small scattering angle assumption, it can only be strictly justified for energies above 1.0 GeV/A. Nevertheless, we have included it in the calculation of $^{12}C + {}^{40}Ca$ at 0.4 GeV/A and also for the case of $^{40}Ar + {}^{12}C$ at 0.2 GeV/A, but those results should be seen as a suggestion that a modified version of the proposed mechanism may be occurring.

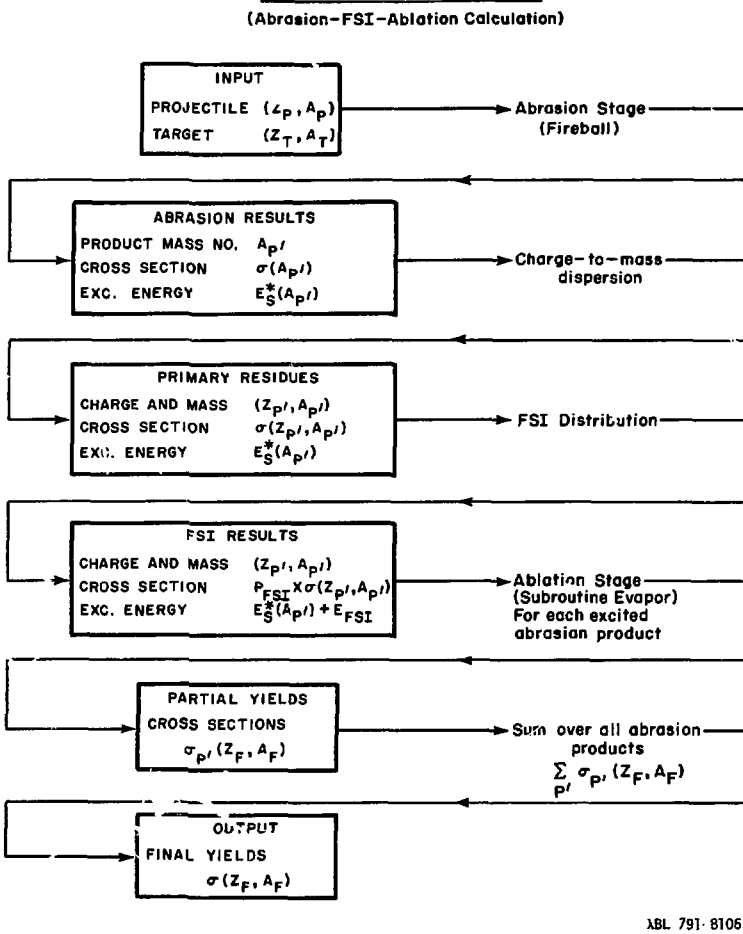
COMPUTATIONAL PROCEDURE
(Abrasion-FSI-Ablation Calculation)
INPUT
PROJECTILE (Z_P, A_P)
TARGET (Z_T, A_T)
Abrasion Stage (Fireball)
ABRASION RESULTS
PRODUCT MASS NO. $A_{P'}$
CROSS SECTION $\sigma(A_{P'})$
EXC. ENERGY $E_S^*(A_{P'})$
Charge-to-mass dispersion
PRIMARY RESIDUES
CHARGE AND MASS $(Z_{P'}, A_{P'})$
CROSS SECTION $\sigma(Z_{P'}, A_{P'})$
EXC. ENERGY $E_S^*(A_{P'})$
FSI Distribution
FSI RESULTS
CHARGE AND MASS $(Z_{P'}, A_{P'})$
CROSS SECTION $P_{FSI} \times \sigma(Z_{P'}, A_{P'})$
EXC. ENERGY $E_S^*(A_{P'}) + E_{FSI}$
Ablation Stage (Subroutine Evapor) For each excited abrasion product
PARTIAL YIELDS
CROSS SECTIONS
$\sigma_{P'}(Z_F, A_F)$
Sum over all abrasion products
$\sum_{P'} \sigma_{P'}(Z_F, A_F)$
OUTPUT
FINAL YIELDS
$\sigma(Z_F, A_F)$
XBL 791-8106

Fig. IV.5.

IV.3 Abrasion-FSI-Ablation: New Comparisons

^{56}Fe Projectile Fragmentation

In Fig. IV.6(a,b,c) we show a comparison between the results of our calculations with FSI (solid lines) and the same experimental data of Fig. IV.2.[4] The inclusion of FSI makes the calculated results flatter than the previous theoretical results (no FSI), and particularly it significantly reduces the cross sections for production of elements close to the target. The agreement between theory and experiment is now generally better than before, except for Z = 25 which is now lower than the experimental value.

We interpret the discrepancy at Z = 25 as an indication of the effects of other peripheral processes not included in our calculations, such as Coulomb dissociation via the giant E1 resonance of the projectile,[64,65] or a dissociation of the projectile in the nuclear field in the target.[19] The former has indeed been observed by Heckman and Lindstrom[66] for the case of ^{12}C and ^{16}O fragmentation (2.1 GeV/A bombarding energy). They observed that such process is negligible for light targets (low Z), but becomes very important for higher Z ones. In the present case (^{56}Fe fragmentation), Coulomb dissociation is certainly negligible for ^{12}C targets, but it may very well account for some of the missing cross section at Z = 25 for the other targets, because the Coulomb-excited ^{56}Fe nucleus mainly deexcites by emitting one nucleon. Indeed we see from Fig. IV.6(A,b,c) that for the heaviest targets the cross section for Z = 25 isotopes increases much more than those for any other Z, and the discrepancy between

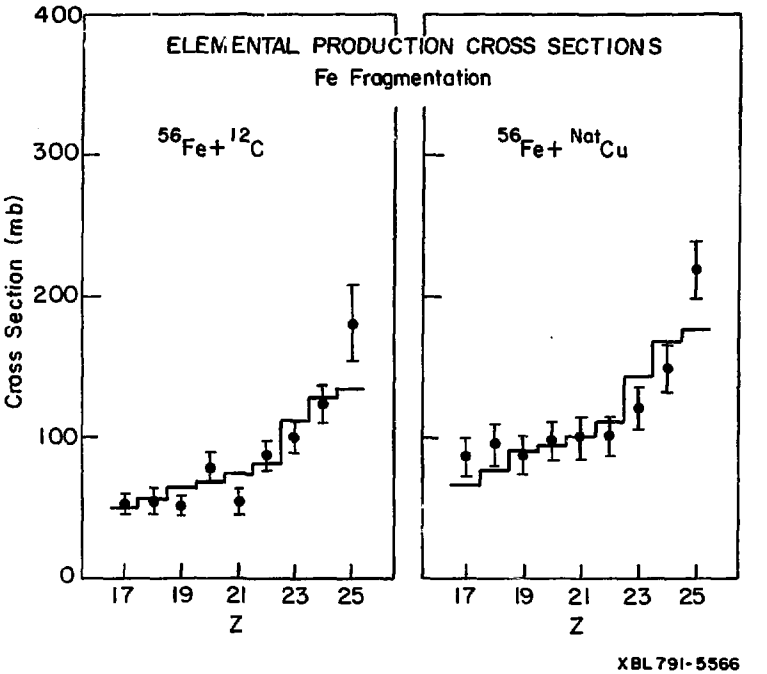

Fig. IV.6(a). Same as Fig. IV.2(a) but with FSI included in the calculations.

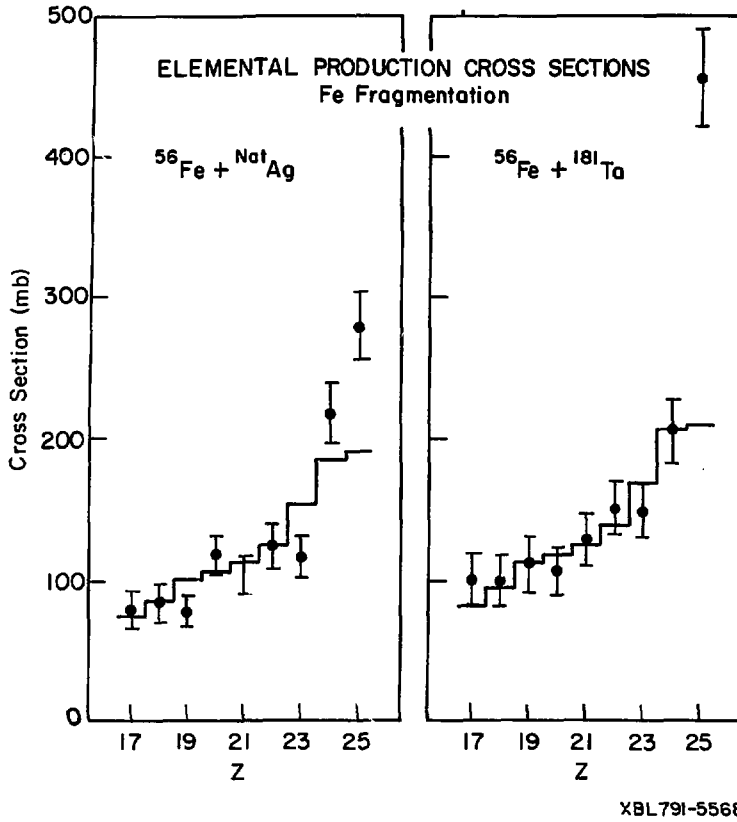

Fig. IV.6(b). Same as Fig. IV.6(a).

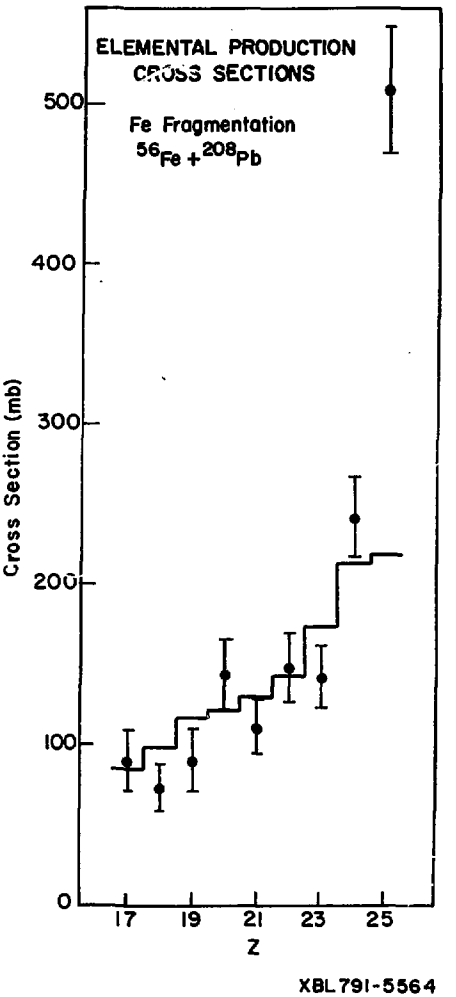

Fig. IV.6(c). Same as Fig. IV.6(a).

the experimental data and the results of our model becomes more pronounced, reflecting the above discussion.

The dependence of the elemental cross sections on the target mass number is presented in the next section.

^{40}Ca Target Fragmentation

A comparison of the results of our calculation and the experimental results of the TOSABE group[30] is shown in Fig. IV.7. They utilized in-beam gamma ray techniques to study the fragmentation of ^{40}Ca following interaction with high-energy alpha and carbon projectiles. We have plotted only the cross sections for the even-even products observed during the beam spills, because the intensity of their $2^+ \rightarrow 0^+$ transitions gives a more reliable measure of their yield. Also a few radioactive isotopes (shown on the left side of Fig. IV.7) were identified by measuring the off-beam spectra between the one-second beam spills. The histograms represent the experimental data, and the full and dashed lines are, respectively, the results of our calculations with and without FSI. Again the inclusion of FSI substantially improves the results, especially for those isotopes with masses close to the target mass.

Shibata et al[30] compared their Ca fragmentation data (both with alpha and carbon projectiles) with data resulting from Ca bombardment by π^- and proton projectiles. Figure IV.8 was replotted from their work with the inclusion of our theoretical results for ^{12}C projectiles. A feature clearly observed in this figure is the development of a plateau for yields corresponding to the heavier projectiles in contrast to the monotonic fall-off of yields resulting from the lighter ones. Such a

Fig. IV.7. A comparison of the calculated isotope production cross sections with the measured data of Shibata et al.[30] The solid and the traced lines are from the abrasion-ablation calculations with and without FSI respectively, and the histograms are the experimental data. The experimental errors are indicated by the dashed lines in the histograms.

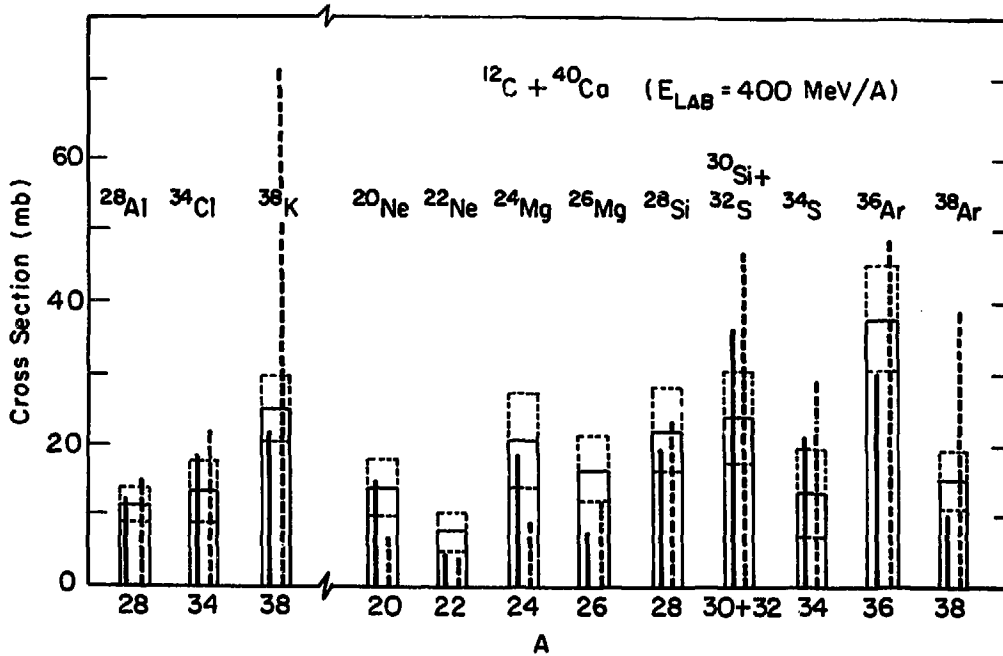

XBL 784-4923

Fig. IV.7

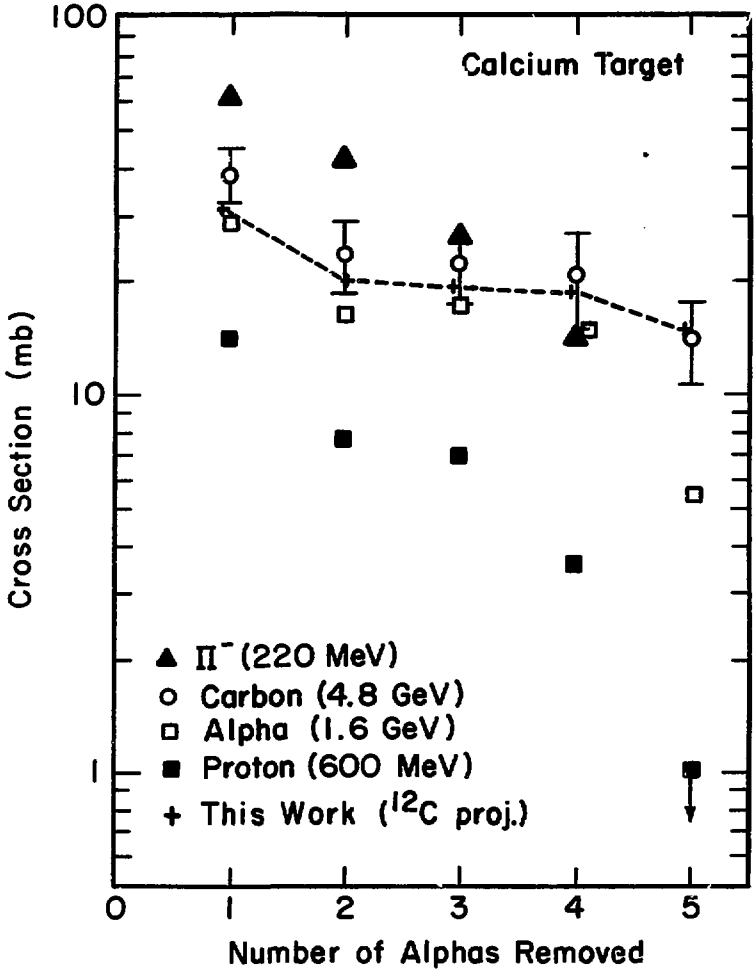

XBL 776-8895 A

Fig. IV.8. ^{40}Ca fragmentation yields of so-called alpha nuclei as a function of the number of alpha particles removed from the target. The line connecting the theoretical results is merely to guide the eyes. For experimental references, see Ref. 30.

plateau is well reproduced by the present theoretical results. It was suggested[30] that plateau formation for the carbon data reflects the great range of intermediate excited products formed at various impact parameters during the fast initial collision process, while the monotonic fall-off of the pion yields mostly represents statistical nucleon and alpha evaporation from excited ^{40}Ca or its nearest neighbors. Within the context of our model, their suggestion is equivalent to saying that production of a wide range of primary products in the abrasion-type process gives the distinctive plateau associated with the heavier projectiles.

^{nat}Cu Target Fragmentation

Several target fragmentation studies with high-energy projectiles have been performed in the past five years at the Bevalac which used radiochemical techniques in the identification of final products (see Table I.1 for references).

Here we compare our theoretical results with the experimental data of Cumming et al.[36] They performed radiochemical studies of the spallation products from a natural copper target irradiated with 80 GeV ^{40}Ar ions, measuring cross sections for production of 35 radioactive nuclides.

In Table IV.2 we present the results of our calculations with and without FSI for the heaviest 22 isotopes along with their respective experimental values. We restrict the comparison to the heaviest isotopes due to their sure origin in peripheral-type collisions. From Table IV.2 we see that the general trend of the data is fairly well reproduced by both calculations, although the FSI results are a factor of 1.5-2.0 lower than the data for most isotopes. But the best way to compare the results

TABLE IV.2. Comparison between theoretical results (with and without FSI) and experimental Cu spallation yields (from Ref. 36). Both calculations were performed with the hypergeometric charge dispersion.

Isotope	Experiment	Calculation without FSI	Calculation with FSI
^{64}Cu	64.0 ± 15.0	50.8	25.4
^{61}Cu	32.0 ± 6.0	43.0	15.9
^{57}Ni	1.87 ± 0.28	3.51	1.08
^{56}Ni	0.1 ± 0.8	1.5	0.1
^{60}Co	31.0 ± 13.0	38.0	15.2
^{58}Co	37.0 ± 7.0	39.9	42.5
^{57}Co	51.0 ± 5.0	25.6	25.9
^{56}Co	17.6 ± 1.4	16.6	8.0
^{55}Co	3.15 ± 0.22	7.7	1.48
^{59}Fe	5.9 ± 0.9	29.4	3.4
^{52}Fe	0.35 ± 0.07	1.95	0.30
^{56}Mn	9.1 ± 1.6	23.0	5.8
^{54}Mn	47.2 ± 1.8	28.5	29.9
^{52}Mn	17.3 ± 0.2	12.2	14.4
^{51}Cr	51.9 ± 1.7	24.4	26.9
^{48}Cr	0.92 ± 0.05	3.48	0.76
^{48}V	26.8 ± 1.1	19.1	20.3
^{48}Sc	1.73 ± 0.17	8.3	0.77
^{47}Sc	7.56 ± 0.37	11.2	3.4
^{46}Sc	21.0 ± 1.4	14.4	9.1
^{44}Sc	25.8 ± 2.3	18.9	19.8
^{43}Sc	8.5 ± 3.5	11.2	9.0

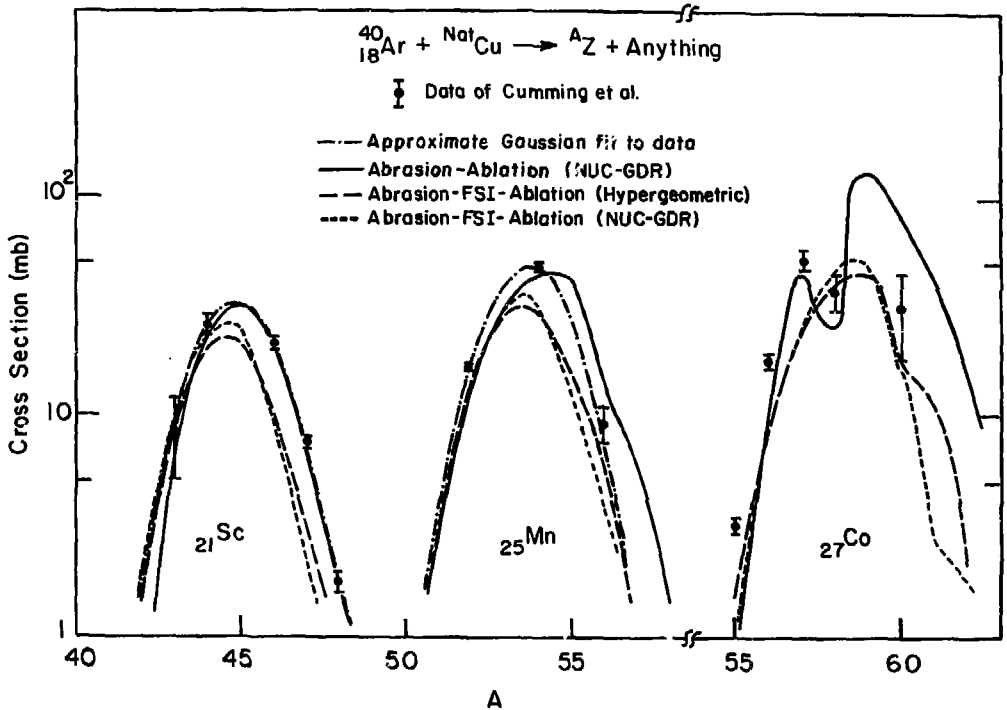

XBL 791-5575

Fig. IV.9(b). Same as Fig. IV.9(a).

for both charge dispersions, which fit the data fairly well if the overall normalization is neglected. This means that at least in the case of copper fragmentation, nuclear ground state correlations cannot be detected if enough excitation energy is pumped into the primary products in the initial stages of the reaction. In other words, the whole reaction process seems to be completely dominated by the evaporation (ablation) stage, with the final products clustering around the valley of beta-stability. We will come back to this discussion in section IV.5, when we discuss the results of other light element fragmentation experiments (^{40}Ar and ^{48}Ca).

IV.5 Factorization of Fragmentation Cross Sections

Projectile fragmentation experiments,[29,36] have been performed at the Bevalac which revealed an interesting feature of relativistic heavy-ion reactions: the large fragment production cross sections from the fragmentation of relativistic projectiles (1.0 to 2.0 GeV/A) follow the factorization hypothesis, within experimental uncertainties. Factorization is a result of the large difference in rapidity ($y = \tanh^{-1} \beta_L$, $\beta_L \equiv$ longitudinal velocity) between the target and projectile fragments in high-energy reactions, and it seems to hold only for products of peripheral collisions. In particular, Wang[67] has calculated the total cross sections for relativistic nucleus-nucleus scattering using Glauber theory, and concluded that those cross sections do not factorize.

In the language of heavy-ion fragmentation, factorization means that the cross section for production of a particular fragment F from the fragmentation of a beam B incident on target T, can be written

$$\gamma_{BT}^{F} = \gamma_T \gamma_B^F \tag{15}$$

where γ_B^F depends only on the projectile and the observed fragment, and γ_T is a target-dependent factor.

Our results for the elemental production cross sections from ^{56}Fe fragmentation are shown in Table IV.3 for ^{12}C, ^{64}Cu, ^{109}Ag, ^{181}Ta, and ^{208}Pb, along with the corresponding experimental values of Westfall et al.[36]

Theoretical (full circles) and experimental[36] target factors are plotted in Fig. IV.10 and one can see that they agree very well. The experimental values (open circles with error bar) were determined by choosing γ_T for the carbon target equal to 1.92 and minimizing the equation

$$\chi^2 = \sum_{T,F} (\sigma_{BT}^F - \gamma_T \gamma_{BF})^2 / \delta\sigma_{BT}^F \tag{16}$$

where T ranged over all targets[68] but F was restricted to the range Z_F = 18-24.

By taking the experimental target factor for ^{12}C (γ_C = 1.92), we obtained the theoretical values of γ_T for another target, by dividing each value of σ_{BT}^F for that target by the corresponding value of σ_{BT}^F for ^{12}C, and multiplying by 1.92. Averaging over the fragments from Z_F = 18-25, we obtained average target factors equal to 2.57, 2.88, 3.19, and 3.30, respectively, for ^{64}Cu, ^{108}Ag, ^{181}Ta, and ^{208}Pb.

The determination of the experimental target factors did not include the Z_F = 25 fragments because their experimental cross sections are not expected to follow the factorization hypothesis. Indeed, it has

TABLE IV.3. Elemental production cross sections (mb) from ^{56}Fe fragmentation.

Target	C		Cu		Ag		Ta		Pb		Target
Z_F	Theory[a]	Exper.[b]	Theory	Exper.	Theory	Exper.	Theory	Exper.	Theory	Exper.	Z_F
25	134	181 ±27	176	219 ±20	192	280 ±23	211	457 ±34	218	509 ±40	25
24	128	134 ±13	168	149 ±16	186	218 ±21	208	206 ±22	213	242 ±25	24
23	112	100 ±11	143	121 ±15	155	117 ±15	170	150 ±19	174	142 ±20	23
22	81	87 ±11	112	101 ±14	125	124 ±16	139	152 ±19	143	148 ±22	22
21	74	54 ± 9	101	100 ±15	113	104 ±13	125	129 ±18	129	111 ±17	21
20	68	78 ±11	95	98 ±14	106	118 ±14	118	107 ±17	121	144 ±22	20
19	64	52 ± 7	91	88 ±14	101	79 ±11	113	111 ±20	117	90 ±19	19
18	56	55 ± 9	77	95 ±15	86	84 ±14	95	100 ±18	98	73 ±15	18
17	50	53 ± 7	67	86 ±13	75	79 ±14	83	101 ±18	85	90 ±19	17

[a]Abrasion-FSI-ablation calculation with hypergeometric charge dispersion.
[b]Experimental data of Westfall et al.[4]

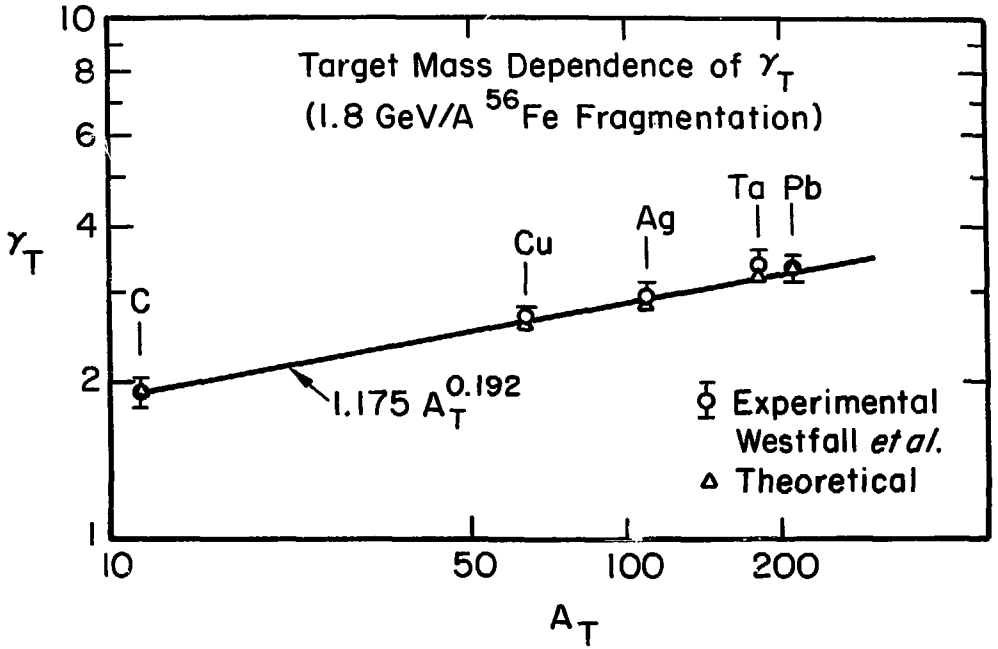

XBL 792-8241

Fig. IV.10. The calculated and the experimental target factors are shown as a function of the target mass number.

been shown by Heckman and Lindstrom[66] that Coulomb dissociation effects, via the giant E1 resonance, are very important for heavy targets but practically negligible for light ones. The Coulomb-excited projectile de-excites mainly by emitting one nucleon, therefore contributing heavily to the Z=25 cross section obtained with the heavier targets. Those cross sections are much enhanced over the corresponding ones (Z_F = 25) for the lighter targets, and therefore do not follow the factorization systematics. Since Coulomb dissociation effects are not included in our calculations, we have averaged over the fragments from Z_F = 18 to 25.

Both the experimental and theoretical target factors can be very well fitted by a target-mass-number dependence of the form

$$\gamma_T = a\, A_T^d \quad . \tag{17}$$

The best fit to the theoretical results (straight line on Fig. IV.4) is given by

$$\gamma_T^{theor} = 1.175\, A_T^{0.192}$$

and the experimental points are best fit by $a = 1.272 \pm 0.044$ and $d = 0.177 \pm 0.010$. These results are quite consistent with previous ^{16}O and ^{12}C projectile fragmentation data,[29] and confirm the expected peripheral nature of the large fragment production process.

IV.6 ^{40}Ar and ^{48}Ca Fragmentation Results

Until very recently only two nuclei (^{16}O and ^{12}C) had been used in the study of high energy projectile fragmentation[29] because of limitations of the Bevalac's capability to deliver heavier beams with reasonable intensities. After the most recent Bevalac upgrading (see Ref. 4), it

became possible to accelerate ^{56}Fe ions up to 2.0 GeV/A with intensities of the order of 10^5 particles/sec. The first experiment designed to study the results of peripheral collisions induced by the new beams was that of Westfall et al,[36] which we have already discussed in the preceding section.

Here we compare the results of our calculations with the recently completed experiment on projectile fragmentation with an ^{40}Ar beam.[31] We also extend our predictions to the upcoming experiment with a ^{48}Ca beam,[58] and discuss the possibilities of detecting nuclei far from beta-stability in that experiment, as suggested by Symons et al.[32]

The experiment of Viyogi et al[31] used the ^{40}Ar beam with an intensity of 10^8 particles/sec to bombard a 140 mg/cm^2 ^{12}C target. The incident energy was 213 MeV/A. Projectile fragments were detected in a multi-element telescope consisting of nine 5-mm thick silicon detectors, which could stop projectile fragments heavier than nitrogen. Isotope production cross sections determined in that experiment are shown in Fig. IV.11(a,b,c) for each element from oxygen to sulphur. Also appearing in Fig. IV.11 are four theoretical curves, two of which are the results of pure abrasion-ablation calculations. The other two result from the inclusion of FSI according to the scheme of Fig. IV.5. Numerical values can be read from the tables in Appendix B.

Before discussing the results, let us mention that the hypothesis of a frictional spectator interaction (FSI) as presented in section IV.3 <u>cannot</u> be justified at energies of the order of 200 MeV/A because of the breakdown of the small angle scattering assumption. This approximation can only be justified at energies above 1.0 GeV/A as indicated by the

experimental nucleon-nucleon cross section. Moreover, the "frozen-nucleus approximation" implicitly used in the FSI calculation is probably also a poor approximation at energies of 200 MeV/A. This latter approximation implies neglecting the Fermi motion of the nucleons in comparison with the high velocity of relative motion of the collision partners. Since the Fermi energy is of the order of 50 MeV, it is likely to play a role in a heavy-ion collision at 200 MeV/A.

Nevertheless, we have chosen to include the curves calculated with FSI in Fig. IV.11, but they should be viewed with care. The reason for their inclusion resides in the fact that we know a priori that the extra-surface energy gives only a lower limit to the excitation of the primary fragments, and we are interested in seeing what happens if the average excitation is increased over that of the surface energy term. Therefore, the long and short dashed curves in Fig. IV.11(a,b,c) were obtained according to the scheme of Fig. IV.5 with E_{FSI} = 40 MeV, which is comparable to the values of Table III.2.

Three conclusions can be immediately drawn from the mass yield diagrams of Fig. IV.11(a,b,c):

i) The pure abrasion-ablation calculation with the hypergeometric charge dispersion (dotted line) gives much broader mass yield distributions than the experimental points, which is inconsistent with what we have seen in the case of Cu target fragmentation.

ii) The pure abrasion-ablation calculation with the NUC-GDR charge dispersion (solid lines) fits the data distributions very nicely except at Z=8. The disagreement at Z=8 is probably due to the fact that we stopped the calculations

Fig. IV.11(a,b,c). A comparison of the calculated isotope production cross sections with the data from the projectile fragmentation (^{40}Ar at 215 MeV/A) experiment of Viyogi et al.[31]

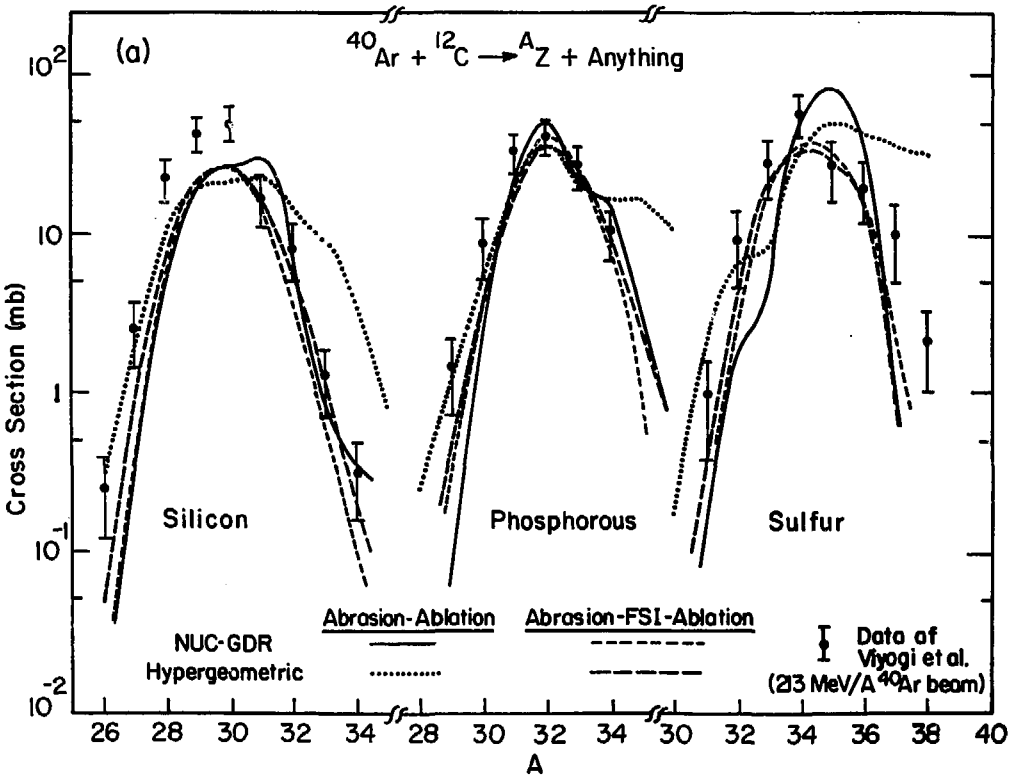

XBL791-5572

Fig. IV.11(a)

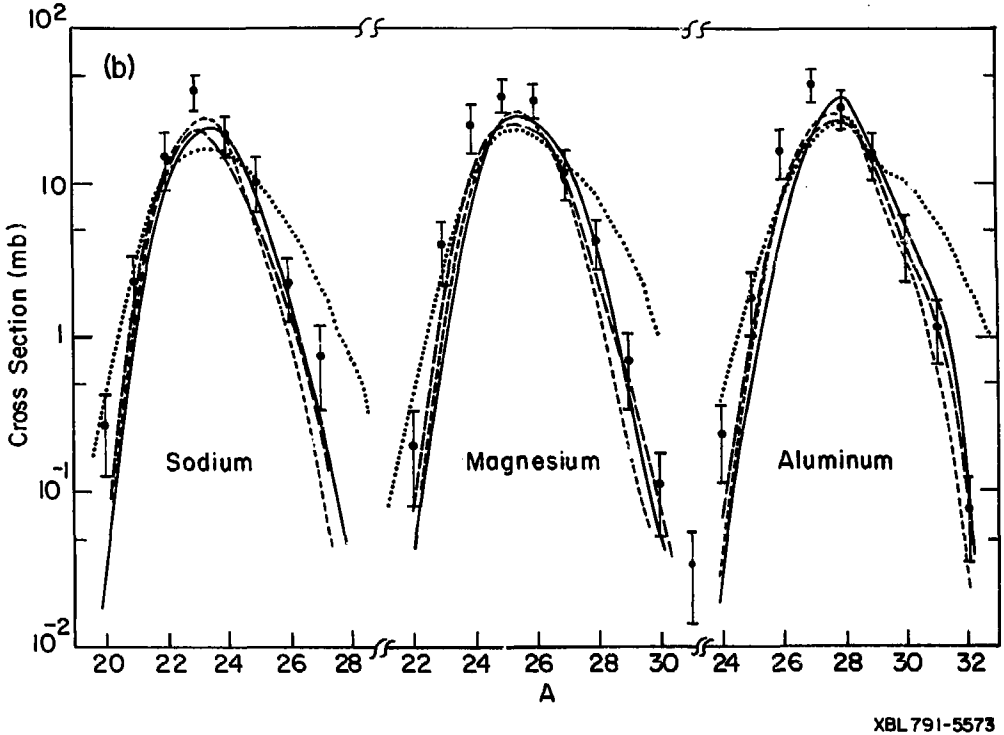
(b)
Cross Section (mb)
10^2
10
1
10^{-1}
10^{-2}
Sodium
Magnesium
Aluminum
20 22 24 26 28
22 24 26 28 30
24 26 28 30 32
A
XBL 791-5573

Fig. IV.11(b)

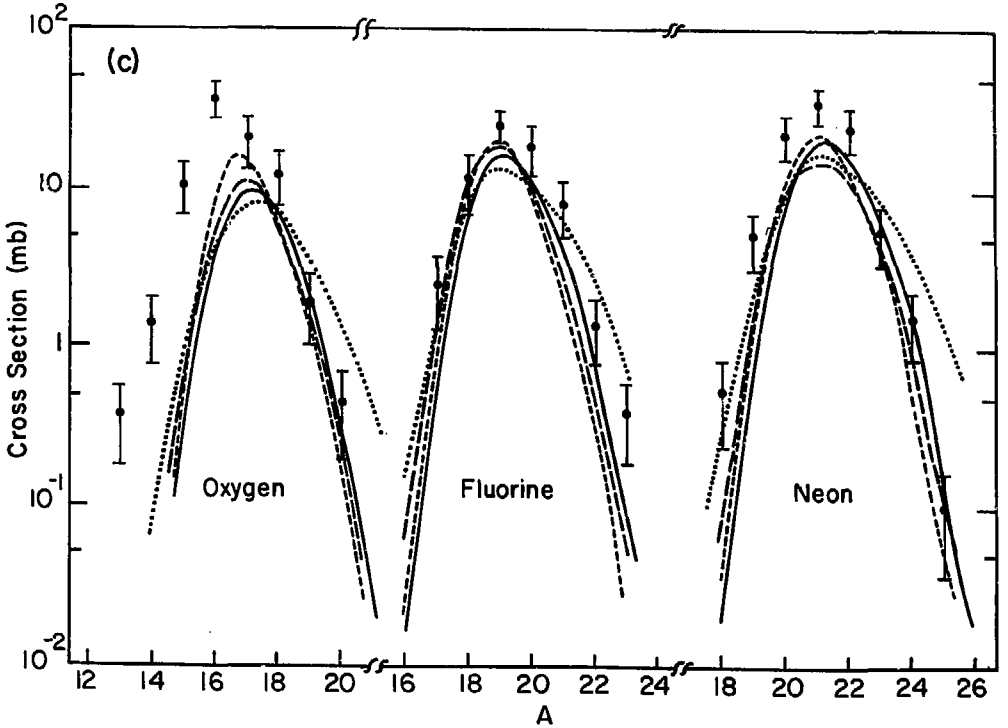

XBL791-5574

Fig. IV.11(c).

before the oxygen isotopes with mass numbers lower than 19 had been completely filled. We proceeded that way because the evaporation calculations become less reliable at low mass numbers.

iii) There are no significant differences between the two calculations with the additional excitation energy (traced lines), and both curves can describe the width and peak of the distributions fairly well. Let us mention that no attempt was made to fit any of the theoretical curves to the experimental points, despite the fact that the absolute normalization of the data is uncertain within a factor of two.[31]

In summary, what can we conclude from the curves on Fig. IV.11? Points i) and ii) seem to indicate that indeed nuclear ground state correlations, such as that of the giant dipole resonance (isospin correlation), can be seen in high-energy projectile fragmentation results. But what happens if more excitation energy is pumped into the primary fragments? In this case, iii) points in the opposite direction, i.e., the differences between the two pictures (correlated and uncorrelated) are washed out by the evaporation stage. Therefore, both traced curves would mainly reflect the shape of the valley of β-stability. But the doubt still persists since we cannot justify the inclusion of FSI at a bombarding energy of 200 MeV/A, as we explained before.

One experiment which could shed some light on this question, and possibly settle the above doubt once and for all, is the planned experiment with the ^{48}Ca beam at the Bevalac.[58] In Fig. IV.12 we present

the results of our calculations for the isotopic yield distributions of sulphur, chlorine and argon,[69] produced by the fragmentation of ^{48}Ca on ^{12}C. Because ^{48}Ca is such an unusual stable light nucleus (N/Z = 1.4), the effects of the evaporation stage (valley of β-stability) should be more strongly manifested than in the case of ^{40}Ar. Indeed, this can be easily seen in Fig. IV.12. The arrows in that figure indicate the N/Z value of the projectile, which is the position of the peak of the corresponding primary product distributions for each of these elements. After the evaporation stage the peaks of the Nuc-GDR mass yield distributions are shifted an average of 2.6 mass units (for the three elements shown) from the projectile N/Z towards the β-stability line. Furthermore, if additional excitation (FSI) is included in the calculations the peaks are again shifted another mass unit in the same direction. The dashed lines become clearly separated from the solid lines (compare with the situation in Fig. IV.11(a)). This means that the data could be capable of discerning between the two situations. Besides predicting different peaks and shapes, the pure abrasion-ablation calculation with the Nuc-GDR charge dispersion (solid lines) gives absolute isotope production cross sections which are substantially different from those predicted by the inclusion of additional excitation energy for most isotopes. Therefore it is very important that the experimental overall normalization be less uncertain than that of the ^{40}Ar experiment.

Using the abrasion-ablation model to calculate isotope production cross sections from the fragmentation of very heavy nuclei, Bondorf, Fai and Nielsen have concluded that some correlation effects are still visible after the evaporation stage has occurred. Among the light

Fig. IV.12. Theoretical results for the mass distributions of some elements produced in the fragmentation of a high-energy ^{48}Ca beam incident on ^{12}C target. Numerical results for all elements from Al to Ar are tabulated in Appendix B.

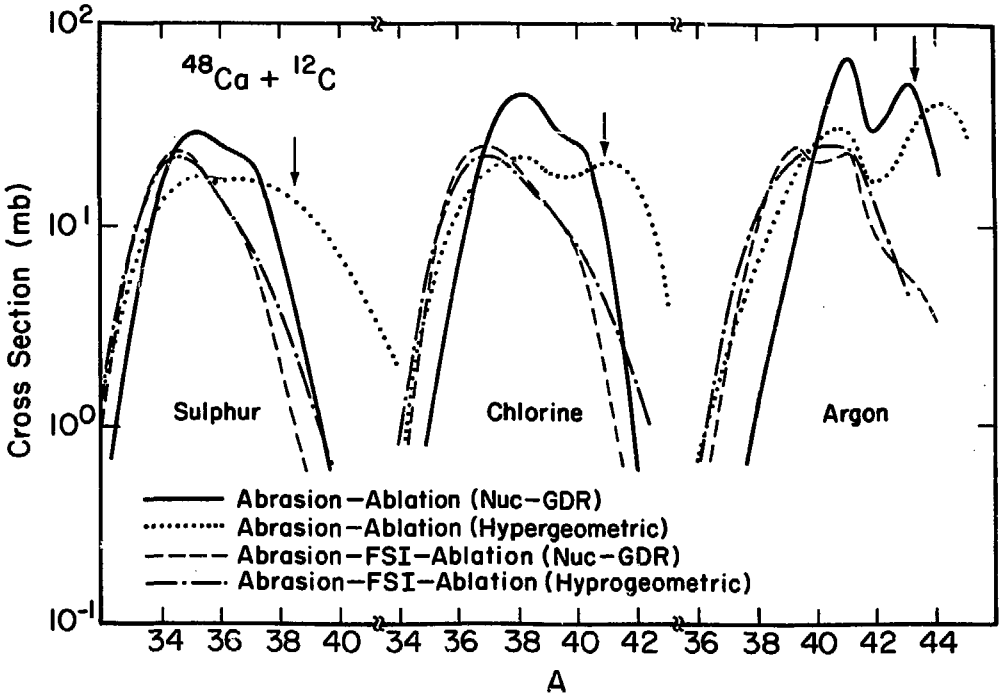

XBL 791-8102

Fig. IV.12

stable nuclei, ^{48}Ca (N/Z = 1.4) is the one most resembling the heavier isotopes (^{208}Pb, N/Z = 1.54), and the fact that correlation effects can be observed in the ^{48}Ca fragmentation cross sections is consistent with the conclusions of Ref. 25.

Let us now turn our attention to another very interesting aspect of the ^{40}Ar and ^{48}Ca fragmentation experiments being described in this section: the production of neutron-rich exotic light nuclei.

Until now the production of neutron-excess light nuclei has been achieved mainly in two types of experiments: heavy-ion multinucleon transfer reactions[70] and spallation of heavy nuclei by high energy protons.[71,72] In both techniques the exotic reaction products appear with low laboratory energy making them difficult to detect.

In the case of high energy projectile fragmentation, the exotic nuclei are produced in peripheral collisions, and we have already seen (Chapter I) that the products of a peripheral collision emerge with the full beam velocity, close to 0° in the laboratory. Therefore, they are suitable for detecting by using conventional ΔE-E telescopes and time-of-flight techniques.[73]

By combining a zero degree magnetic spectrometer[74] and two detector telescopes mounted in the focal plane of the spectrometer, Symons et al[32] were able to detect three new exotic nuclei (^{35}Al, ^{33}Mg, and ^{28}Ne -- see Fig. IV.13)[75] produced in the fragmentation of 205 MeV/nucleon ^{40}Ar by a carbon target. They also confirmed the particle stability of six neutron-rich nuclei that have been observed previously only in a single experiment.

Within the context of the abrasion-ablation model, a nucleus such as ^{35}Al could possibly be produced from an ^{40}Ar projectile through the

Fig. IV.13. Exotic light nuclei predicted to be found in the fragmentation of a high-energy ^{48}Ca beam. For the numerical values of the predicted cross sections see Table IV.4.

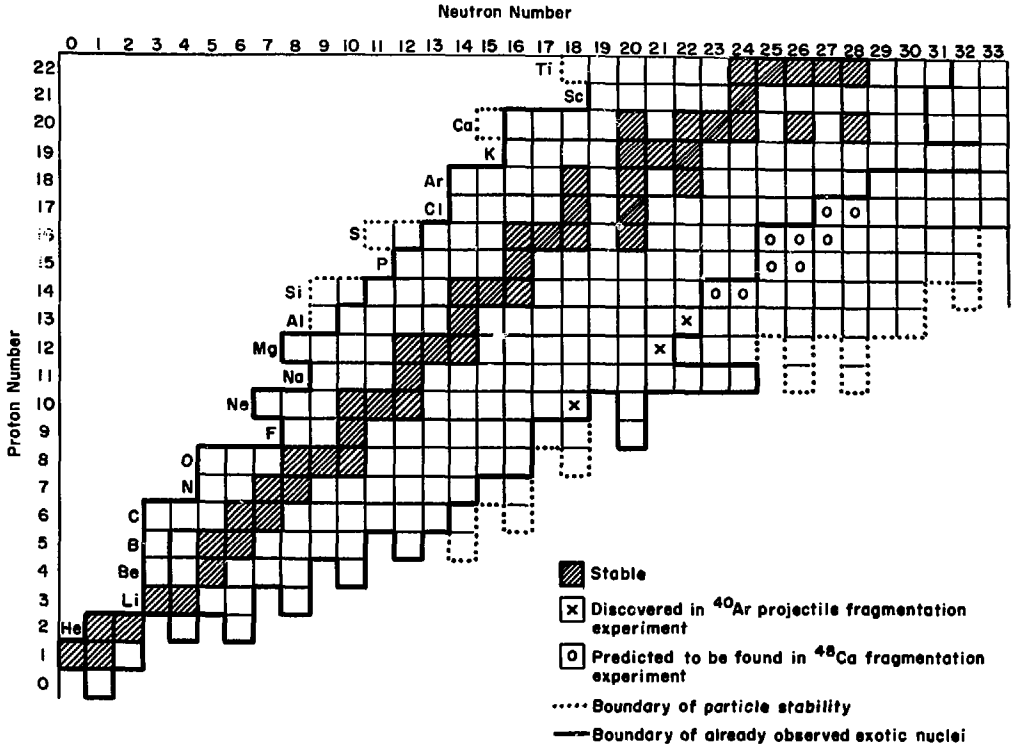
Neutron Number
Proton Number
He
Li
Be
B
C
N
O
F
Ne
Na
Mg
Al
Si
P
S
Cl
Ar
K
Ca
Sc
Ti
Stable
Discovered in ^{40}Ar projectile fragmentation experiment
Predicted to be found in ^{48}Ca fragmentation experiment
Boundary of particle stability
Boundary of already observed exotic nuclei

XBL 791-8107

scraping of three protons in the fast process and the subsequent evaporation of two other protons from the excited ^{37}P primary fragment. Of course, such a process has a very small cross section (tens of nanobarns).

As a modest contribution to the upcoming ^{48}Ca projectile fragmentation experiment[58] we would like to present some predictions for production of new exotic nuclei. Because of the unusual position of ^{48}Ca in the chart of nuclides, our calculations indicate that at least nine new neutron-rich isotopes (indicated by a circle in Fig. IV.13) may be observed. Their predicted numerical cross sections are given in Table IV.4. Comparing the results of columns 3 and 4 we see that the abrasion-FSI-ablation with the Nuc-GDR charge dispersion predicts values which are at least one order of magnitude lower than those calculated with the hypergeometric distribution. This is clearly an effect of the restrictions imposed on the primary product distributions by the Nuc-GDR distribution, for many exotic primary products, which would decay to the final exotic nuclei, cannot be produced under such restrictions. That effect survived the evaporation stage (even with the FSI energy included), and could be used to distinguish between the two charge dispersions. But, of course, this is a very difficult experimental task because of the smallness of those cross sections.

TABLE IV.4. Cross sections (μb) for production of exotic nuclei in the fragmentation of ^{48}Ca by ^{12}C predicted by the abrasion-ablation model.

Exotic nucleus	Abr-Abl (Nuc-GDR)	Abr-FSI-Abl (Nuc-GDR)	Abr-FSI-Abl (Hypergeometric)
^{45}Cl	<0.01	0.01	8.
^{44}Cl	0.03	0.6	75.
^{43}S	0.2	0.02	0.1
^{42}S	2.3	0.3	2.8
^{41}S	30.0	5.0	34.
^{41}P	<0.01	<0.01	0.07
^{40}P	0.3	0.1	1.5
^{38}Si	<0.01	0.01	0.6
^{37}Si	2.1	0.4	6.0

V. FIRESTREAK ABRASION

V.I Introduction

In this chapter we explore the possibility of using the geometrical and kinematical assumptions of the firestreak model of Myers[20,21] to calculate the abrasion stage of a high-energy heavy-ion reaction. In this model the colliding nuclei are subdivided into infinitesimal streaks (or tubes) parallel to the direction of the incoming projectile (see Fig. II.2). Assuming straight-line trajectories, each projectile tube collides with the target tube directly in its path for a given impact parameter. The streak-on-streak collisions are assumed to be completely inelastic, with the matter within each composite streak assumed to thermally equilibrate all energy in excess of the translational kinetic energy for momentum-conserving center-of-mass motion of the streak.

Each composite tube is completely characterized by the parameter

$$\eta_p = \frac{m_p}{m_p + m_T} \tag{1}$$

where m_p and m_T are, respectively, the amount of projectile and target material in the tube.

The novelty of this approach is that it recognizes the existence of a velocity shear across the overlap zone which depends locally on η, whereas the fireball model does not. Another advantage of the firestreak model is that it permits the use of a more realistic diffuse nuclear density distribution rather than the sharp sphere density imposed by the fireball model.

In section V.2 we give a detailed description of the geometrical and kinematical calculations, and explain how the abrasion cross sections are calculated. Results for the primary product mass distributions and excitation energies are presented and compared to the corresponding fireball abrasion results. In section V.3 we also present results for the final product distributions and discuss the problems encountered in this approach. Possible solutions to those problems are also discussed in the same section.

V.2 Firestreak Abrasion: Geometry and Kinematics

Let us assume a projectile (Z_P, A_P) is aimed at a target (Z_T, A_T) with a given impact parameter b. Let us calculate here the cross section and excitation energy of the target primary fragments, but as we have pointed out before, the calculations apply equally well to the projectile primary fragments by simply exchanging the subscripts P and T in the following equations.

By numerically integrating the target and projectile densities inside a streak one calculates η_P of each streak. This was done by projecting the density distributions onto the x-y plane and using a grid point space of 0.2 fm for the x- and y-integrations. The density distributions used here were obtained by folding a Yukawa function into the equivalent sharp spherical distribution.[20] This procedure gives

$$\rho(r) = \rho_0 \begin{cases} \left[1 - \left(1 + \frac{R}{a}\right) e^{-R/a} \frac{\sinh(r/a)}{r/a}\right], & r < R \\ \left[\frac{R}{a}\cosh(R/a) - \sinh(r/a) \frac{e^{-r/a}}{r/a}\right], & r > R \end{cases} \tag{2}$$

where $R = 1.2\ A^{1/3}$ and $a = \sqrt{\tfrac{1}{2}}$.

Once η_p of a streak is obtained, the laboratory momentum (per particle) of the streak is given by

$$P_s = \eta_p[t_p(t_p + 2m)]^{\frac{1}{2}} \tag{3}$$

and its total energy (per particle) by

$$E_s = m + \eta_p t_p \tag{4}$$

where t_p is the lab kinetic energy (per nucleon) of the projectile and m is the bound nucleon mass. Using Eqs. (3) and (4) we can express the rest mass of the streak in terms of η as

$$\begin{aligned} M &= (E_s - P_s)^{\frac{1}{2}} \\ &= m\left[1 + 2\eta_p(1-\eta_p)\frac{t_p}{m}\right]^{\frac{1}{2}} \quad . \end{aligned} \tag{5}$$

The internal energy per particle t_s of a streak is obtained from Eq. (5) by subtracting the bound nucleon mass

$$t_s = m\left[1 + 2\eta_p(1-\eta_p)\frac{t_p}{m}\right]^{\frac{1}{2}} - m \quad . \tag{6}$$

From Eq. (6) we see that t_s depends only on η and on the lab kinetic energy of the projectile.

Escaping Tube Criterion

To determine which composite streaks are retained in the target spectator and which ones join the escaping firestreak mass we use the following escaping tube criterion: all composite tubes which have an

internal energy per particle less than a critical value ε_c remain in the target spectator (primary products), otherwise they escape. Since the internal energy per particle, t_s, [Eq. (6)] depends only on the parameter η_p at a given projectile lab energy, one can easily calculate the critical value η_p^c by making $t_s = \varepsilon_c$ in Eq. (6). Therefore, our criterion can be more generally written in terms of the parameter η_p of each composite streak:

$$\begin{aligned} \eta_p &< \eta_p^c && \text{target spectator} \\ \eta_p^c < \eta_p &< 1 - \eta_p^c && \text{escaping firestreak} \qquad (7) \\ \eta_p &> 1 - \eta_p^c && \text{projectile spectator} \end{aligned}$$

We think that ε_c should be the order of the average binding energy per nucleon (8 MeV), but we have also performed calculations for higher values of ε_c and the results are discussed in the next section.

The excitation energy of each primary product is calculated by adding the excitation energy of all tubes which are retained in the target spectator. This excitation energy is then assumed to thermalize in the target spectator.

Using the above criterion we constructed two functions of the impact parameter b: $A_{T'}(b)$ and $E^*_{T'}(b)$. The former gives the mass number of the surviving spectator fragment and the latter its excitation energy. From the inverse function $b(A_{T'})$ we calculated the abrasion cross section for production of a primary fragment of mass $A_{T'}$ by the same procedure used for the fireball abrasion, i.e.

$$\sigma(A_{T'}) = \pi\left[b(A_{T'} - 0.5)^2 - b(A_{T'} + 0.5)^2\right] \quad . \qquad (8)$$

The excitation energy of $A_{T'}$ is determined from $E^*_{T'}(b)$ by interpolating at the corresponding $b(A_{T'})$. Once the abrasion cross sections and excitation energies are calculated, one can obtain the final product distribution by following either one of the procedures illustrated in Figs. IV.1 and IV.5.

V.3 Discussion

In Table V.1 we present the abrasion cross sections and excitation energies obtained with the firestreak geometry and kinematics for the cases of $^{56}Fe + ^{12}C$ at 1.8 GeV/nuc and $^{12}C + ^{40}Ca$ at 0.4 GeV/nuc. Results for values of ε_c equal to 8, 12, 16, 20, 30 and 40 MeV/nuc are listed in that table. The most realistic case should be that of $\varepsilon_c = 8$ MeV/nuc, i.e., a composite tube is ejected from the spectator if its excitation energy per particle is higher than the average binding energy per nucleon. It is evident from the table that the cross sections are far too large, even for $\varepsilon_c = 8$ MeV/nuc. Indeed, the total firestreak reaction cross sections (shown at the bottom of the table) are much higher than the experimental[76] or calculated[47,48] ones, which are slightly less than the geometrical cross sections. It is true that by taking higher values of ε_c the cross sections decrease, for it becomes more difficult to eject a streak from the spectator, but even for $\varepsilon_c = 40$ MeV/nuc, that decrease is not very significant (as can be seen from Table V.I). On the other hand, the excitation energy distribution is very sensitive to the value of ε_c, increasing very quickly with higher values of ε_c. As a consequence of the higher excitation energies, no fragments close to the target would survive in any significant amount,

a result which certainly contradicts the experimental observations.

The large cross section values are a direct consequence of the assumption of completely inelastic collisions and the diffuse tail of the nuclear density. It is obvious from the results in Table V.1 that some modification has to be introduced into the firestreak model to account for the fact that peripheral collisions which involve tubes situated in the diffuse tail cannot be treated as totally inelastic, particularly at bombarding energies above 1 GeV/nuc.

One simple way out of this difficulty is to assume sharp rather than diffuse nuclear densities,[19] but then the firestreak calculations give only a very slight improvement over the fireball abrasion-ablation results, because with the very low η_p^c used in the firestreak abrasion calculations the vast majority of the composite tubes leave the target spectator. This is exactly what is assumed in the fireball abrasion, i.e., all target nucleons in the overlap zone are ejected from the target.

As cautioned by Myers,[20] nuclear matter transparency effects become important at very high energies. A more refined change to the firestreak abrasion assumptions is to allow for transparency effects, particularly for the tail tube collisions. This can be done by relaxing the assumption of complete inelasticity, and assuming instead the streak-on-streak collisions to be collisions with friction.

The projectile tube loses energy while passing through the target tube which becomes excited. The rate at which energy is transferred can be estimated from the equation used before, $dE/dx = - \alpha E/\lambda$, with the appropriate value of α. At high energies a projectile tube may pass

through the target without being captured. The corresponding target tube would be excited, but possibly not sufficiently excited to be ejected from the target. This effect should tend to decrease the abrasion cross sections. Unfortunately, our preliminary calculations have shown this effect to be small, and the cross sections to be about the same as those for the completely inelastic case. Nevertheless, further investigations along these lines are currently going on.

TABLE V.1. Firestreak abrasion cross sections (mb) and excitation energies (MeV) for several values of ε_c (MeV/nuc).

$^{56}Fe + {}^{12}C$ (1.8 GeV/nuc)

$A_{p'}$	$\varepsilon_c = 8$		$\varepsilon_c = 12$		$\varepsilon_c = 16$	
	$\sigma_{A_{p'}}$	$E^*_{A_{p'}}$	$\sigma_{A_{p'}}$	$E^*_{A_{p'}}$	$\sigma_{A_{p'}}$	$E^*_{A_{p'}}$
55	1103	8	1017	12	1010	17
54	369	15	354	20	331	26
53	246	20	225	28	224	38
52	192	23	205	35	201	48
51	183	27	129	40	119	53
50	114	30	127	43	126	57
49	112	31	101	46	103	61
48	100	33	105	48	95	65
47	85	35	102	53	92	69
46	91	36	80	57	87	75
45	74	38	71	59	73	80
44	70	39	69	61	62	82
43	69	41	58	62	59	84
42	67	42	60	63	60	86
41	62	44	60	65	55	89
σ_{tot}	3925		3474		3576	

TABLE V.1 (continued)

$^{56}Fe + {}^{12}C$ (1.8 GeV/nuc)

$A_{p'}$	$\varepsilon_c = 20$		$\varepsilon_c = 30$		$\varepsilon_c = 40$	
	$\sigma_{A_{p'}}$	$E^*_{A_{p'}}$	$\sigma_{A_{p'}}$	$E^*_{A_{p'}}$	$\sigma_{A_{p'}}$	$E^*_{A_{p'}}$
55	906	21	987	34	935	47
54	430	35	344	57	343	80
53	213	49	215	75	243	101
52	175	56	181	93	142	126
51	150	70	130	100	124	136
50	119	74	118	108	117	147
49	95	79	107	122	95	162
48	94	83	99	133	109	181
47	81	88	74	141	67	192
46	77	91	68	145	71	192
45	77	97	67	150	63	206
44	66	102	62	156	58	213
43	61	105	58	161	57	219
42	63	110	54	165	53	227
41	54	115	50	169	49	234
σ_{tot}	3497		3387		3244	

TABLE V.I (continued)

$^{12}C + ^{40}Ca$ (400 MeV/nuc)

$A_{p'}$	$\varepsilon_c = 8$		$\varepsilon_c = 12$		$\varepsilon_c = 16$	
	$A_{p'}$	$E^*_{A_{p'}}$	$\sigma_{A_{p'}}$	$E^*_{A_{p'}}$	$\sigma_{A_{p'}}$	$E^*_{A_{p'}}$
39	788	9	860	14	840	18
38	375	14	320	24	307	32
37	205	20	220	30	201	38
36	144	21	127	37	141	48
35	151	25	120	40	112	53
334	104	28	105	43	100	56
33	88	30	89	47	87	61
32	79	31	89	50	75	65
31	78	33	71	56	69	67
30	67	35	60	57	68	72
29	58	35	62	59	57	76
28	59	36	52	62	52	78
27	56	38	47	62	51	81
26	51	39	47	64	45	85
25	46	40	43	65	39	86
σ_{tot}	3780		2692		2594	

TABLE V.1 (continued)

$^{12}C + ^{40}Ca$ (400 MeV/nuc)

$A_{p'}$	$\varepsilon_c = 20$		$\varepsilon_c = 30$		$\varepsilon_c = 40$	
	$A_{p'}$	$E^*_{A_{p'}}$	$A_{p'}$	$E^*_{A_{p'}}$	$\sigma_{A_{p'}}$	$E^*_{A_{p'}}$
39	820	24	772	43	654	56
38	301	42	272	64	284	87
37	181	51	174	85	142	117
36	148	62	121	96	129	137
35	103	69	111	108	120	160
34	100	74	95	122	72	175
33	73	79	78	133	77	184
32	78	85	68	138	56	195
31	69	86	62	148	59	200
30	62	96	52	153	58	216
29	47	96	46	157	44	224
28	55	98	44	159	42	231
27	48	106	45	165	37	235
26	38	105	43	173	37	342
25	39	107	37	180	31	248
σ_{tot}	2499		2296		2073	

VI. CONCLUSIONS

In this thesis we have applied the abrasion-ablation model to the problem of calculating the isotopic and elemental production cross sections resulting from the fragmentation of relativistic heavy-ions. Two different models (fireball and firestreak) were used to describe the fast abrasion process, and a subroutine (EVAPOR), which performs standard statistical evaporation of nucleons, deuterons and alphas, was used to obtain the final isotopic yields.

The primary product distributions obtained with the simple fireball abrasion models were compared to those predicted by the multiple scattering abrasion of Hüfner et al.[22,23,42] The results of the two calculations were shown to be in good agreement except for the most peripheral collisions which involve the removal of one nucleon from the target or projectile.

Elemental and isotope production cross sections obtained with the fireball abrasion plus statistical evaporation model were compared to a variety of fragmentation experimental data. The calculated yields for the elements with masses very close to the target (or projectile) mass were shown to be much higher than the data. The reason for this lack of agreement was considered to be the low values of the primary product excitation energy, as calculated assuming only an excess surface contribution. This led us to introduce a frictional spectator interaction (FSI) in the calculations. The FSI process takes into account the energy lost by a struck nucleon that happens to go through the spectator pieces. This increases the average excitation energy of the primary products and improves the results considerably in most cases.

The possibility of observing nuclear ground state correlations was explored through the use of two different charge-to-mass dispersions: one which considers no correlation between the proton and neutron distributions inside the nucleus (hypergeometric distribution) and one which is based on the zero-point oscillations of the giant dipole resonance[24] (Nuc-GDR). Isotope production cross sections obtained with these two charge dispersions were compared to the ^{40}Ar (213 MeV/nucleon) fragmentation of Viyogi et al.[31] The mass distributions (for each element) predicted by the abrasion-ablation (without FSI) with the Nuc-GDR charge dispersion are shown to be in good agreement with the measured mass distributions, whereas those calculated with the hypergeometric charge dispersion are much broader than the data. This fact by itself would indicate that the correlation effects survived the evaporation stage, but by artificially adding more excitation energy to the primary products we have shown that the new mass distributions predicted by the two charge dispersions agree with each other and with the data (neglecting the overall normalization since the data is uncertain by a factor of two). We have concluded that the ^{40}Ar data cannot answer unambiguously to the question raised by Bondorf, Fai and Nielsen[25] on the possibility of observing ground state correlations in RHI fragmentation reactions. However, we have shown that the predictions of the different theoretical assumptions for the mass distributions resulting from a ^{48}Ca fragmentation experiment are sufficiently different as to allow one to distinguish the correlation effects and possibly to answer the question of how much excitation energy is pumped into the primary products. The advantage of ^{48}Ca lies in its unusual position with respect to the valley of beta stability.

Primary product cross sections calculated with the diffuse fire-streak abrasion model were shown to be exceedingly high as compared to experimental data. We have concluded that this is a direct consequence of the assumption of completely inelastic tube-on-tube collisions. It is our opinion that this assumption cannot be valid for the most peripheral collisions because nuclear matter transparency effects are not taken into account.

To conclude this work we would like to quote from a great theoretician (and a good friend of ours). In presenting his model calculations in a seminar during the NATO/NSF Advanced Studies Institute in Madison, Wisconsin, he said: "This model has no free parameters other than the model itself." His words apply equally well to our calculations, but we would like to remark that one should not give up trying to find simple methods and models even when more complicated computer codes can fit the data well. To really understand a subject, simple methods and models are of great importance because of the greater transparency implied in their simplicity. The abrasion-ablation model does not only satisfy this criterion, but also gives often a quantitative description of the problem.

APPENDIX A
DERIVATION OF THE Nuc-GDR CHARGE DISPERSION

The derivation contained in this Appendix is an extended version of that presented in Ref. 24, whose authors we would like to thank for kindly allowing us to include it in this work.

In order to have a specific frame of reference, all equations in this Appendix are written in terms of the target participant and spectator nucleons, but they are obviously valid for the projectile as well.

The basic assumption of the Nuc-GDR charge dispersion is that in a "clean-cut" sudden interaction such as that implied in the fireball abrasion picture, the fluctuations in the number of participant target protons are due to zero point vibrations of the giant dipole resonance of the target nucleus. In the Goldhaber-Teller picture,[77] the giant dipole resonance is described as an out-of-phase vibration of the neutrons against the protons. Studying the GDR in terms of the droplet model of the nucleus,[78] Myers et al derived a harmonic oscillation (HO) potential to describe the motion of the neutrons against the protons, which can be approximated by

$$V(\alpha) \approx \tfrac{1}{2} C \alpha^2 \tag{A.1}$$

with

$$C = \frac{2}{3} Q A^{4/3} \frac{u}{1+u} \tag{A.2}$$

and

$$u = \frac{3J}{Q A^{1/3}} \tag{A.3}$$

where A is the target mass number, J is the nuclear symmetry energy

coefficient and Q is the effective neutron skin stiffness. Here J and Q are taken as 25.76 MeV and 11.9 MeV, respectively, which correspond to 70% of the values quoted in Ref. 78. The smaller values of J and Q used here are meant to compensate for the fact that Myers et al[78] had to use an effective nucleon mass $m^* = 0.7\,m$ in order to obtain good agreement with the measured values of the mean energy of the GDR.

The zero-point frequency of the HO [Eq. (A.1)] is given by[78]

$$\omega_o = \left(\frac{8J}{m}\right)^{1/2} [r_o A^{1/3} (1+u)^{1/2}]^{-1} \tag{A.4}$$

where r_o is the nuclear radius parameter taken as 1.18 fm and m is taken to be 938.9 MeV, the average of the neutron and proton rest masses. Myers et al[78] have also shown that the relativistic displacement of centers of the neutron and proton spheres d in the GT mode of the GDR can be approximately written

$$d = \frac{u}{1+u}\,\alpha R \tag{A.5}$$

where R is the radius of the vibrating nucleus ($R = r_o A^{1/3}$).

The classical turning point of the zero point oscillation, i.e., the maximum displacement from the origin can be easily obtained from

$$E = T + V = V = 1/2\, C\, \alpha^2 \tag{A.6}$$

or

$$\alpha_{CTP} = \sqrt{2E/C}\,. \tag{A.7}$$

In quantal notation the zero point energy is given by

$$E_o = 1/2\, \hbar\omega_o \quad , \tag{A.8}$$

Therefore, semiclassically one obtains

$$\alpha_{CTP} = \sqrt{\frac{\hbar\omega_o}{C}} \tag{A.9}$$

Substituting ω_o from Eq. (A.4) into Eq. (A.9),

$$\alpha_{CTP} = \left[\frac{\hbar}{r_o A^{1/3}} \left(\frac{8J}{m}\right)^{1/2} \frac{1}{C(1+u)^{1/2}}\right]^{1/2}$$

$$= \left[\frac{\hbar C}{r_o A^{5/3}} \left(\frac{8J}{mC^2(1+u)}\right)^{1/2} \frac{3(1+u)}{2Qu}\right]^{1/2}$$

$$= \left[\frac{\hbar C}{r_o A^{5/3}} \frac{3}{2Q} \left(\frac{8J}{mC^2} \frac{(1+u)^2}{(1+u)u^2}\right)^{1/2}\right]^{1/2}$$

or

$$\alpha_{CTP} = \left[\frac{3}{2Q} \frac{\hbar C}{r_o} A^{-5/3} \left(\frac{8J}{mC^2} \frac{1+u}{u^2}\right)^{1/2}\right]^{1/2} . \tag{A.10}$$

Substituting the numerical values one obtains

$$\alpha_{CTP} = \frac{3.139}{A^{5/6}} \left(\frac{1+u}{u^2}\right)^{1/4} . \tag{A.11}$$

Substituting Eq. (A.11) into Eq. (A.5), one obtains

$$d_{CTP} = \frac{3.704}{A^{1/2}} \left(\frac{u^2}{(1+u)^3}\right)^{1/4} . \tag{A.12}$$

The distribution in displacements of the neutrons relative to the protons can be obtained from the displacement expectation values using the wave function for the lowest state of the harmonic oscillator

represented in Eq. (A.1), i.e.,

$$\psi_o(\alpha) = N_o e^{-y^2/2} \tag{A.13}$$

where

$$y = \left(\frac{m\omega_o}{\hbar}\right)^{1/2} \alpha = \left(\frac{C}{\hbar\omega_o}\right)^{1/2} \alpha = \frac{\alpha}{\alpha_{CTP}} \quad . \tag{A.14}$$

The probability of finding the system at a given α is

$$|\psi_o(\alpha)|^2 = N_o^2 e^{-y^2} = N_o^2 e^{-\alpha^2/\alpha_{CTP}^2} \quad . \tag{A.15}$$

Similarly, in d coordinate one obtains

$$|\psi_o(d)|^2 = \text{const} \times e^{-d^2/d_{CTP}^2} \quad . \tag{A.16}$$

Equation (A.16) is a Gaussian of width

$$\sigma_{disp} = \frac{d_{CTP}}{\sqrt{2}} \quad . \tag{A.17}$$

Substituting d_{CTP} from Eq. (A.12), σ_{disp} can be written as

$$\sigma_{disp} = \frac{2.619}{A^{1/2}} \left(\frac{u^2}{(1+u)^3}\right)^{1/4} \quad . \tag{A.18}$$

Once the width of the distribution in displacements of the protons relative to the neutrons σ_{disp} has been obtained, one can say that the width of dispersion in the number of target protons removed in the "instantaneous clean-cut" of the RHI interaction at a given impact parameter is given by

$$\sigma_Z = \sigma_{disp} \left(\frac{da_T}{db}\right) \frac{Z_T}{A_T} \tag{A.19}$$

where da_T/db is the rate of change of the number of nucleons removed with impact parameter.

APPENDIX B

Tables of ^{40}Ar and ^{48}Ca Fragmentation Cross Sections

In this Appendix we present two tables with numerical results of our calculations. The organization of the tables is as follows:

Table C-1 contains the calculated and experimental isotope production cross sections from the fragmentation of ^{40}Ar incident on a ^{12}C target. The experimental values are those of Ref. 31. The four columns of theoretical results correspond to the following calculations:

Hyperg — pure abrasion-ablation with hypergeometric charge dispersion (scheme of Fig. IV.1),

Hyperg + FSI — abrasion-FSI-ablation with hypergeometric charge dispersion (scheme of Fig. IV.5),

Nuc-GDR — pure abrasion-ablation with Nuc-GDR charge dispersion,

Nuc-GDR +FSI — abrasion-FSI-ablation with Nuc-GDR charge dispersion.

Table C-2 contains our predictions to the isotope production cross sections to be observed in the fragmentation experiment with a 250 MeV/nuc ^{48}Ca beam incident on a ^{12}C target. The organization of this table is the same as that of Table C-1.

TABLE C.1. Isotope production cross sections (in mb) for the fragmentation of ^{40}Ar (213 MeV/nuc) in a ^{12}C target.

Z_F	A_F	Hyperg.	Hyperg + FSI	Nuc-GDR	Nuc-GDR + FSI	Experiment[31]
	38	31.9			0.17	2.1 ±1.2
	37	38.0	1.03	1.1	1.7	9.8 ±5.0
	36	43.5	17.7	39.2	15.7	19.3 ±8.7
16	35	49.7	26.4	86.1	31.3	27.3±11.0
	34	31.5	33.0	47.7	35.4	58.0±17.4
	33	7.8	18.4	4.2	18.7	27.5±11.0
	32	6.3	3.6	1.8	2.1	9.0 ±4.5
	31	1.7	0.36	0.20	0.13	0.98±0.6
	35	16.3	2.7	3.3	0.82	
	34	16.8	9.8	15.0	7.8	1.5 ±0.7
	33	21.4	27.8	22.4	26.1	8.7 ±3.5
15	32	36.9	33.8	51.8	40.3	33.0 ±9.0
	31	20.8	16.3	19.9	17.0	41.5±10.4
	30	4.6	4.8	2.0	3.7	27.0 ±8.1
	29	1.1	0.5	0.15	0.28	10.4 ±3.5
	34	3.7	0.21	0.36	0.11	0.32±0.16
	33	9.3	1.3	0.82	0.73	1.3 ±0.6
	32	14.4	6.8	8.0	4.3	8.2 ±3.2
	31	22.2	15.3	29.7	15.1	16.8 ±5.9
14	30	21.2	25.0	26.3	26.8	49.5±12.4
	29	19.0	20.3	20.2	21.2	42.5±10.6
	28	9.3	6.4	5.0	5.4	22.4 ±6.7
	27	1.8	0.72	0.32	0.40	2.5 ±1.1
	26	0.25	0.05	0.02	0.02	0.25±0.13

(continued . . .)

TABLE C-1 (continued)

Z_F	A_F	Hyperg.	Hyperg + FSI	Nuc-GDR	Nuc-GDR + FSI	Experiment[31]
	25	1.1	0.11	0.12	0.04	0.52±0.29
	24	3.5	0.78	1.3	0.50	4.9 ±2.0
	23	8.3	4.1	6.2	3.5	21.7 ±6.5
	22	13.2	11.5	15.9	12.1	33.9 ±8.5
10	21	16.2	19.6	20.4	21.1	24.0 ±7.2
	20	8.8	11.9	7.9	12.7	5.4±2.2
	19	2.0	1.7	0.71	1.4	1.5±0.7
	18	0.31	0.09	0.02	0.04	0.09±0.06
	24	0.18				
	23	0.71	0.06	0.09	0.02	0.38±0.2
	22	2.3	0.43	0.7	0.30	1.34±0.6
	21	5.9	2.3	4.2	1.9	7.8 ±3.1
9	20	9.6	8.0	10.6	8.4	17.8 ±6.2
	19	12.5	17.0	15.9	19.9	23.9 ±6.0
	18	7.7	9.8	7.6	11.2	11.4 ±4.6
	17	1.4	1.4	0.4	1.1	2.4 ±1.2
	20	1.2	0.20	0.33	0.14	0.44±0.25
	19	3.5	1.4	2.1	1.1	1.9 ±0.86
	18	6.3	4.7	7.0	5.4	11.9 ±4.5
	17	7.2	10.1	9.2	14.3	20.0 ±7.0
8	16	3.8	5.3	3.7	7.1	36.2 ±9.0
	15	1.0	0.8	0.8	0.6	10.6 ±3.7
	14	0.07	0.03			1.4 ±0.6
	13					0.37±0.19

TABLE C-1 (continued)

Z_F	A_F	Hyperg.	Hyperg + FSI	Nuc-GDR	Nuc-GDR + FSI	Experiment[31]
	32	2.1	0.12	0.06	0.03	0.08±0.04
	31	5.7	1.0	1.8	0.51	1.2 ±0.5
	30	10.0	4.0	6.0	3.2	4.1 ±1.9
	29	14.5	10.2	15.0	9.6	15.3 ±9.0
13	28	25.5	24.1	36.5	25.9	42.6±10.7
	27	15.8	20.1	17.4	21.3	15.8 ±5.5
	26	7.1	8.1	4.4	7.7	1.7 ±0.8
	25	2.2	1.0	0.50	0.66	0.23±0.12
	24	0.37	0.06	0.03	0.03	0.034±0.02
	23	0.046				
	30	0.98	0.06	0.05	0.03	0.11±0.07
	29	3.3	0.46	0.40	0.17	0.67±0.34
	28	7.9	2.3	4.1	1.6	4.0 ± 1.4
	27	12.8	8.1	13.7	7.7	11.5 ± 4.0
12	26	18.7	20.1	24.7	21.4	33.0 ± 8.3
	25	19.9	22.1	24.8	23.6	36.0 ± 9.0
	24	9.1	9.7	7.3	9.5	23.0 ± 8.0
	23	2.2	1.3	0.64	1.0	3.8 ± 1.7
	22	0.37	0.08	0.03	0.04	0.2 ± 0.12
	27	2.1	0.26	0.31	0.1	0.27±0.15
	26	5.3	1.4	1.9	1.0	2.3 ± 1.0
	25	10.1	5.6	8.6	5.0	14.8 ± 5.9
	24	16.5	14.7	21.3	15.9	38.9 ± 9.7
11	23	16.6	22.0	20.3	23.8	20.3 ± 6.0
	22	10.0	11.4	9.0	11.6	10.3 ± 4.0
	21	2.5	1.6	0.9	1.2	2.2 ± 1.0
	20	0.37	0.09	0.02	0.04	0.76±0.42

(continued . . .)

TABLE C-2. Predicted isotope production cross sections (in mb) for the fragmentation of ^{48}Ca in a ^{12}C target.

Z_F	A_F	Hyperg.	Hyperg + FSI	Nuc-GDR	Nuc-GDR + FSI
	46	83.0	20.7	156.6	39.1
	45	57.1	25.2	108.1	27.8
	44	37.4	30.0	32.8	31.1
	43	11.9	45.6	2.1	36.7
19	42	12.2	33.1	1.9	54.1
	41	9.7	17.1		23.3
	40	2.7	8.6		7.5
	39	0.27	2.3		1.9
	38		0.18		
	45	28.0	0.7		
	44	40.2	1.3	22.2	3.3
	43	28.1	4.6	52.9	5.9
	42	16.1	12.5	30.5	8.8
	41	32.5	25.8	73.8	23.7
18	40	26.5	23.3	37.9	21.4
	39	16.4	21.2	7.4	24.0
	38	5.4	12.1	1.2	11.0
	37	3.5	4.2	0.2	2.7
	36	0.68	0.7		0.19
	43	3.9	0.35		
	42	15.9	1.2	0.63	0.21
	41	20.8	3.8	9.3	1.7
	40	18.1	7.7	26.3	7.7
	39	19.1	12.2	32.8	12.7
17	38	21.8	17.6	45.5	18.9
	37	18.4	22.4	27.7	25.1
	36	12.5	17.7	7.0	19.5
	35	4.0	6.2	1.0	5.6
	34	0.63	0.78		0.46

(continued . . .)

TABLE C-2 (continued)

Z_F	A_F	Hyperg.	Hyperg. + FSI	Nuc-GDR	Nuc-GDR + FSI
	40	6.5	0.30	0.19	
	39	12.0	1.3	1.9	0.38
	38	14.5	3.5	6.7	2.0
	37	16.3	8.1	20.4	7.9
16	36	16.3	13.7	23.8	13.9
	35	18.1	21.2	28.5	22.2
	34	13.5	19.2	15.9	20.4
	33	6.4	8.6	3.0	8.4
	32	1.4	1.3	0.16	0.96
	38	3.2	0.12	0.20	
	37	6.6	0.49	1.0	0.15
	36	9.7	1.7	4.9	0.89
	35	11.2	4.2	8.4	3.4
	34	15.8	10.4	19.6	11.0
15	33	17.4	17.3	23.5	19.0
	32	14.2	19.5	14.9	20.9
	31	6.7	10.3	4.8	10.4
	30	1.8	2.1	0.45	1.6
	29	0.24	0.13		
	35	3.0	0.17	0.35	
	34	6.3	0.79	2.2	0.39
	33	9.5	2.8	8.0	2.0
	32	12.6	7.1	14.5	6.6
14	31	15.0	13.8	21.0	15.2
	30	14.9	18.4	17.6	21.0
	29	8.5	10.6	6.1	11.1
	28	2.3	2.5	0.75	1.7
	27	0.3	0.14		

REFERENCES

1. P.Freier, E.J.Lofgren, E.P.Ney, F.Oppenheimer, H.L.Bradt, and B.Peters, Phys. Rev. 74 (1948) 213.
2. P.Freier, E.J.Lofgren, E.P.Ney, and F.Oppenheimer, Phys. Rev. 74 (1948) 1818.
3. M.G.White, M.Isaila, K.Prelec, and H.L.Allen, Science 174 (1971) 1121.
4. H.A.Grunder, W.D.Hartsough, and E.J.Lofgren, Science 174 (1971) 1128.
5. For information about other high energy heavy-ion accelerators (planned or in operation) see the review paper by A.S.Goldhaber and H.H.Heckman, Ann. Rev. Nucl. Part. Sci. 28 (1978) 161.
6. T.D.Lee and G.C.Wick, Phys. Rev. D9 (1974) 2291; T.D.Lee, Rev. Mod. Phys. 47 (1975) 267.
7. W.Scheid, H.Muller, and W.Greiner, Phys. Rev. Lett. 32 (1974) 741; H.Baumgardt, J.V.Scott, Y.Sakamoto, E.Schopper, H.Stocker, J.Hoffman, W.Scheid, and W.Greiner, Z. Phys. A273 (1975) 359.
8. A.B.Migdal, ZhETF (USSR) 61 (1971) 2209, Nucl. Phys. A210 (1973) 421; Phys. Lett. 45B (1973) 448, 47B (1973) 96, 52B (1974) 172, Phys. Rev. Lett. 31 (1973) 257.
9. P.J.Lindstrom, D.E.Greiner, H.H.Heckman, B.Cork and F.S.Bieser, Lawrence Berkeley Laboratory Report LBL-3650 (1975).
10. J.Papp, J.Jaros, L.Schroeder, J.Staples, H.Steiner, A.Wagner, and J.Wiss, Phys. Rev. Lett. 34 (1975) 601.
11. B.Cork, Talk presented at the Sixth Int. Conf. on High Energy Physics and Nuclear Structure, Albuquerque, New Mexico (1975), and LBL-4203.

12. S.Y.Fung, W.Gorn, G.P.Kierman, F.F.Liu, J.J.Lu, Y.T.Oh, J.Ozawa, R.T.Poe, C.Van Dalen, L.Schroeder, and H.Steiner, Phys. Rev. Lett. 40 (1978) 292.

13. H.H.Heckman, D.E.Greiner, P.J.Lindstrom, and D.D.Tuttle, "An Atlas of Heavy-Ion Fragmentation Topology," LBL, unpublished.

14. J.Gosset, H.H.Gutbrod, W.G.Meyer, A.M.Poskanzer, A.Sandoval, R.Stock, and G.D.Westfall, Phys. Rev. C16 (1977) 629.

15. D.K.Scott, LBL-7727, Lectures delivered at the NATO/NSF Advanced Studies Institute on Theoretical Methods in Medium-Energy and Heavy-Ion Physics, Madison, Wisconsin, June 12-23, 1978.

16. J.D.Bowman, W.J.Swiatecki, and C.F.Tsang, LBL-2908 (1973) unpublished.

17. G.D.Westfall, J.Gosset, P.J.Johansen, A.M.Poskanzer, W.G.Meyer, H.H.Gutbrod, A.Sandoval, and R.Stock, Phys. Rev. Lett. 37 (1976) 1202.

18. L.F.Oliveira, R.Donangelo, and J.O.Rasmussen, to be published in Phys. Rev. C.

19. J.Rasmussen, R.Donangelo, and L.F.Oliveira, Proceedings of the IPCR Symposium on Macroscopic Features of Heavy-IonCollisions and Pre-Equilibrium Processes, Hakone, Japan (1977) 440.

20. W.D.Myers, Nucl. Phys. A296 (1978) 177.

21. J.Gosset, G.D.Westfall, and J.I.Kapusta, Phys. Rev. C18 (1978) 844.

22. J.Hüfner, K.Schäfer, and B.Schürmann, Phys. Rev. C12 (1975) 1888.

23. J.Hüfner, Lectures delivered at the NATO/NSF Advanced Studies Institute on Theoretical Methods in Medium-Energy and Heavy-Ion Physics, Madison, Wisconsin, June 12-23 (1978).

24. D.J.Morrissey, W.R.Marsh, R.J.Otto, W.Loveland, and G.T.Seaborg, Phys. Rev. C18 (1978) 1267.

25. J.P.Bondorf, G.Fai and O.B.Nielsen, Phys. Lett. 41B (1978) 398.

26. J.P.Bondorf, G.Fai and O.B.Nielsen, Nucl. Phys. A312 (1978) 149.

27. W.J.Swiatecki, LBL (1976) unpublished.

28. Z.Fraenkel and Y.Yariv, private communication (to be published).

29. P.J.Lindstrom, D.E.Greiner, H.H.Heckman, B.Cork, and F.S.Bieser, LBL-3650 (1975) unpublished.

29a. H.H.Heckman, D.E.Greiner, P.J.Lindstrom, and F.S.Bieser, Phys. Rev. Lett. 28 (1972) 926.

30. T.Shibata, H.Ejiri, J.Chiba, S.Nagamiya, K.Nakai, R.Anholt, H.Bowman, J.G.Ioannou, E.A.Rauscher, and J.O.Rasmussen, Nucl. Phys. A308 (1978) 513.

31. Y.P.Viyogi, T.J.M.Symons, P.Doll, D.E.Greiner, H.H.Heckman, D.L. Hendrie, P.J.Lindstrom, J.Mahoney, D.K.Scott, K.Van Bibber, G.D.Westfall, H.Wieman, H.J.Crawford, C.McParland, and C.K.Gelbke, Phys. Rev. Lett. 42 (1979) 33.

32. T.J.M.Symons, Y.P.Viyogi, G.D.Westfall, P.Doll, D.E.Greiner, H.Faraggi, P.J.Lindstrom, D.K.Scott, H.J.Crawford, and C.McParland, Phys. Rev. Lett. 42 (1978) 40.

33. G.D.Westfall, L.W.Wilson, P.J.Lindstrom, H.J.Crawford, D.E.Greiner, and H.H.Heckman, LBL-7162 (to be published in Phys. Rev. C).

34. J.B.Cumming, P.E.Haustein, R.W.Stoenner, L.Mausner, and R.A.Naumann, Phys. Rev. C10 (1974) 739.

35. J.B.Cumming, R.W.Stoenner, and P.E.Haustein, Phys. Rev. C14 (1976) 1554.

36. J.B.Cumming, P.E.Haustein, T.J.Ruth, and G.J.Virtes, Phys. Rev. C17 (1978) 1632.

37. C.R.Rudy and N.T.Porile, Phys. Lett. 59B (1975) 240.

38. W.Loveland, R.J.Otto, D.J.Morrissey, and G.T.Seaborg, Phys. Lett. 69B (1977) 284.

39. W.Loveland, R.J.Otto, D.J.Morrissey, and G.T.Seaborg, Phys. Rev. Lett. 39 (1977) 320.

40. D.J.Morrissey, W.Loveland, and G.T.Seaborg, Z. Phys. A289 (1978) 123.

41. Y.Eisenberg, Phys. Rev. 96 (1954) 1378.

42. A.Y.Abul-Magd and J.Hufner, Nucl. Phys. A308 (1978) 429.

42a. In this section (II.3) all equations are written in terms of the target primary products, but they apply equally well to the projectile primary products.

43. R.J.Glauber, in "Lectures in Theoretical Physics," Vol. I, edited by W.E.Brittin and L.G.Dunham (Interscience Publishers, N.Y., 1959), pp. 315-414.

44. R.J.Glauber, Proceedings of Third Int. Conf. on High Energy Physics Nucl. Structure, edited by S.Devons (Plenum Press, N.Y., 1970), pp. 207-264.

45. W.Czyz and L.C.Maximon, Ann. Phys. (N.Y.) 52 (1969) 59.

46. P.M.Fishbane and J.S.Trefil, Phys. Rev. D10 (1974) 3005 and 3128.

47. S.Barshay, C.B.Dover, and J.P.Vary, Phys. Rev. C11 (1975) 360.

48. P.J.Karol, Phys. Rev. C11 (1975) 1203.

49. J.M.Eisenberg and W.Greiner, "Nuclear Theory," Vol. II [Excitation Mechanisms of the Nucleus] (North-Holland, 2nd edition, 1976) 123.

50. M.Blann, OVERLAID ALICE, USAEC Report COO-3494-29 (unpublished).

51. V.F.Weisskopf and D.H.Ewing, Phys. Rev. 57 (1940) 472.

52. W.D.Myers and W.J.Swiatecki, Nucl. Phys. 81 (1966) 1; Ark Fys. 36 (1967) 343.

53. T.F.Cleghorn, P.S.Freier, and C.J.Waddington, Can. J. Phys. 46 (1968) 572.

54. J.Benecke, T.T.Chou, C.N.Yang, and E.Yen, Phys. Rev. 188 (1969) 2159.

55. F.P.Feynman, Phys. Rev. Lett. 23 (1969) 1415.

56. H.R.Collard, L.R.B.Elton, and R.Hofstadter, in "Nuclear Radii," edited by H.Schopper (Springer-Verlag, Berlin, 1967), Landolt-Börnstein, New Series, Vol. 2.

57. K.Chen, A.Fraenkel, G.Friedlander, J.R.Grover, J.M.Miller, and Y.Shimamoto, Phys. Rev. 166 (1968) 949.

58. D.K.Scott, private communication.

59. S.T.Buttler and C.A.Pearson, Phys. Rev. Lett. 7 (1961) 69, and Phys. Rev. 129 (1963) 836.

60. H.H.Gutbrod, A.Sandoval, P.J.Johansen, A.M.Poskanzer, J.Gosset, W.G.Meyer, G.D.Westfall, and R.Stock, Phys. Rev. Lett. 37 (1976) 667.

61. O.Benary, L.R.Price, and G.Alexander, "NN and ND Interactions (above 0.5 GeV/c) – A Compilation," UCRL-20000 (1970).

62. Martin L. Perl, "High Energy Hadron Physics," (John Wiley & Sons, 1974), p.7.

63. J.Hüfner, C.Sanders, and G.Wolschin, Phys. Lett. 73B (1978) 289.

64. X.Artru and G.B.Yodth, Phys. Lett. 40B (1972) 43.

65. R.Jackle and H.Pilkuhn, Nucl. Phys. A247 (1975) S21.

66. H.H.Heckman and P.J.Lindstrom, Phys. Rev. Lett. 37 (1976) 56.

67. W.L.Wang, Phys. Lett. 52B (1974) 143.

68. G.D.Westfall et al[36] have used ten different targets, and the minimization of Eq. IV.16 is performed over all of them.

69. Numerical results are presented in Appendix B.

70. A.G.Artukh, V.V.Avdeichikov, G.F.Gridnev, V.L.Mikheev, V.V.Volkov, and J.Wilczynski, Nucl. Phys. A176 (1971) 284.

71. R.Klapisch, C.Thibauld, A.M.Poskanzer, R.Prieels, C.Rigaud, and E.Roeckl, Phys. Rev. Lett. 29 (1972) 1254.

72. G.W.Butler, D.G.Perry, L.P.Remsberg, A.M.Poskanzer, J.B.Natowitz, and F.Plasil, Phys. Rev. Lett. 38 (1977) 1380.

73. F.S.Goulding and B.G.Harvey, Ann. Rev. Nucl. Sci. 25 (1975) 167.

74. D.E.Greiner, P.J.Lindstrom, F.S.Bieser, and H.H.Heckman, Nucl. Instr. Meth. 116 (1974) 21.

75. Figure IV.13 was drawn after J.Cerny and A.Poskanzer, Sci. Am. 238 (June 1978) 60.

76. H.H.Heckman, D.E.Greiner, P.J.Lindstrom, and H.Shwe, Phys. Rev. C17 (1978) 1735.

77. M.Goldhaber and E.Teller, Phys. Rev. 74 (1948) 1046.

78. W.D.Myers, W.J.Swiatecki, T.Kodama, L.El-Jaick, and E.R.Hilf, Phys. Rev. C15 (1977) 2032.

U.S.GPO:1979-689-058(F)3